ANALYSIS AND MEASUREMENT OF ANTI-RECIPROCAL SYSTEMS

BY

NOORI KIM

DISSERTATION

Submitted in partial fulfillment of the requirements
for the degree of Doctor of Philosophy in Electrical and Computer Engineering
in the Graduate College of the
University of Illinois at Urbana-Champaign, 2014

Urbana, Illinois

Doctoral Committee:

Associate Professor Jont B. Allen, Chair
Professor Stephen Boppart
Professor Steven Franke
Associate Professor Michael Oelze

ABSTRACT

Loudspeakers, mastoid bone-drivers, hearing-aid receivers, hybrid cars, and more - these "anti-reciprocal" systems are commonly found in our daily lives. However, the depth of understanding about the systems has not been well addressed since McMillan in 1946. The goal of this study is to provide an intuitive and clear understanding of the systems, beginning from modeling one of the most popular hearing-aid receivers, a balanced armature receiver (BAR).

Models for acoustic transducers are critical in many acoustic applications. This study analyzes a widely used commercial hearing-aid receiver, manufactured by Knowles Electronics, Inc (ED27045). Electromagnetic transducer modeling must consider two key elements: a *semi-inductor* and a *gyrator*. The semi-inductor accounts for electromagnetic eddy-currents, the "skin effect" of a conductor, while the gyrator accounts for the anti-reciprocity characteristic of Lenz's law. Aside from the work of Hunt to our knowledge, no publications have included the gyrator element in their electromagnetic transducer models. The most prevalent method of transducer modeling evokes the *mobility method*, an ideal transformer alternative to a gyrator followed by the dual of the mechanical circuit. The mobility approach greatly complicates the analysis. The present study proposes a novel, simplified, and rigorous receiver model. Hunt's two-port parameters as well as the electrical impedance $Z_e(s)$, acoustic impedance $Z_a(s)$, and electro-acoustic transduction coefficient $T_a(s)$ are calculated using transmission and impedance matrix methods. The model has been verified with electrical input impedance, diaphragm velocity *in vacuo*, and output pressure measurements. This receiver model is suitable for designing most electromagnetic transducers, and it can ultimately improve the design of hearing-aid devices by providing a simplified yet accurate, physically motivated analysis.

As a utilization of this model, we study the motional impedance (Z_{mot}) that was introduced by Kennelly and Pierce in 1912 and highlighted by many researchers early in the 20th century. Our goal for this part of the study is to search for the theoretical explanation of the negative real part (resistance) observed in Z_{mot} in an electromechanical system, as it breaks the positive-real (PR) property of Brune's (1931) impedance, as well as the conservation of

energy law. Specifically, we specify conditions that cause negative resistance in the motional impedance using simple electro-mechanical network models. Using Hunt's two-port system parameters (a simplified version of an electro-acoustic system), Z_{mot} is defined as $-\frac{T_{em}T_{me}}{Z_m}$, where the subscript m stands for mechanic, T_{em} and T_{me} are transfer impedances, and Z_m is the mechanical impedance of the system. Based on the simplified electromechanical model simulation, we demonstrate that $Z_{mot}(s)$ is a minimum-phase function, but does not have to be a positive-real (PR) function. Any electro-mechanical network with shunt losses in the electrical side (including a semi-inductor and a resistor) sees a negative real part in Z_{mot}, which may arise when there are frequency-dependent real parts. In conclusion, Z_{mot} is not a PR impedance because of the phase lag.

Several significant topics will be discussed in addition to these two larger issues (modeling the balanced armature receiver and investigating Z_{mot}). We generalize the gyrator with the non-ideal gyrator, analogous to the ideal vs. non-ideal transformer cases. This formula is reinterpreted via electromagnetic fundamentals. This work helps to transparently explain the anti-reciprocal property embedded in a gyrator. Explaining the matrix composition method is another contribution, which is characterized by the Möbius transformation. This is a significant generalization of the transmission matrix cascading method. Systems where the quasi-static approximation fails will also be considered (i.e., derivation of Kirchhoff's circuit laws from Maxwell's equations). This leads us to the definition of "wave impedance," which is distinct from the traditional Brune impedance, discussed in modern network theory by Vanderkooy. The Brune impedance is defined by a reflectance that is minimum phase which is a significant limitation on this classical form of impedance. The typical example of a non-Brune impedance is a transmission line. This non-Brune distinction is important,s and we believe it to be a novel topic of research

To my parents, Iljoo Kim and Jihyun Koh, to my brother, Sanghyuk, and to my husband Seungjun, for their love and support

ACKNOWLEDGMENTS

I cannot express enough thanks to my Ph.D. advisor Jont Allen, and other committee members for their continued support and encouragement (Professors Stephen Boppart, Steven Franke, and Michael Oelze). I offer my sincere appreciation for the learning opportunities provided by them. Also I appreciate my Master's degree advisor Myoung-Hee Kim for her continuous mentoring and guidance throughout my career.

Many thanks to my friends supported to keep me well-balanced along the way, including the Human Speech Recognition group at UIUC (Sarah Robinson, you are special to me), members at both Jesus-Love church and Mimosa Acoustics (special thanks to Pat Jeng), and Soo-Kyung Shin, my best friend. Most of all, I should thank my husband Seungjun Roh for being the closest friend and partner in my life. I couldn't have done it without their support, they walked into my life when I thought the world walked out from my life.

Finally, I thank Christ Jesus, my Lord, who has given me strength.

This material is based upon work supported by the STTR grant from Office of Naval Research under the contract number N00014-11-C-0498.

CHAPTER 1

INTRODUCTION

A typical hearing-aid consists of three parts: a microphone (picks up sound), an amplifier (transforms sound into different frequencies, filters noise, and selectively amplifies each frequency region based on the difference in individual hearing loss[1] via multi-band compression), and a receiver (sends the processed signal from the amplifier into the ear). A proper understanding of each component in the hearing-aid can facilitate better and clearer sound quality

The current study starts by modeling one of the most important and complex hearing-aid components, the balanced armature receiver (BAR). The BAR is an electromagnetic loudspeaker that converts an electrical signal (current) into acoustical pressure (or force, in the case of an electromechanical system). It is referred to as an electromagnetic transducer because small magnets are involved. These miniature loudspeakers are widely used and remain one of the most expensive components of modern hearing-aids; they are also the most poorly understood. Therefore, a detailed understanding of these transducers is critical to optimize their design.

In the electromagnetic transducer models of both Weece and Allen (2010) and Thorborg et al. (2007), an ideal transformer was used to convert electrical current into mechanical force (or acoustical pressure) in the transducer. As described in Beranek (1954), the mobility analogy (Firestone, 1938), along with an ideal transformer, is a valid way to represent electrical-to-mechanical transduction when modeling anti-reciprocal electromagnetic transducers. The mobility method, which requires using the dual network (swapping current and voltage), fails to provide an intuitive explanation of the anti-reciprocity characteristic of the electromagnetic transducer, which follows from Maxwell-Faraday's law and Lenz's law. The impedance and mobility methods are mathematically equivalent, meaning one can use either method to describe the system. However, including the gyrator in transducer models allows

[1]The percentage of people in the United States who are suffering from hearing loss is 12.7% at age of 12 years and older (Lin et al., 2011). Also two-thirds of Americans older than 70 years have experienced mild to severe hearing loss. The importance of designing hearing-aids properly, therefore, is come to the fore in contemporary society along with the population ageing. Population ageing is a shift in the distribution of a country's population towards older ages (http://en.wikipedia.org/wiki/Population_ageing).

for a logical, intuitive, and accurate interpretation of the physical properties. For example, when using a gyrator to represent the mechanical and electrical transformation, stiffness can be represented as a capacitor and mass as an inductor in the series combination. Given the mobility (dual) network, it is necessary to swap the inductor and capacitor, placing them in parallel combination. Thus, we believe that the dual network combined with the mobility method is less intuitive and more difficult to quantify when describing the system.

Kim and Allen (2013) suggested a two-port network model of the BAR (Fig. 1.1) having a *semi-inductor*, a *gyrator* (two poorly understood elements of special interest in the electromagnetic transducer), and a *pure delay*. Our network has two wave speeds, the speed of light (3×10^8 [m/s]) and the speed of sound (345 [m/s]). Both speeds are important for proper modeling. The acoustic delay becomes significant due to the relatively slow speed of sound. This pure delay is represented using a transmission line in the model. With a *quasi-static* (QS) assumption, there is no pure delay in the system.

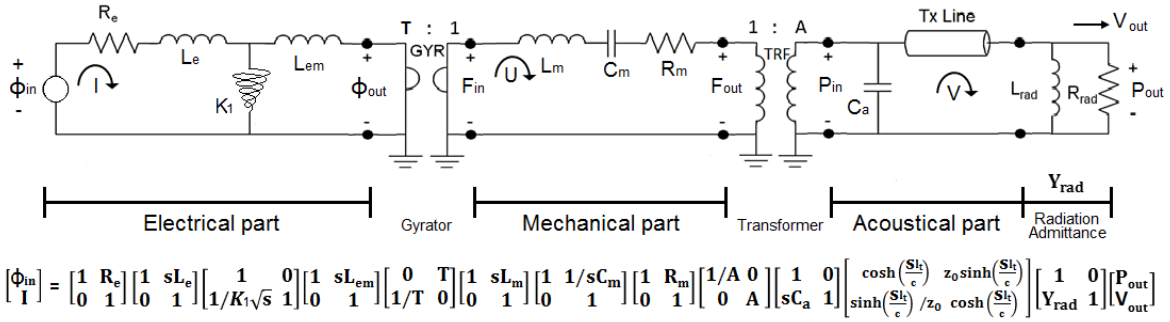

$$\begin{bmatrix}\Phi_{in}\\ I\end{bmatrix} = \begin{bmatrix}1 & R_e\\ 0 & 1\end{bmatrix}\begin{bmatrix}1 & sL_e\\ 0 & 1\end{bmatrix}\begin{bmatrix}1 & 0\\ 1/K_1\sqrt{s} & 1\end{bmatrix}\begin{bmatrix}1 & sL_{em}\\ 0 & 1\end{bmatrix}\begin{bmatrix}0 & T\\ 1/T & 0\end{bmatrix}\begin{bmatrix}1 & sL_m\\ 0 & 1\end{bmatrix}\begin{bmatrix}1 & 1/sC_m\\ 0 & 1\end{bmatrix}\begin{bmatrix}1 & R_m\\ 0 & 1\end{bmatrix}\begin{bmatrix}1/A & 0\\ 0 & A\end{bmatrix}\begin{bmatrix}1 & 0\\ sC_a & 1\end{bmatrix}\begin{bmatrix}\cosh\left(\frac{Sl_t}{c}\right) & z_0\sinh\left(\frac{Sl_t}{c}\right)\\ \sinh\left(\frac{Sl_t}{c}\right)/z_0 & \cosh\left(\frac{Sl_t}{c}\right)\end{bmatrix}\begin{bmatrix}1 & 0\\ Y_{rad} & 1\end{bmatrix}\begin{bmatrix}P_{out}\\ V_{out}\end{bmatrix}$$

Figure 1.1: The balanced armature receiver (BAR) circuit as a model (Kim and Allen, 2013) as defined by a transmission (ABCD) matrix representation. The chained properties of an ABCD matrix are followed by the Möbious transformation. This factored nature of the ABCD matrix is discussed in detail in Section 2.3. The electrical and mechanical circuits are coupled by a gyrator (GYR, realizing an anti-reciprocal network), while a transformer (TRF) is used for the coupling of the mechanical and acoustical circuits. The $K1$ is a semi-inductor representing electromagnetic diffusion due to the skin effect. The $TXLine$ stands for a transmission line to involve a pure delay in the system, violating a quasi-static assumption in this electroacoustic system. Using this non-quasi-static element is the proper way to model this system. In this model, the input and output potentials for each section are specified as voltage (Φ), force (F), and pressure (P). Current (I), particle velocity (U), and volume velocity (V) represent the flow for each of the three physical sections.

The semi-inductor component is necessary to account for eddy current diffusion (the "skin effect"). In 1989, Vanderkooy demonstrated that, at high frequencies, the behavior of the impedance of a loudspeaker changes from the behavior of a normal inductor to that of a semi-inductor because of the eddy current diffusing into the iron pole structure of the loudspeaker (i.e., the skin effect). Using a Bessel function ratio, Warren and LoPresti (2006) represented Vanderkooy's semi-inductor model as a "diffusion ladder network," a continued fraction expansion or a combination of resistors and inductors. In 2010, Weece and Allen

used this representation in a bone-driver model. After demagnetizing the bone-driver, they established the $\sqrt{s}$ behavior and determined the ladder network elements from the measured electrical impedance of the transducer. Thorborg et al. (2007) also introduced a loudspeaker model with lumped circuit elements, including a semi-inductor.

In 1946, McMillan introduced the anti-reciprocal component as a network element. Two years later, Tellegen (1948) coined the term *gyrator* and categorized it as a fifth network element, along with the capacitor, resistor, inductor, and ideal transformer. Other than Hunt's 1954 publication, we remain unaware of any publication which implements anti-reciprocity in its electromagnetic transducer model using a gyrator.

Leading to their new circuit model of the BAR (Fig. 1.1), Kim and Allen (2013) measured the electrical input impedance, solving for the Hunt parameters (1954)[2] of the receiver. An intuitive design of an electromagnetic transducer was developed by using the gyrator and the asymptotic property as $\omega \to \infty$ (Vanderkooy, 1989) was properly described by using a parallel relationship between a semi-inductor and a normal inductor (electrical part in Fig. 1.1). Approximations for two extreme frequency limits of the input impedance ($Z_{in} = \sqrt{s}||s$) are defined as follows:

$$Z_{in}(s) = \frac{1}{\frac{1}{\sqrt{s}} + \frac{1}{s}} \approx \begin{cases} \frac{1}{\frac{1}{\sqrt{s}} + \frac{1}{\cancel{s}}} = \sqrt{s}, & s \to \infty \\ \\ \frac{1}{\frac{1}{\cancel{\sqrt{s}}} + \frac{1}{s}} = s, & s \to 0 \end{cases} \tag{1.1}$$

where s is the Laplace frequency ($j\omega$). This model is presented in Fig. 1.1, and the modeled BAR[3] and its internal structure are shown in Fig. 1.2.

1.1 Comparison of a telephone receiver and a moving-coil receiver

The oldest telephone receiver is the BAR type, and it is still in use. The original technology goes back to the invention of the electric loudspeaker by A. G. Bell in 1876. Attraction and release of the armature are under the control of the current in the windings of an electromagnet (Beranek and Mellow and Hunt, 1954, Chapter 7). As the electrical current goes into the electric terminal of the receiver, it generates an alternating current (AC) magnetic field surrounded by a coil. Due to the polarity between the permanent magnet

[2]The electrical impedance Z_e, the mechanical impedance Z_m, and electromechanic transduction coefficients T_{em}, T_{me}. More detail about the Hunt parameters is discussed in Section 2.1.

[3]ED7045 Knowles Electronics, Itasca, IL (http://www.knowles.com).

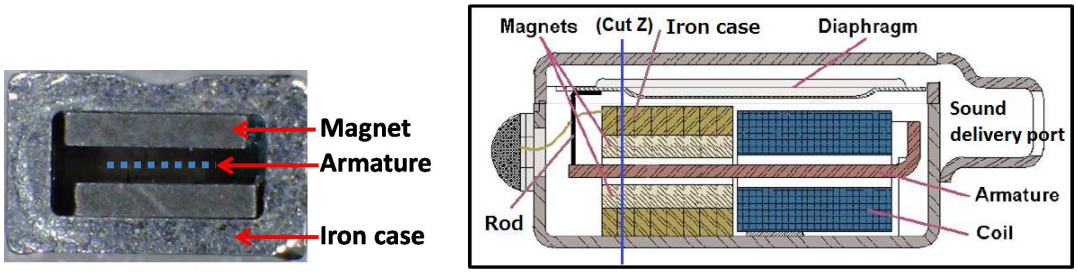

(a) The cross-sectional view of the receiver

(b) The structure of ED7045 receiver

Figure 1.2: (a) The picture of the BAR at the "Cut Z" line in panel (b). There is space for the armature to vibrate vertically between the magnets. Magnets are sandwiching the armature (the blue, dotted line). A laminated iron case surrounds the magnets and the armature. (b) A schematic of a BAR. An electrical current in the coil comes from the transducer's electrical input terminals; the current induces a Lorentz force on the armature via the induced magnetic field (modified from Knowles documentation of the ED receiver series). Note that the port location of the ED7045 receiver is rotated 90^o to the longer side.

and the generated magnetic field, an armature, which sits within the core of the coil and the magnet, feels a force. The very basic principles for explaining this movement are Hooke's law (F_{hook}) and the magnetic force due to a current $\mathbf{I}$ ($\mathbf{F_{mag}}$) [4]

$$F_{hook} = k\xi, \tag{1.3}$$

where ξ is the displacement, and k is a constant characterizing stiffness of spring (or armature in our case), and

$$\mathbf{F}_{mag} = \mathbf{I} \times \mathbf{B_0}, \tag{1.4}$$

where $\mathbf{I}$ is the current and $\mathbf{B_0}$ is the static magnetic field.

As shown in Fig. 1.2, since a diaphragm is connected to the end of the armature, when the armature moves, so does the diaphragm. The sound wave is propagated out of the sound delivery port. A large number of coil turns is required since the generated magnetic field (from the coil, time-varying magnetic field) should be compatible with the static direct

[4] A new theory about operation of the BAR was introduced by Jensen et al. (2011). This paper derives a non-linear time-domain force for the BAR-type receiver. Based on their theory, the input force of the moving-armature transducer system employs "the tractive force," which attempts to minimize the air gap between the armature and the magnet. According to this theory

$$F_{bar} = \frac{\mathbf{S_a B^2}}{2\mu_0} = \frac{\Psi_0^2}{2\mu_0 \mathbf{S_a}}, \tag{1.2}$$

where $\mathbf{B}$ [Wb/m^2] is the magnetic field across the air gap, S_a [m^2] is the transverse area of the armature with the permanent magnet, μ_0 is the permeability in free space ($4\pi 10^{-7}$ [H/m]), and $\Psi_0 (= \mathbf{B}_0 S_a)$ [Wb] is the total magnetic flux in the air gap. To justify this theory, one must construct a relationship between F_{bar} in Eq. 1.2 and current similar to the relationship shown in Eq. 1.4 due to the gyrator nature in electromagnetic system.

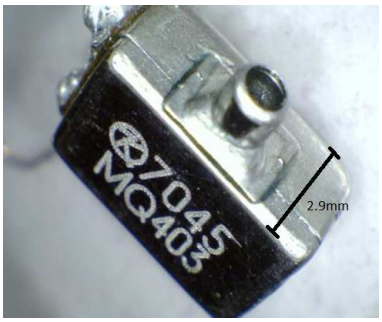

Figure 1.3: A picture of the ED7045, a BAR used in this study. The black line shows the depth of the transducer, 2.9 [mm].

current (DC) magnetic field (permanent magnet) to balance the mutual magnetic force. The size, weight, and sensitivity of this type can be greatly improved by using a light (low-mass) pole piece (i.e., armature) with small permanent magnets. This is the main reason for using this type of transducer in hearing-aid products.

Knowles Electronics[5] ED series receivers shown in Fig. 1.2(a) and Fig. 1.3, including the ED7045 and ED1913, are BARs, used in all hearing-aids. The ED receiver is $6.32 \times 4.31 \times 2.9$ [mm] in size. These receivers consist of a coil, an armature, two magnets, and a diaphragm. Unlike the alternative moving-coil drivers, the coil of the BAR has a fixed position (Jensen et al., 2011), thereby reducing the internal mass and providing more space for a much longer coil. As a result of the lower mass, the BAR frequency response is higher, and due to the greater coil length, the sensitivity is greater.

The armature used for the ED7045 is an E-shaped metal reed (Bauer, 1953), whereas a U-shaped armature was widely used for early telephone instruments (Mott and Miner, 1951). Both shapes have advantages and disadvantages. For example, the U-shaped armature has better acoustic performance (i.e., wide-band frequency response) while the E-shaped armature lowers the vibration of the body more effectively. The armature is placed through the center of the coil and in between two magnets, without touching them. The movement of the armature is directly connected to the diaphragm through a thin rod (Fig. 1.2 (b)). Figure 1.4 shows the types of ring armature receivers adapted from Mott and Miner (1951).

The other popular type of speaker is the moving-coil, or dynamic, speaker proposed by Oliver Lodge in 1898 (Hunt, 1954) (Fig. 1.5). In this type of speaker, a voice coil surrounds a magnet and the coil is attached to a diaphragm (or sound cone). When there is input through the coil, the coil is forced to move (up and down), as described by Faraday's law. The coil drives the cone, which radiates the sound. As a result, the air particles around the sound cone vibrate; therefore, sound waves are created.

[5]Knowles Electronics, Itasca, IL (http://www.knowles.com).

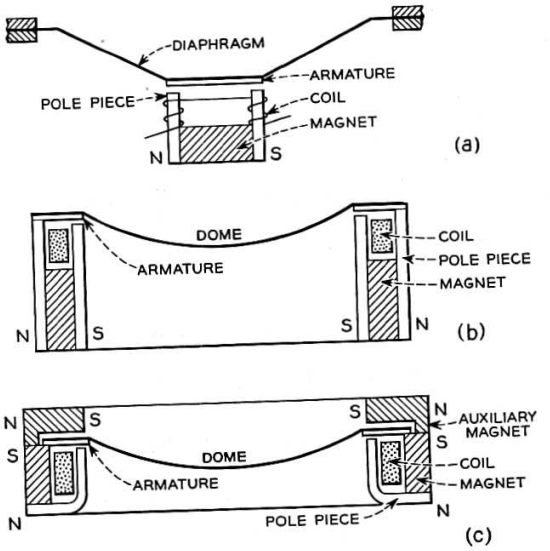

Fig. 2—(a) Early composite diaphragm receiver.
(b) Simple ring armature receiver.
(c) Ring armature receiver with auxiliary magnet.

Figure 1.4: Sectional view of ring armature receivers (three types) adapted from Mott and Miner (1951), Fig. 2 in the original manuscript.

To limit the mass of the coil in the dynamic speaker, the number of coil turns must be greatly reduced (e.g., 100 times less than in the BAR case). The dynamic speaker needs a strong core magnet to float the cone (with the coil), which leads to a size generally larger than the BAR. This acoustic characteristic of the dynamic speaker is easier to understand after controlling the speaker mass and the stiffness of the diaphragm.

1.2 Goal of this study

The goal of this study is to provide clear insight into anti-reciprocal (or broadly non-reciprocal) system. We are exposed to anti-reciprocal systems in our daily lives; however, the depth of our understanding of them has not been well addressed since McMillan in 1946. The keyword is "anti-reciprocity."

As discussed in the appendix C, the motivation for this study began with a PSPICE simulation using the BAR-type ED series receiver model from Knowles Electronics (Kim and Allen, 2013, Fig. C.1). We then proceeded to redefine a new circuit model to characterize a BAR-type receiver, the Knowles ED7045, and then developed theoretical insights and observations critical to understanding the BAR.

The specific concepts covered in this study follow from a conceptual version of the BAR model shown in Fig. 1.6. There are six highlighted parts in this figure labeled with capital

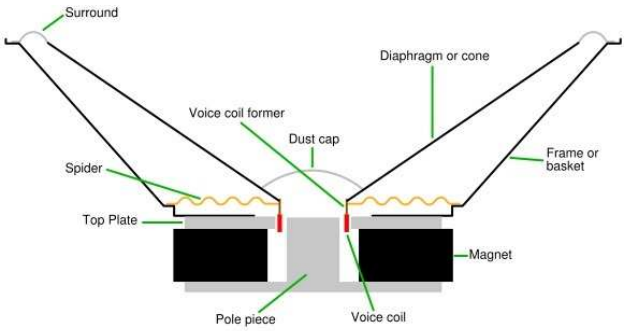

Figure 1.5: The cross-section view of the moving-coil loudspeaker. Up-and-down motion of the voice coil around an permanent magnet creates a time-varying magnetic field. As a voice coil moves around the pole piece, it becomes an electromagnet. The image is from http://i1-news.softpedia-static.com.

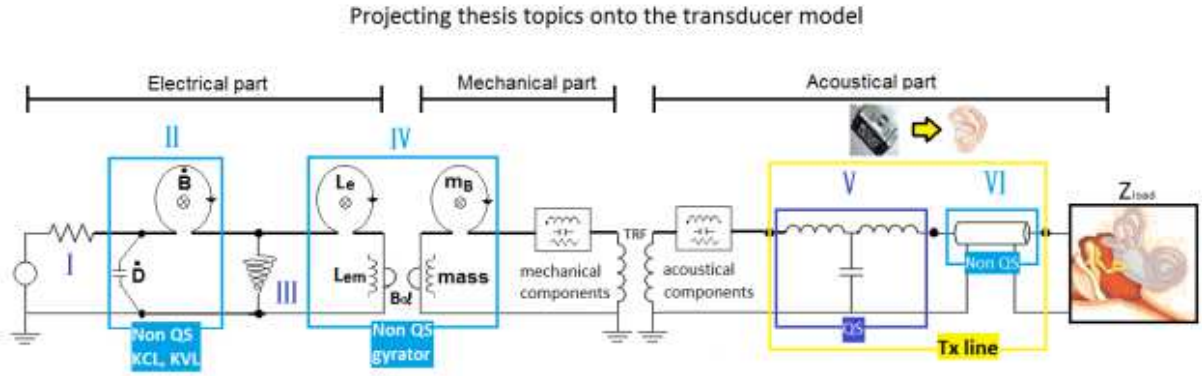

Figure 1.6: Overview of this study via the BAR model. All concepts discussed in this thesis can be tied together to understand the BAR transducer. The important concepts are highlighted using Roman numerals. Note that the *quasistatic* (QS) components are marked as dark blue and the non-QS components are in light blue.

Roman numerals. Dark blue represent QS elements, while light blue shows non-QS elements. The left-most resistor (part I) on the electrical side stands for the DC resistance of wire. It depends on the real part of the wire resistance, with the internal noise attributed to the Brownian (thermal) motion of the electrons in the resistor. The second part (II) defines two missing parameters (Lewin, 2002a) in classic circuit theory (KVL and KCL) lead inductance due to the electromotive force (emf) created by the magnetic field ($\dot{\mathbf{B}}$), and stray capacitance due to displacement current ($\dot{\mathbf{D}}$), respectively (Lewin, 2002b). These components are frequency-dependent terms embedded in Faraday's law and Ampere's law. According to Woodson and Melcher (1968) either the lead inductance or the stray capacitance must be zero when defining QS circuits. They define two cases: the stray capacitance ($\dot{\mathbf{D}}$) is zero for electrostatic and the lead inductance ($\dot{\mathbf{B}}$) is zero for magnetostatic.

There are two types of leakage inductances. One is due to the air side of the coil (L_e in

part IV) and the other is from the semi-inductor leakage (part III) due to the magnetic field diffusion which leads to the eddy current in the iron core (Vanderkooy, 1989). This diffusive current is described by the skin depth of the ferromagnetic material ($\sqrt{\frac{2}{\mu\sigma\omega}}$), where μ, σ are the permeability and conductivity of the material and ω is the angular frequency.

Part IV characterizes the behavior of a non-ideal gyrator. Two loop inductors (L_e, m_B) due to the induced magnetic fields are associated with the self-inductor (mass in the mechanical side). The ideal gyrator, introduced by Tellegen (1948), does not employ these non-ideal loop inductors, considering only the DC magnetic field of permanent magnets and the wire's self-inductances (i.e., $F = B_0 l I$ relationship from an ideal gyrator, where B_0 is static magnetic field density due to the permanent magnet and l is the length of the wire). Note that the non-ideal coupling coefficients (or transfer impedances) are analogues to mutual inductance of a non-ideal transformer. Both the ideal and non-ideal gyrators assume the QS approximation. This gyrator describes the transfer impedances of electromechanical (or electroacoustic) systems, namely T_{em}, T_{me}, which have anti-reciprocal characteristics due to Lenz's law.

Parts V and VI represent transmission lines, with (V) and without (VI), the QS approximation. The behavior of this line in the low-frequency region can be estimated by lumped circuit elements, as shown in part V. However, any pure delay, identified by the non-QS transmission line, cannot be modeled via the QS approximation. Infinite numbers of resonance and anti-resonance (poles and zeros) are observed in the magnitude of the impedance of the non-QS transmission line (VI). Therefore, it is critical to clearly understand the transmission line, whether it is QS or non-QS, to describe the system correctly. A typical and important application of this kind of transducer is the human ear, as depicted in Fig. 1.6 as the terminating impedance, Z_{load}. The outer ear (i.e, ear canal) and tympanic membrane (TM) can be modeled as a lossless transmission line (Puria and Allen, 1998; Robinson and Allen, 2013; Parent and Allen, 2010), and then the specific load is the middle ear.

Along with these concepts (parts I - VI), we also study the *motional impedance* Z_{mot}, a unique characteristic of anti-reciprocal systems discovered early in the 20th century. It was first introduced experimentally (Kennelly and Pierce, 1912; Kennelly and Affel, 1915; Kennelly and Nukiyama, 1919; Kennelly and Kurokawa, 1921; Kennelly, 1925); however, it has rarely been explained theoretically (Mott and Miner, 1951). Along with the modeling work, we investigate Z_{mot}, based on an in-depth analysis of the anti-reciprocal system. For this, we reduce the complexity of the proposed BAR model, leaving only the essential elements, to represent a simpler electromagnetic motor network.

We also reconsider the Z_{mot} formula based on each parameter's spatial relationship. When Maxwell formulated his equations, he used quaternions working in 4D space (x, y, z in the

spatial domain plus time t). This work is critical because when we perform circuit simulation, we usually do not consider the spatial variation of each variable. Using quaternions to reformulate the definitions of the Hunt parameters and Z_{mot} does not change the original formulas (Appendix D).

1.2.1 A note about the electrical-computer engineering (ECE) curriculum

When modeling transducers, frequency domain tools are critical for both analysis and understanding. These include 1-port and 2-port network theory (Van Valkenburg, 1964, 1960). These tools naturally include the Fourier and Laplace transforms, power, impedance, and various generalizations of these tools including the Impedance and transmission (ABCD) matrix, scattering matrices, reflectance (Smith chart). Also important are time domain tools, especially for nonlinear systems. Popular tools include Matlab (ECE310/311) and Spice (ECE-342/343). At the heart of such analysis is the QS approximation, which is typically defined in terms of the ratio of the wavelength over the dimensions of the physical structure being analyzed. This ratio is typically quoted as $ka \ll 1$, where $k = 2\pi/\lambda$ and a is the radius of the system or object being modeled.

Digital signal processing (DSP) is based on time domain processing but also uses the frequency domain in the form of the DFT and Z-transform. The quasi-static approximation is not typically assumed in DSP processing, since there is explicit pure delay built into the analysis in terms of the sampling period, based on an estimate of the highest frequency being analyzed. Thus again an upper bound on frequency is assumed, but not in terms of QS. This is a different model that explicitly includes the pure delay.

Once the student is introduced to Maxwell's equations (ME), all these superficial distinctions are replaced by vector calculus, the wave equation, Gauss's law, and Poynting's power theorem ($\mathbf{E} \times \mathbf{H}$).

In this thesis all of these ideas necessarily come into play at the same time. This is in part due to the merging of acoustics, with its slow wave speed, thus short wavelengths relative to the EM wavelengths (i.e., speed of sound and speed of light). While we use the QS approximation and its associated Brune impedance relationships, we must also generalize impedance to include the *wave impedance* seen in EM and acoustics. These two types of impedance complement each other. Wave impedance requires delay, as we have learned from DSP, whereas the Brune impedance obeys the QS approximation.

1.3 Historical notes

Two people inspired this study. The first is Arthur Edwin Kennelly (Fig. 1.7 (a)), who was born in 1861 in India. Kennelly was 15 years old when Bell submitted the telephone patent and 16 years old when Edison invented the carbon microphone. He is famous for working with Edison starting in 1887 to supplement Edison's weaknesses (i.e., math, AC, and electromagnetic studies); he was 26 years old when he joined Edison's group. He was a professor of electrical engineering at Harvard University from 1902-1930. He wrote his first paper on a loudspeaker in 1912 and worked at the Massachusetts Institute of Technology (MIT) from 1913-1924. Also, he was the first person to use the term impedance for AC circuits (Kennelly, 1893). In this paper, he discussed the first use of complex numbers as applied to Ohm's law in alternating current circuit theory.

(a) A. E. Kennelly (b) F. V. Hunt

Figure 1.7: (a) A. E. Kennelly (b) F. V. Hunt

Along with these academic achievements in electroengineering, the first analysis of the magnetically driven moving-coil speaker's behavior, seen from the electrical side, was highlighted by Kennelly and Pierce (1912) and he, the creator of *impedance* analogy in AC circuits, called it motional *impedance* (Z_{mot}). This concept was intensively studied early in the 20th century based on experimental facts, without theoretical criticism. Kennelly actively published many investigations on Z_{mot}, making him a pioneer in loudspeaker analysis. However, a significant problem regarding Z_{mot} is its negative real part, which appears to be a violation of energy conservation (Eq. A.1). Including Kennelly's papers, the negative real

part in Z_{mot} has never been clarified with regard to its physical properties (Littler; Fay and Hall; Hanna).

The second person who inspired this study was Frederick Vinton Hunt (Fig. 1.7 (b)), who was born in 1905 in Barnesville, Ohio. He was a professor at Harvard University, working in acoustic engineering. He contributed to underwater acoustics during World War II by developing the first modern sonar system. Other inventions and studies, including room acoustics, regulated power supply, lightweight phonograph pickups, and electronic reproduction equipment, are also important contributions he made to the field of electrical engineering.

Hunt published *Electroacoustics* in 1954, which is the basis of the current thesis. In that book, he analyzed and synthesized the electroacoustic (or electromechanical) system by modeling it as a 2×2 matrix using scalar forms of Lorenz's force and Maxwell's equations (i.e., Ampere's law and Faraday's law).[6]

The actual contributions from this study which are tied together to understand the BAR transducer intuitively can be summarized as follows:

1) Our distinctive BAR model involves a gyrator, semi-inductor, and a transmission line, representing anti-reciprocal, diffusive, and non-QS network (Fig. 1.1), respectively.

2) In-depth investigation of the anti-reciprocal network. Reinterpreting the gyrator's formula via electromagnetic basics and expending the formula to non-ideal case.

3) Reinterpretation of the QS considering pure delay in the system.

The remainder of this study is structured as follows: Chapter 2 introduces the theoretical concepts specifically related to designing electromagnetic transducer models. Chapter 3 presents the experimental methods used in the study of the BAR. Chapter 4 includes the results from both the theoretical and experimental methods. Finally, the conclusions and contributions of this study are summarized in Chapter 5.

[6]It was done by distinguishing two constants $j = \sqrt{-1}$ for a 90° phase shift and $k = \sqrt{-1}$ for a 90° spatial phase shift. Hunt (1954) Chapter 3 pp.114, $F = BlkI$, $\Phi = Blku$, where F, I, Φ, u, B, l are force, current, voltage, velocity, magnetic intensity, and length of wire respectively.

CHAPTER 2

THEORETICAL METHODS

In this chapter, we research important theoretical concepts to appreciate anti-reciprocal networks, such as Hunt's two-port network, Möbious transformation, Carlin's network postulate, a gyrator, a semi-inductor, and the motional impedance.

It will be useful to discuss a proper way to choose frequency domains for signals (i.e., Φ, I) and systems (i.e., power and impedance) at this point. Laplace frequency $s = \sigma + j\omega$ is used to indicating a positive-real (PR) characteristic of a system. In a Laplace frequency plane, the abscissa (x-axis) is for a real part (σ referring to any loss in a system) while the ordinate (y-axis) is for an imaginary part ($j\omega$ where ω is an angular frequency or a Fourier frequency). PR functions are strictly non-negative on the right half of the Laplace plane to assume they obey the passive condition (see, C3 in Section 2.2). However, Φ and I are classified as signals (not systems). They do not need to obey the PR property. Therefore the angular Fourier frequency ω is used for $\Phi(\omega)$ and $I(\omega)$. For example, one can use the Fourier transform to convert a voltage in the time domain to a voltage in the frequency domain. But to convert power from one domain to the other, the Laplace transform must be applied. Since impedance is a necessary part of power, the concept of impedance ($\mathcal{Z}$) is also described as a system, especially in a frequency domain; therefore we use the Laplace frequency s for $\mathcal{Z}(s)$. It is true for one or two-port systems.

2.1 Two-port anti-reciprocal network with Hunt parameters

Hunt (1954) modeled an electromechanic system into a simple 2×2 impedance matrix relationship. There are four Hunt's two-port network parameters, following Wegel (1921), $Z_e(s)$, $Z_m(s)$, $T_{em}(s)$, and $T_{me}(s)$, where $s = \sigma + j\omega$ is the Laplace frequency.

To explain each parameter, we convert a two-port ABCD matrix to the Hunt impedance matrix. A schematic representation of this network is shown in Fig. 2.1 as depicted by Kim and Allen (2013). As shown in Fig. 2.1, each network element may be represented with a 2×2 ABCD matrix, with the velocity U defined as flowing out of the element (resulting in a negative sign). Thus multiple elements' matrices can be 'chained' (i.e., factored) in

accordance with different combinations of the elements (i.e., series or shunt). This allows one to represent the network using matrix multiplication, which enables convenient algebraic manipulation. Since the current (flow) is always defined as going into the port, when we transform the ABCD matrix to an impedance matrix, it is necessary to force a negative sign for the volume velocity to maintain tradition matrix requirements.

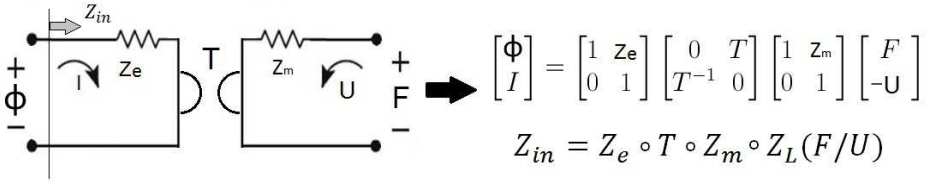

Figure 2.1: A schematic representation of an electromechanic system using Hunt parameters and Möbious composition of the ABCD matrix (Kim and Allen, 2013). Note how the ABCD matrix method factors the model into a 2×2 matrix. This allows one to separate the modeling from the algebra.

In practical electromechanical systems, all variables in the system (Φ, I, $\mathbf{F}$, $\mathbf{U}$) are constrained to a fixed direction of action (without considering spatial dependency); therefore relationships between each quantity become scalar (Hunt, 1954). Especially when we analyze the system using the ABCD matrix, we must treat all variables as the scalars.

The Hunt impedance matrix representation of the same system is

$$\begin{bmatrix} \Phi(\omega) \\ F(\omega) \end{bmatrix} = \begin{bmatrix} Z_e(s) & T_{em}(s) \\ T_{me}(s) & Z_m(s) \end{bmatrix} \begin{bmatrix} I(\omega) \\ U(\omega) \end{bmatrix}, \tag{2.1}$$

where $s = \sigma + j\omega$, and

$$Z_e(s) = \frac{\Phi(\omega)}{I(\omega)} \text{ when U}(\omega)\text{=0}, \tag{2.2}$$

$$T_{em}(s) = \frac{\Phi(\omega)}{U(\omega)} \text{ when I}(\omega)\text{=0}, \tag{2.3}$$

$$T_{me}(s) = \frac{F(\omega)}{I(\omega)} \text{ when U}(\omega)\text{=0}, \tag{2.4}$$

$$Z_m(s) = \frac{F(\omega)}{U(\omega)} \text{ when I}(\omega)\text{=0}. \tag{2.5}$$

For DC electromagnetic coupling, $-T_{em} = T_{me} = T = B_0 l$, where B_0 and l are the DC magnetic field and length of wire, respectively. Along with Eq. 2.1, the two-port electromechanic transducer equation can alternatively be represented in ABCD (a.k.a. transmission matrix) form, as given by

$$\begin{bmatrix} \Phi(\omega) \\ I(\omega) \end{bmatrix} = \begin{bmatrix} A(s) & B(s) \\ C(s) & D(s) \end{bmatrix} \begin{bmatrix} F(\omega) \\ -U(\omega) \end{bmatrix}. \tag{2.6}$$

Here A, B, C, D are functions of s to show they are causal (see, C4 in Section 2.2) and complex analytic system variables. The signal variables Φ, I, F, U, on the other hand, are functions of ω, to indicate they are neither causal, nor analytic.

The fundamental difference between the two matrix representations lies in the coupling of the electromechanic transducer, between the mechanical and the electric signals. Specifically, the electrical input parameters Φ and I on the left side of the network and Eq. 2.6 are expressed in terms of the mechanical variables, the force F and the velocity U, on the right side of the network, via the four frequency dependent parameters A, B, C, and D.

Conversion between Eq. 2.6 and Eq. 2.1 has the following relationships:

$$\mathcal{Z} = \begin{bmatrix} z_{11}(s) & z_{12}(s) \\ z_{21}(s) & z_{22}(s) \end{bmatrix} = \frac{1}{C} \begin{bmatrix} A(s) & \Delta_T(s) \\ 1 & D(s) \end{bmatrix}, \tag{2.7}$$

$$\mathcal{T} \begin{bmatrix} A(s) & B(s) \\ C(s) & D(s) \end{bmatrix} = \frac{1}{T_{me}(s)} \begin{bmatrix} Z_e(s) & \Delta_Z \\ 1 & Z_m(s) \end{bmatrix}, \tag{2.8}$$

where $\Delta_Z = Z_e Z_m - T_{em} T_{me}$ and $\Delta_T = AD - BC$. Note that if $C = 0$, Z does not exist. Eq. 2.8 represents Eq. 2.7's inverse transformation, the conversion from impedance matrix to transmission matrix.

Note that the impedance matrix is useful when making measurements. For instance, a system's electrical input impedance and output acoustic impedance (or output mechanical impedance) can be represented with the impedance matrix elements, z_{11} and z_{22}. The ABCD matrix representation is useful for network modeling, but then may be transformed into an impedance matrix for experimental verification. Symmetry relationships of the network (i.e., reversibility, reciprocity) based on Eq. 2.7 are discussed in Section 2.2.

2.1.1 Calibration of Hunt parameters for an electroacoustic transducer

In this section, we employ Hunt parameters to electroacoustic systems, Z_e, Z_a, and T_a, where subscript 'a' stands for acoustic. The electroacoustic Hunt parameters can be estimated from Z_{in} given three different acoustic load conditions. Similar to Eq. 2.1, the BAR can be represented by its electroacoustic impedance matrix as

$$\begin{bmatrix} \Phi(\omega) \\ P(\omega) \end{bmatrix} = \begin{bmatrix} Z_e(s) & -T_a(s) \\ T_a(s) & Z_a(s) \end{bmatrix} \begin{bmatrix} I(\omega) \\ V(\omega) \end{bmatrix}. \tag{2.9}$$

The acoustic load impedance Z_L is defined by Ohm's law as

$$Z_L \equiv \frac{P}{-V}, \tag{2.10}$$

where V is volume velocity defined as flowing into the port.

Combining Eq. 2.9 and Eq. 2.10 and solving for V gives

$$V = \frac{-T_a I}{Z_L + Z_a}. \tag{2.11}$$

Replacing V in Eq. 2.9 gives an expression for the loaded electrical input impedance ($V \neq 0$)

$$Z_{in} \equiv \frac{\Phi}{I} = Z_e + \boxed{\underbrace{\frac{T_a^2}{Z_L + Z_a}}_{Z_{mot}}}, \tag{2.12}$$

where Z_{mot} is denoted the *motional impedance* due to the acoustic load shown in the electric terminals (Hunt, 1954). Note that the sum of Z_a and Z_L in Z_{mot}'s denominator is treated as total acoustic impedance when it is looked at from the electrical side. Thus the Z_{in} obtained through measurements depends on the acoustic load, Z_L. Varying the acoustic load, which can be done by varying the length of the acoustic tube, results in different Z_{in} values (see Fig. 3.2 in Chapter 3). The algebraic details are provided in Appendix E.

2.2 Network postulates

An important terminology may be used to describe one-port and two-port networks, as defined in this section. One can relate the limitations of the Brune's impedance based on the one-port network theory (Brune, 1931; Serwy, 2012). To cross from one physical modality from the other (Table A.1), a two-port network must be used (Hunt, 1954; Carlin and Giordano, 1964).

Carlin and Giordano (1964) summarized two-port networks in terms of 6 postulates: C1-linearity, C2-time-invariance, C3-passivity, C4-causality, C5-real-time function, and C6-reciprocity. Note that C6 only applies to two-port networks while the others are for both one-port or two-port networks.

C1 Linearity (*vs.* non-linearity): A system obeys superposition.

$$\alpha f(x_1) + \beta f(x_2) = f(\alpha x_1 + \beta x_2). \tag{2.13}$$

C2 Time-invariance (*vs.* time-variance): A system does not depend on the time of excitation.

$$f(t) = f(x(t)) \rightarrow f(t - t_1) = f(x(t - t_1)). \tag{2.14}$$

C3 Passivity (*vs.* Active): Conservation of energy law, Eq. A.1. A system cannot provide more power than supplied amount, where power is defined as

$$power(t) = \int^t i(t) \cdot v(t) dt. \tag{2.15}$$

C4 Causality (*vs.*non-causality *vs.* anti-causality): A response of a system cannot be affected by a future response.

C5 Real-time function (*vs.* complex-time function): The system's time response is real.

The systems' stability can be discussed via the impulse response, the transfer function, and the poles and zeros of the system. An impedance can be interpreted as a transfer function for one-port systems, and through the inverse Laplace transform ($\mathfrak{L}^{-1}$), we can have its impulse response. In terms of region of convergence (ROC) of the transfer function, the imaginary axis of the s-plane is included in the ROC for a stable system. Specifically, for a system to be stable and bounded, all poles are in the left half plane (LHP) in a causal system case, whereas all poles must be in the right half plane (RHP) in an anti-causal bounded system case. A third category exists if the system is causal and unbounded, when the poles are in the RHP. In this case, (there may be multiple ROCs but usually) the ROC is the right side plane from the right-most pole.[1] Either BAR or dynamic speaker, both types of transducers are categorized as two-port electroacoustic systems, converting electrical energy into acoustic pressure. Other examples of the two-port network can be easily found in our daily lives. Table 2.1 shows some real-life examples of the two-port networks.

Table 2.1: Example of two-port networks

Two-port network system	Examples
electromechanic	motors, bone vibrators
electroacoustic	loud speakers, ear-phones

All one-port postulates we discussed (C1-C5) can also be applied to two-port networks. One strictly two-port postulate is Carlin's last postulate:

[1]If a pole (s_k) is represented as $s_k = \sigma_0 + j\omega_0$, where σ_0 and ω_0 are the real and the imaginary parts of the pole, then the right-most pole of the system has the largest, the most positive σ_0.

C6 Reciprocity (*vs.* non-reciprocity vs. anti-reciprocity): To be a reciprocal network, in terms of conjugate variables described in Table A.1, a generalized force is swapped to a flow across one modality to the other (Eq. 2.16a). In other words, the two transfer impedances (the two off-diagonal components) of the system's impedance matrix must be equal. The anti-reciprocal network swaps the force and the flow, but one variable changes to the opposite direction (Eq. 2.16b). A non-reciprocal network is a network which does not have reciprocal characteristics. Note that the special case of a non-reciprocal networks are the anti-reciprocal network (McMillan, 1946).

$$\begin{bmatrix} \Phi \\ F \end{bmatrix} = \begin{bmatrix} 0 & 1 \\ 1 & 0 \end{bmatrix} \begin{bmatrix} I \\ U \end{bmatrix} \tag{2.16a}$$

$$\begin{bmatrix} \Phi \\ F \end{bmatrix} = \begin{bmatrix} 0 & -1 \\ 1 & 0 \end{bmatrix} \begin{bmatrix} I \\ U \end{bmatrix} \tag{2.16b}$$

$$\begin{bmatrix} \Phi \\ F \end{bmatrix} = \begin{bmatrix} 1 & 0 \\ 0 & 1 \end{bmatrix} \begin{bmatrix} I \\ U \end{bmatrix} \tag{2.16c}$$

There is another important property denoted *reversibility* (Van Valkenburg, 1964), where the diagonal components in a system's impedance matrix are equal (input impedance = output impedance; Eq. 2.16c). In other words, the input force and flow are proportional to the output force and flow, respectively. This postulate is only defined for the two-port network.

For the reader's benefit, the six types of network symmetry are defined, as followed:

1) Reciprocal network: If $z_{12} = z_{21} \Leftrightarrow \Delta_T = 1$ with $C \neq 0$.

2) Non-reciprocal network: all systems that are not reciprocal.

3) Anti-reciprocal network: $-z_{12} = z_{21} \Leftrightarrow \Delta_T = -1$ with $C \neq 0$.

4) Reversible network: $z_{11} = z_{22} \Leftrightarrow A = D$, $C \neq 0$.

5) Reciprocal and reversible network: $z_{11} = z_{12}$ & $z_{21} = z_{22} \Leftrightarrow A = D$ & $\Delta_T = 1$, with $C \neq 0$.

6) Anti-reciprocal and reversible network: $-z_{12} = z_{21}$ & $z_{11} = z_{22} \Leftrightarrow A = D$ & $\Delta_T = -1$, with $C \neq 0$,

where Δ_T is the determinant of the transmission matrix. When $C = 0$ or $z_{21} = 0$, conversion between transmission matrix and impedance matrix is not possible.

Note that all categorized postulates are independent,[2] including the reversibility (Carlin and Giordano, 1964).

2.2.1 Additional postulates to include Brune's impedance

In addition to Carlin's postulates for the one-port network (C1-C5), one should consider Brune's impedance as a highly limited extension of the one-port network properties. Otto Brune synthesized the properties of one-port (or two terminals) PR networks in his Ph.D. thesis at MIT (Brune, 1931). However, the critical limitation of his network theory is that it assumes a quasi-static approximation. This limitation has been addressed by Serwy 2012.

B1 Positive-real (PR): $Z(s) = \Re(\sigma, \omega) + j\Im(\sigma, \omega)$, where $s = \sigma + j\omega$. Then $\Re(\sigma \geq 0) \geq 0$. Note that PR functions (i.e., impedances) are a subset of minimum phase functions. Therefore impedance is a positive-definite (PD) operator. Moreover the order difference between numerator and denominator is ± 1 for PR. This concept is an expanded version of C1-C5.

B2 Quasi-static (QS) (vs. non-quasi-static or what we call the *Einstein causality*): A QS system always assumes that the system size is much smaller than the wave length λ. Only when the QS system is band limited, can it exhibit a finite system delay. The complement concept is Einstein causality, meaning that the pure delay ($\tau = \frac{x}{c}$) depends on a distance (x) where c is the wave speed (sound or light; $\delta(t - x/c)$).

For further explanation of B1, $Z(s)$ is represented as a rational polynomial fraction (pole-zero pairs). It can be factored into first-order terms in s (Van Valkenburg, 1964),

$$Z(s) = \frac{\Pi_{i=1}^{L} K_i(s - n_i)}{\Pi_{k=1}^{N} K_k(s - d_k)} = \frac{|\rho| e^{j\theta_n}}{|r| e^{j\theta_d}} = \left|\frac{\rho}{r}\right| e^{j(\theta_n - \theta_d)}, \tag{2.17}$$

where K_i and K_k are scale factors. The s values for which $Z(s)$ is zero ($s = n_i$) and infinite ($s = d_k$) are called the system's zeros and poles. In the first definition of $Z(s)$ in Eq. 2.17, any poles and zeros that have the same complex location, $n_i = d_k$, (pairwise pole-zero, a.k.a. removable singularities) are canceled. Then, the product of zeros and poles can be represented in polar form (middle definition in Eq. 2.17 with magnitude: ρ, r, and phase: θ_n, θ_d). Finally $Z(s)$ has a reduced form with its magnitude $\frac{\rho}{r}$ and phase $\theta_n - \theta_d$. If a system

[2]It is not an absolute statement. There is an exception to this rule.

satisfies the PR property, then the phase difference $|\theta_n - \theta_d|$ must be less than $\frac{\pi}{2}$. This means $Z(s)$ is always positive in the right half plane. It follows that the difference in order between numerator and denominator cannot be more than ± 1 or $|L-N| \leq 1$ (Van Valkenburg, 1960).

This PR property is closely related to the positive definite (PD) matrix (operator property). For an example, a 2×2 impedance matrix $\mathcal{Z}$ for a two-port network must have,

$$\begin{bmatrix} \mathcal{I}_1 & \mathcal{I}_2 \end{bmatrix} \begin{bmatrix} z_{11} & z_{12} \\ z_{21} & z_{22} \end{bmatrix} \begin{bmatrix} \mathcal{I}_1 \\ \mathcal{I}_2 \end{bmatrix} \geq 0, \quad \forall\, \mathcal{I}_1, \mathcal{I}_2 \tag{2.18}$$

or

$$\mathcal{I}^T \cdot \mathcal{Z}(s) \cdot \mathcal{I} \geq 0, \quad \forall\, \mathcal{I}(\omega). \tag{2.19}$$

Note this generalizes to a $\mathcal{Z}_{2\times 2}$ matrix, for example, $\mathcal{Z}(s)$ and $\mathcal{I}(\omega)$ are 2×2 and 2×1 matrices, respectively, and $\mathcal{I}^T$ is the transpose of $\mathcal{I}$. Since $\mathcal{Z}$ is PR, the matrix version of $\mathcal{Z}$ is a PD operator.

The quasi-static property (B2) is an alternative way to specify C4. The definition of quasi-static is "not having pure delay," that is (τ [s] $= \frac{\Delta_x \text{ [m]}}{c \text{ [m/s]}} = 0$) in a system. An equivalent definition inherently exists in most classical circuit analysis such as KCL and KVL. Especially when we deal with an electromagnetic system, one or both of the time-dependent terms in Maxwell's equation ($\dot{\mathbf{B}}$ and $\dot{\mathbf{D}}$, where a dot represents the first-order time derivative) are zero. This point will be discussed later in Section 2.5.2.

The antithesis of QS is non-QS, or Einstein causality, a delay existing in a system proportional to a distance. The most relevant example is reflectance Γ, defined as

$$\Gamma(s) = \frac{Z(s) - 1}{Z(s) + 1}, \tag{2.20}$$

where $\mathcal{L}^{-1}$ of $Z(s)$ is $z(t) \leftrightarrow Z(s)$, such that $z(t) = 0 \forall t < 0$. Compared to C4, B2 limits the causal boundary to be physical. Assuming we live in a world within the theory of relativity of Einstein, Einstein causality is an appropriate characteristic to define a network when we talk about the causality. All physical networks must obey B2.

Note that B1-B2 can be applied to both one- and two-port networks.

It is worth discussing the difference between static and quasi-static. The static system is not time-varying ($\frac{d}{dt} = 0$). Serwy (2012) describes two types of QS based on the definition of the speed of light, $c = \frac{1}{\sqrt{\mu_0 \epsilon_0}}$; $\epsilon \to 0$ and $\mu \to 0$ to realize $c \to \infty$. However this definition is inadequate since it conflicts with the definition of characteristic impedance ($\sqrt{\mu/\epsilon}$).

The concept of quasi-static still remains vague and needs a better definition. We claim that it is necessary to move beyond quasi-static: one main reason is to handle the case of a

physical system, such as ear canal delay (i.e., the canal impedance needs to be factored into a pure delay and a minimum-phase component, and this means that it will not be a Brune impedance[3] (Robinson and Allen, 2013)). Details of this topic are discussed in Section 2.5.1.

2.3 Generalization of the ABCD matrix using Möbius transformation

In this section, we explain how the Möbius transformation or bilinear transformation is an important generalization of the ABCD transformation. In characterizing the ABCD transformation, a cascading series of ABCD matrices is necessary to simplify the algebra. It is equivalent to the composition of Möbius transformations (Boas, 1987). This is a visual way of describing the ABCD matrix (Fig. 2.2).

Figure 2.2: Möbious strip sculpture at the Beckman Institute, University of Illinois, Urbana-Champaign. A Möbious transformation matrix is presented underneath the sculpture.

The relationship (conversion) between the impedance matrix and the ABCD matrix formula defined in Eq. 2.8 may be found in most electrical engineering texts and is taught in undergraduate classes. The impedance matrix is a generalization of Ohm's law. One side of each equation has a force variable; the other side involves the relation between two flows in the system. The conversion to the ABCD matrix results once the two equations are rewritten in terms of the first port's two variables, force and flow. The derivation is straightforward; however, it is not completely clear why the ABCD cascading method works. One can find the root of this method in the composition of the Möbius transformation.

[3]The impedance at the probe can be fit to a Brune's form, but the ear canal is definitely better modeled as a delay line

Let us start with an example. The general form of a Möbius transformation is defined as a rational function. We define two rational functions $M_{a,b,c,d}(s)$ and $M_{A,B,C,D}(z)$,

$$M_{a,b,c,d}(s) = \frac{as+b}{cs+d}\,, \text{ and } \; M_{A,B,C,D}(z) = \frac{Az+B}{Cz+D} \tag{2.21}$$

where $a, b, c, d, A, B, C,$ and D are any complex numbers satisfying $AD - BC \neq 0$ and $ad - bc \neq 0$. When $ad = bc$ or $AD = BC$, Eqs. 2.21 are not Möbius transformations.

For better visualizing of each Möbius function, four steps of transformation (compositions) are introduced. Taking one of the two formulas in Eq. 2.21, $M_{a,b,c,d}(s)$ can be decomposed into four different functions,

$$M_{a,b,c,d}(s) = M1_{a,b,c,d}(s) \circ M2_{a,b,c,d}(s) \circ M3_{a,b,c,d}(s) \circ M4_{a,b,c,d}(s), \tag{2.22}$$

where

1) $M1_{a,b,c,d}(s)$: $s + \frac{d}{c}$ translation by $\frac{d}{c}$,

2) $M2_{a,b,c,d}(s)$: $\frac{1}{s}$ taking an inverse,

3) $M3_{a,b,c,d}(s)$: $\frac{bc-ad}{c^2}s$ expansion and rotation, and

4) $M4_{a,b,c,d}(s)$: $s + \frac{a}{c}$ translation by $\frac{a}{c}$.

Composing the two functions in Eq. 2.21 leads to the function $Q(z)$,

$$Q(z) = M_{a,b,c,d}(s) \circ M_{A,B,C,D}(z) = \frac{as+b}{cs+d} \circ \frac{Az+B}{Cz+D} = \frac{a\left(\frac{Az+B}{Cz+D}\right)+b}{c\left(\frac{Az+B}{Cz+D}\right)+d}. \tag{2.23}$$

Finally we have

$$Q(z) = \frac{(aA+bC)z + (aB+bD)}{(cA+dC)z + (cB+dD)}. \tag{2.24}$$

Write two 2×2 matrices based on the four coefficients in both $M_{a,b,c,d}(s)$, $M_{A,B,C,D}(z)$ in Eq. 2.21, and cascade the two matrices,

$$\begin{bmatrix} a & b \\ c & d \end{bmatrix} \begin{bmatrix} A & B \\ C & D \end{bmatrix} = \begin{bmatrix} aA+bC & aB+bD \\ cA+dC & cB+dD \end{bmatrix}. \tag{2.25}$$

It is therefore demonstrated that the composition of Möbious transformations (in Eq. 2.24 and Eq. 2.23) is equivalent (i.e., isomorphic) to the cascaded matrix of Eq. 2.25. It also applies to multiple matrix computation. As shown in Eq. 2.23, computational complexity will be increased as the order of the composition is increased. In such a case, the cascading

matrix method is superior over composition. Cascading ABCD matrices in circuit theory is the best example of Möbious composition. When we compose a circuit system, we need many circuit components (e.g., Fig. 1.1). Therefore when analyzing a circuit using the ABCD matrix multiplication method, the algebra becomes trivial.

Example 1

Figure 2.3 depicts a circuit model with a series impedance Z. There are two inputs (Φ_1, I_1) and two outputs (Φ_2, I_2) to form this simple network. A well-known ABCD matrix of a

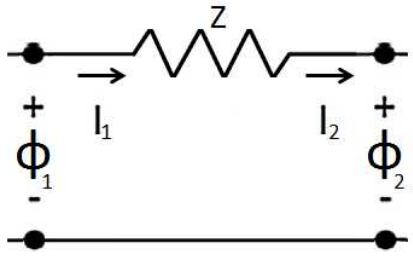

Figure 2.3: A series impedance (Z) representation with inputs (Φ_1, I_1) and outputs (Φ_2, I_2). Note that, in this figure, all currents are defined as going out of the network.

series impedance (Z) is given as

$$\begin{bmatrix} \Phi_1 \\ I_1 \end{bmatrix} = \begin{bmatrix} 1 & Z \\ 0 & 1 \end{bmatrix} \begin{bmatrix} \Phi_2 \\ I_2 \end{bmatrix}, \tag{2.26}$$

where Φ and I are the voltage and the current, which is defined as going out of the network. The subscripts 1 and 2 stand for the input port and the output port, respectively. To form a rational function using this relationship, take a ratio of the first and the second rows in Eq. 2.26 to have input impedance Z_{in} as a function of the output impedance, Z_{out},

$$Z_{in}(Z_{out}) = \frac{\Phi_1}{I_1} = \frac{\Phi_2 + ZI_2}{0 + I_2} = \frac{\Phi_2/I_2 + Z}{0 + 1} = \frac{Z_{out} + Z}{0Z_{out} + 1}, \tag{2.27}$$

where the Eq. 2.27 may be changed by a multiple of the Z_{in} matrix itself. Representing Eq. 2.27 in Möbious composition form,

$$M_{1,Z,0,1}(Z_{out}) = \frac{Z_{out} + Z}{0Z_{out} + 1} \quad : \quad [M] = \begin{bmatrix} 1 & Z \\ 0 & 1 \end{bmatrix}, \tag{2.28}$$

which is identical to the impedance matrix shown in Eq. 2.26. In summary, Eq. 2.26 is the matrix form while Eq. 2.28 is the composition form.

As discussed early in this section, the parameter C (Eq. 2.6) for Eq. 2.27 is zero; therefore $Z_{in}(\infty) = \infty$. Conversion to the impedance matrix is impossible for this case.

Example 2

This theory can be directly applied into any domain-changing relationship such as the conversion between reflectance Γ and impedance Z. The relationship between Γ and Z is

$$\Gamma_{1,-r_0,1,r_0}(Z) = \frac{Z - r_0}{Z + r_0} \quad : \quad [\Gamma] = \begin{bmatrix} 1 & -r_0 \\ 1 & r_0 \end{bmatrix}, \tag{2.29}$$

and its inversion relationship is

$$[\Gamma]^{-1} = Z = \frac{1}{2r_0} \begin{bmatrix} 1 & -r_0 \\ 1 & r_0 \end{bmatrix}, \tag{2.30}$$

where r_0 is surge impedance.

In general we may show this as

$$Z_{A,B,C,D}(s) = \frac{As + B}{Cs + D} \quad : \quad [Z] = \begin{bmatrix} A & B \\ C & D \end{bmatrix}, \tag{2.31}$$

where s is the Laplace frequency. It is standard to use round brackets $Z(s)$ on the composition form and square brackets $[Z]$ on the matrix form. Composing Eq. 2.31 with Eq. 2.29,

$$\Gamma(Z) = \frac{\frac{As+B}{Cs+D} - 1}{\frac{As+B}{Cs+D} + 1} = \frac{(A - C)s + B - D}{(A + C)s + B + D}. \tag{2.32}$$

The coefficients in Eq. 2.32 are equivalently shown from the following matrix multiplication, cascading Eq. 2.31 and Eq. 2.29 with $z_0 = 0$ in Eq. 2.29,

$$\begin{bmatrix} 1 & -1 \\ 1 & 1 \end{bmatrix} \begin{bmatrix} A & B \\ C & D \end{bmatrix} = \begin{bmatrix} A - C & B - D \\ A + C & B + D \end{bmatrix}. \tag{2.33}$$

We have shown an example of the conversion relationship from Z to Γ. Now in Fig. 2.4 we consider an inverted case, representing a relationship from Γ to Z with a simple diagram. We believe that it will give us a better understanding of the composition method behind the algebra.

For the case of a lossless transmission line,

$$\Gamma(s) = e^{-s2L/c} \leftrightarrow \delta(t - 2L/c), \tag{2.34}$$

where L/c represents delay in the transmission line.

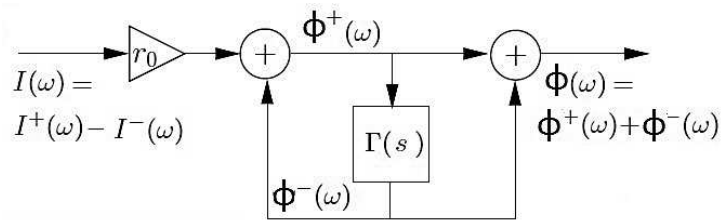

$$\Phi^-(\omega) = r_0\, I^-(\omega) \qquad \Phi^-(\omega) = \Gamma(s)\Phi^+(\omega)$$
$$\Phi^+(\omega) = r_0\, I^+(\omega) \qquad I^-(\omega) = \Gamma(s) I^+(\omega)$$

$$\mathcal{Z}(s) \equiv \frac{\Phi}{I} = \frac{\Phi^+ + \Phi^-}{I^+ - I^-}$$
$$= \frac{\Phi^+}{I^+} \cdot \frac{1+\Gamma(s)}{1-\Gamma(s)} = r_0 \frac{\Gamma(s)+1}{-\Gamma(s)+1}$$

$$Z(\Gamma)_{r_0, r_0, -1, 1} = r_0 \frac{\Gamma+1}{-\Gamma+1} : [Z](\Gamma) = \begin{bmatrix} r_0 & r_0 \\ -1 & 1 \end{bmatrix}(\Gamma)$$

Figure 2.4: Inverted relationship between reflectance (Γ) and the wave impedance (Z) shown in Eq. 2.33, where the conversion is made from Z to Γ. When we convert from Γ to Z, the matrix diagonal elements are swapped compared to Eq. 2.33.

To summarize, multiplying 2×2 matrices is isomorphic to composition of the bilinear transformation.

2.4 Motional impedance (Z_{mot})

Kennelly's first paper on Z_{mot} was published in 1912 (Kennelly and Pierce, 1912); it is referenced frequently in the extensive literature. The main point of this 1912 paper is that the impedance of a telephone receiver (when the diaphragm is free to vibrate) is different from when the diaphragm's motion is damped or blocked (Hunt, 1954). Kennelly defined Z_{mot} as the difference between the two (input) impedances with different boundary conditions, namely $Z_{mot} = Z_{in}|_{free} - Z_{in}|_{blocked}$. Details of the Z_{mot} definition may be found in Section 2.4.1.

Three years later, Kennelly published a second paper about Z_{mot} (Kennelly and Affel, 1915). In this paper, Z_{mot} is characterized in the Z-plane (real and imaginary parts of the impedance, Z) as a circle-shaped impedance passing through the origin of coordinates, with its diameter depressed through a certain angle (depressed compared to the circle in

undamped impedance). Kennelly and Affel addressed these distinctive features in terms of the electrical and mechanical properties of the system. They described Z_{mot} using four constants, A (force factor), m (equivalent mass), r (motional resistance), and k (stiffness constant). There are four unknowns; therefore, four equations are needed to solve for Z_{mot}. Each of the four constants has the following relationships,

1) The resonant angular frequency $\omega_0 = \sqrt{\frac{k}{m}}$.

2) The damping constant $\Delta = \frac{r}{2m}$.

3) The magnitude of the $|Z_{mot}| = \frac{A^2}{r}$.

The missing fourth equation can be supplied by measuring any one of the four constants directly. In practice, what Kennelly actually did was to iterate for the four parameters (assuming one of the constant is known) using the least square method to estimate the Z_{mot} circle diagram. This is related to Eq. 2.31. From the difference between the two Z_{mot} circle diagrams, the last independent equation can be found. The precise procedure may be found in Appendix E and in Ramo et al. (1965).

Kennelly's third paper about Z_{mot} was published in 1919 (Kennelly and Nukiyama, 1919). In this paper, he focused on the power concept of Z_{mot}, and introduced the motional power diagram to better physical understanding. The motional power diagram is drawn based on the mmf (magneto motive force) generated by the vibration of the diaphragm in the permanent magnetic field. The motional power can be regarded as a scaled motional impedance diagram. In their view, power is a better concept for understanding the system, compared to impedance.[4] He explained the motional power circle by means of "active mechanical power (P_m)", which is defined as a difference between electrical power (P_e) and hysteresis power (P_h):

$$P_m = P_e - P_h. \tag{2.35}$$

The mechanical power observed from the electrical side (the motional power circle) is depicted in Fig. 2.5. This image is reproduced from Kennelly and Nukiyama (1919). Based on the definition of P_m in Eq. 2.35, the negative real parts shown in the motional power diagram (Fig. 2.5) can be redefined as purely active mechanical power, looking at the electric part of the system.

Kennelly and Kurokawa published a fourth technical paper in 1921. The objective of this paper is to describe some techniques to measure acoustic impedance, including various constants introduced in his three previous papers. Starting from definition of mechanical

[4] In 1919, impedance had not yet to be defined properly, which finally came about 12 years later in Brune's PhD thesis.

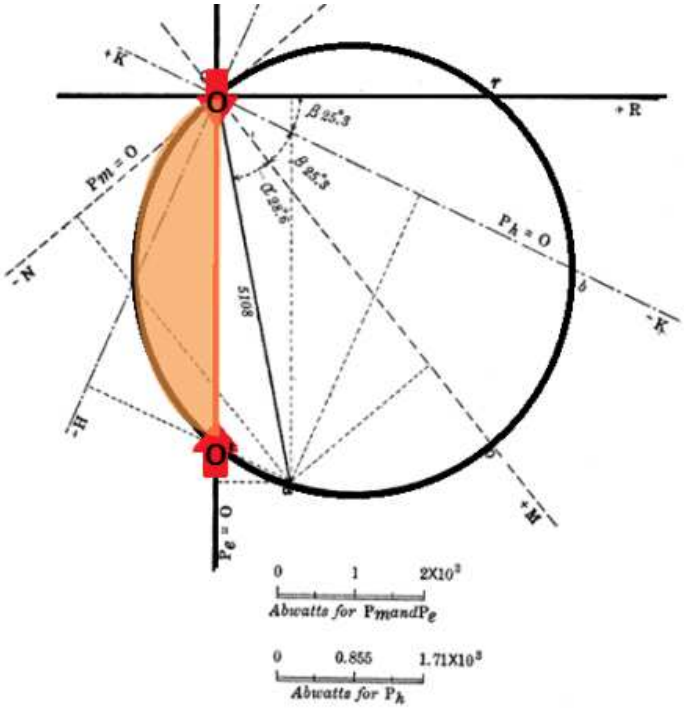

Fig. 27—Motional Power Diagram

Figure 2.5: An example of the motional power diagram introduced by Kennelly and Nukiyama (1919). The x-axis and y-axis show resistive and reactive parts of the motional power, respectively. When the resistance becomes negative (the left shaded part of the red line, O-O', on the circle), power supplied from the electric part of the system no longer exists (It does not provide the mechanical power onto the diaphragm). Therefore (referencing the electrical side) this part of the power is "active mechanical (motional) power". All power in this region is consumed for hysteresis loss when the diaphragm is released (i.e., diaphragm is going back to its original position).

impedance, the authors explain specific ways of measuring the motional impedance, mechanical impedance, and surge impedance. They also introduce a method to calculate the mechanical impedance (z_m) from Z_{mot}

$$z_m = \frac{A^2}{Z_{mot}} \text{ [vector ohm]}, \tag{2.36}$$

where A is a complex constant, representing the force factor. Note that this equation is presented as Equation 16 in the original paper (Kennelly and Kurokawa, 1921). This was before the anti-reciprocal gyrator was invented. Dividing the complex constant A^2 by the measured Z_{mot}, z_m at a single frequency (including the size and the slope) is obtained. Repeating this calculation for several frequency points, the total z_m is determined. An example of z_m is shown in Fig. 2.6, along with its theoretical value. The theoretical impedance for a shorted transmission line (the dashed line in Fig. 2.6) is defined as

$$z_0 \tanh(\beta l), \tag{2.37}$$

where z_0, β are the surge impedance and wavenumber ($\beta = 2\pi/\lambda$, λ is the wavelength), and l is the length of the transmission line.

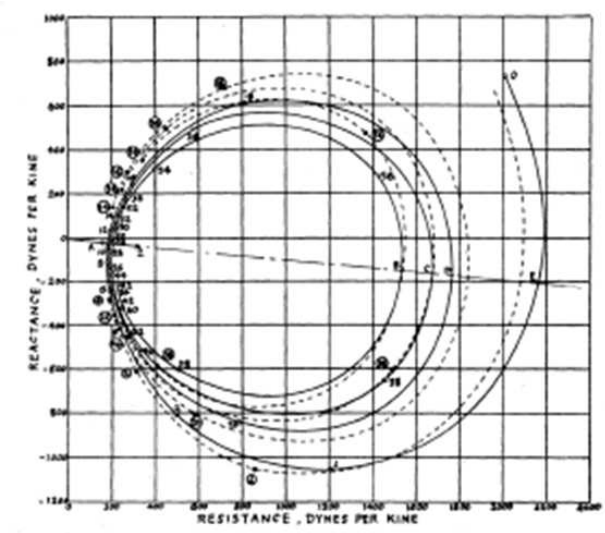

Figure 2.6: The calculated z_m (Eq. 2.36) graph by inverting Z_{mot} and then multiplying by the complex force factor A^2 (Eq. 2.36). Solid curve is obtained by connecting observation values at each frequency point. The dotted line represents the computed (theoretical) values Eq. 2.37. Note that this image is shown as Figure 9 in the original manuscript (Kennelly and Kurokawa, 1921).

Acquiring values to calculate mechanical impedance (z_m, Eq. 2.36) seems somewhat troublesome and inefficient. Historically, this work can be viewed as the first measurement of a mechanical impedance z_m purely from electrical measurements. Four years later Kennelly

published a paper (Kennelly, 1925) specific to this idea based on the preliminary data from the work with Kurokawa(Kennelly and Kurokawa, 1921), for measuring acoustic impedance electrically (Hunt, 1954).

Wegel's Z_{mot} Besides Kennelly, Wegel also considered Z_{mot} in his 1921 paper. This paper is credited by Hunt as the forerunner of Hunt's 1954 two-port matrix representation (Eq. 2.1). Wegel takes account of the general theory of receiver structures using a simple schematic having four coils. As applications, he takes four different specific cases of a receiver: a simple receiver, a receiver with eddy currents in the core, a simple induction-type receiver, and an electrodynamics receiver. One interesting point he mentioned is the effect of the eddy current, which decreases proportional to the square root of the frequency when it flows around the core surface (Wegel, 1921 p.797). However, he did not derive any specific formula for this phenomenon, as it was simply an experimental observation. As a matter of fact, the observation of this phenomenon (the diffusion wave's impedance $\propto \sqrt{\text{frequency}}$) has a long history. To fully appreciate this fact, the observation was related to the eddy current, the current flow from primary magnetic field, and finally analyzed using Maxwell's equation as carefully analyzed by Vanderkooy (1989), leading to the first definition of the semi-inductor with its impedance of $Z_{semi} = K\sqrt{s}$.

Investigation of the circular shape of Z_{mot} In terms of the spolar impedance plane, Z_{mot} is a circle passing through the origin (Kennelly and Affel, 1915). The unusual shape may be explained by the physical nature of the anti-reciprocal electromechanic systems. The left side circuit (1) in Fig. 2.7 describes a (typical) mechanical electromechanic network. The series of a damper, a mass, and a stiffness of the system are represented as circuit components R, L, and C, respectively. The Z_{mot} is defined as a mechanical characteristic observed on the electrical side, therefore simulation of these three main mechanical elements on the electrical side is our main concern.

Two circuits shown in Fig. 2.7 are functionally equivalent, (1) is physically intuitive due to using a gyrator, (2) is a dual version of (1) via the mobility analogy (Firestone, 1938). Figure 2.8 simulates the two circuit cases in Fig. 2.7; the blue line (1) without the gyrator (purely mechanical case) and the red line (2) decoding the gyrator using mobility method to see the mechanical behavior on the electrical input side. The upper and lower plots in left plane represent the magnitude and phase of input impedance and the right polar plot shows the real and imaginary parts of the impedance.

In Fig. 2.8, the red circle on the polar plot (Z_{dual}) shows Z_{mot}, which is the dual of Z_M

namely,

$$Z_M = R + \frac{1}{sC} + sL\Big|_{R,L,C=1} = 1 + \frac{1}{j\omega} + j\omega = \begin{cases} \infty & \omega \to \infty \\ 1 & \omega \to 1 \\ -\infty & \omega \to -\infty \end{cases}, \tag{2.38}$$

$$Z_{dual} = \frac{1}{R}||sC||\frac{1}{sL}\Big|_{R,L,C=1} = \frac{1}{1 + j\omega + \frac{1}{j\omega}} = \begin{cases} 0 & \omega \to 0 \\ 1 & \omega \to 1 \\ 0 & \omega \to \infty \end{cases}. \tag{2.39}$$

The reason we have a circle shape of Z_{mot} is because we are observing mechanical behavior across the gyrator. Note that F_c stands for the transition frequency between C (low-frequency) and L (high-frequency) for both original and dual of magnitude and phase plots. In polar plots, when $\Im Z \to +\infty$, Z is dominated by L and in case of $\Im Z \to -\infty$, Z depends on C.

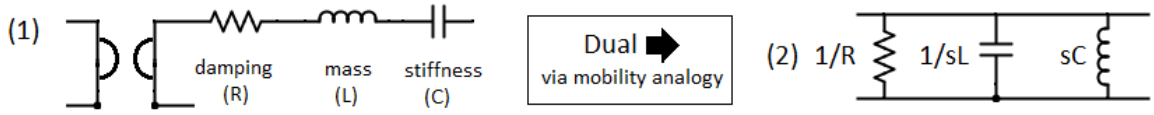

Figure 2.7: The corresponding circuits for Fig. 2.8 (1) and (2), before (1) and after (2) mobility networking. Due to the gyrator, the mechanical components becomes dual when they are seen on the electrical side of the network. As investigated in Fig. 2.8, this makes the shape of the Z_{mot} circle.

One may suggest a refined model of Z_{mot} based on Fig. 2.7. The only difference between the real experimental data of Z_{mot} and the simulation in Fig. 2.8 is the angular rotation (clockwise direction) of the circle pivoted at the origin of the circle, which will introduce the negative real part in Z_{mot}. One way to realize this model is to add a phase delay in the system ($e^{-j\phi(\omega)}$) along with mechanical circuits.

Rotating the circle toward the negative real part is related to any shunt loss in the electrical part of the system. The details are discussed in Section 2.4.3.

2.4.1 Definition of Z_{mot}

Physically, Z_{mot} can be interpreted as the impedance of the mechanical side of the system as seen from the electrical input. Z_{mot} was first defined(Kennelly and Pierce, 1912) by taking a difference between the mechanical open and the short circuit conditions, of electrical input impedance.

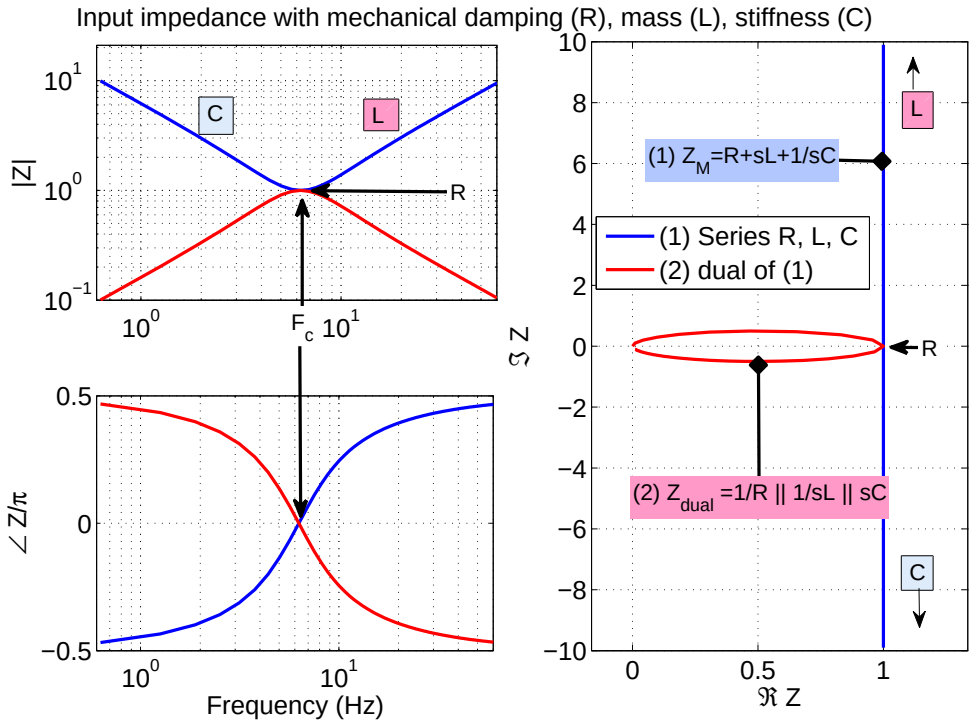

Figure 2.8: This figure explains the circular shape of Z_{mot} where the motion of the mechanical behavior (i.e., damping (loss), mass, and stiffness) projected to the electrical side defines Z_{mot}. When the mechanical behavior is seen on the electrical input side, due to the gyrator, the series mechanical network becomes a dual network based on the mobility analogy. The blue line shows input impedance based on the series relationship ((1) in Fig. 2.7 without considering the gyrator) while the red line represents the dual. The upper-left and lower-left plots show magnitude and phase of impedance and the right plot (polar plot) shows real and imaginary parts of the impedance. The red circle on the polar plot justifies the circular shape of Z_{mot}. F_c stands for the transition frequency between C (low-frequency) and L (high-frequency) for both original and dual of magnitude and phase plots. In polar plots, if $\Im Z \to +\infty$, Z is dominated by L, and in case of $\Im Z \to -\infty$, Z depends on C. Note that this figure only discusses the shape of typical Z_{mot}, not its negative real parts. For simplification, values for L, R, and C, are 1 in this simulation.

Starting from Hunt's impedance matrix (Eq. 2.1), we see that

$$\Phi = Z_e I + T_{em} U, \tag{2.40a}$$

$$F = T_{me} I + Z_m U. \tag{2.40b}$$

When the force F is zero, i.e., "shorting out" the mechanical side, the electrical input impedance is

$$\frac{\Phi}{I} = Z_e + \frac{T_{em} U}{I}, \tag{2.41a}$$

and

$$\frac{U}{I} = -\frac{T_{me}}{Z_m}. \tag{2.41b}$$

The shorted electrical input impedance is

$$Z_{in}|_{F=0} = \frac{\Phi}{I}|_{F=0} = Z_e - \frac{T_{em} T_{me}}{Z_m} = Z_e + Z_{mot}. \tag{2.42}$$

Thus Z_{mot} may be interpreted as the difference between the two mechanical boundary conditions on the electrical impedance (Z_{in})[5]:

1) Z_{in} with freely oscillating (vibrating) mechanical side ($F = 0$: short circuit condition, Eq. 2.42).

2) $Z_{in} = Z_e$ when the mechanical system is not allowed to move ($U = 0$: open circuit condition, Eq. 2.2):

$$\boxed{Z_{mot} = Z_{in}|_{F=0} - Z_{in}|_{U=0}}. \tag{2.43}$$

Z_{mot} definition using Hunt parameters For the computational benefits, we can also define Z_{mot} from the ABCD matrix parameters introduced in Eq. 2.6,

$$Z_{mot} = \frac{\Phi}{I}|_{F=0} - \frac{\Phi}{I}|_{U=0} = \frac{B}{D} - \frac{A}{C} = -\frac{\Delta_T}{DC} = \frac{1}{DC}, \tag{2.44}$$

where A, B, C, D are the transmission matrix parameters described in Eq. 2.6. Note that the determinant of the transmission matrix (Δ_T) for an anti-reciprocal network is always -1.

To satisfy the positive real (PR) property of Brune's impedance (Brune, 1931),

$$\Re Z(s) \geq 0. \tag{2.45}$$

[5]The electrical conditions "open" and "short" are equivalent to the mechanical terms "blocked" and "free", respectively. Electrically "open" means no current, while "blocked" means no velocity.

In Eq. 2.43, it is obvious the two individual terms $Z_{in}|_{F=0}$ and $Z_{in}|_{U=0}$ are PR functions as they are physical, real impedances. A sum or product of two PR functions has to be PR, but a difference, which is Z_{mot}, will not be a PR function when $\Re Z_{in}|_{U=0} > \Re Z_{in}|_{F=0}$. Thus Z_{mot} is not a physically realizable impedance. This is because it is a transfer impedance, not a driving point impedance.

To be more detailed about the problem, Eq. 2.43 may be written as

$$\boxed{Z_{mot} = -\frac{T_{em}T_{me}}{Z_m} = -T_{em}T_{me}Y_m}, \tag{2.46}$$

where $Y_m = \frac{1}{Z_m}$ is mechanical admittance, which is PR. Therefore the answer to our question is reduced to investigation of the two transfer impedances' product $T_{em}T_{me}$. According to Hunt, $T_{em} = B_0 l$, which is real and positive. We know that where $T_{em} = T_{me}$ the system is reciprocal and when $T_{em} = -T_{me}$, the system is anti-reciprocal.

The question here is, if Z_{mot} is PR. If the transfer impedances are real, then Z_{mot} must be PR. However, if they are complex, then Z_{mot} could have negative real parts (negative resistance). It has been observed (e.g., Fig. 2.5), that the motional power has negative real parts.

2.4.2 Z_{mot} interpretation with Eq. 2.46

If we define Z_{mot} using Eq. 2.46 (with Eq. 2.3, Eq. 2.4, and 2.5), Z_{mot} can be reinterpreted as

$$Z_{mot} = -\frac{\Phi_{I=0}}{U_{I=0}}\frac{F_{U=0}}{I_{U=0}}\frac{U_{I=0}}{F_{I=0}}, \tag{2.47}$$

where $U_{I=0}$ terms are in both T_{em} and Z_m canceled out. This definition is interpreted based on the system's signals, is quite different from Kennelly's experimental definition shown in Eq. 2.43. So the remaining four terms represent Z_{mot}, which is

$$Z_{mot} = -\frac{\Phi_{I=0}}{I_{U=0}}\frac{F_{U=0}}{F_{I=0}}. \tag{2.48}$$

Lorenz force ($\mathbf{F_L}$) is

$$\mathbf{F_L} = q(\mathbf{E} + \mathbf{U} \times \mathbf{B}), \tag{2.49}$$

where q, $\mathbf{E}$, $\mathbf{U}$, and $\mathbf{B}$ represent a point charge, electric field, particle velocity, and magnetic field respectively. From Eq. 2.49 one can infer the two terms $F_{U=0}$, $F_{I=0}$ in Eq. 2.48 are $q\mathbf{E}$,

and $q\mathbf{U} \times \mathbf{B}$ (or $q\mu\mathbf{U} \times \mathbf{H}$, $\mathbf{B} = \mu\mathbf{H}$).[6]

Also one may view $\Phi_{I=0}$ in Eq. 2.48 is the Thevenin voltage (Φ_{Th}) considering only the electrical side of the network (one-port system's open circuit voltage). And $I_{U=0}$ is the electrical side's Norton current (I_{No}), as the U across the gyrator becomes Φ; therefore the $U = 0$ is equivalent to $\Phi = 0$, the shorted condition. The ratio of the Thevenin voltage and the Norton current is the Thevenin electrical impedance (Z_{Th}) representing the electrical side of the network ($\frac{\Phi_{Th}}{I_{No}} = Z_{Th}$). Recall and compare Z_{Th} to Z_e from Eq. 2.2, the open circuit electrical impedance.

To sum up: Eq. 2.48 can be rewritten as (scalars in frequency domain)

$$Z_{mot} = -\frac{\Phi_{I=0}}{I_{U=0}}\frac{F_{U=0}}{F_{I=0}} = -\frac{\Phi_{Th}}{I_{No}}\frac{q\underline{\mathrm{E}}}{qU\underline{\mathrm{B}}}, \tag{2.50}$$

where $\underline{\mathrm{B}}$, $\underline{\mathrm{E}}$ represents scalar magnetic flux density and electric field in frequency domain respectively.

Finally we have

$$Z_{mot} = -Z_{Th}\frac{q\underline{\mathrm{E}}}{qU\underline{\mathrm{B}}} = -Z_{Th}\frac{\underline{\mathrm{E}}}{\mu U\underline{\mathrm{H}}}, \tag{2.51}$$

where U, $\underline{\mathrm{H}}$ are scalars in the frequency domain.

From Eq. 2.51, we can consider the motional impedance as affected by the electrical impedance (Z_{Th}), as well as the mechanical velocity (U).

The semi-inductor (related to the magnetic diffusion wave) elaborated on Eq. 2.51 is part of Z_{mot}, causing the negative real parts. When the wave is diffusive, the diffusion time constant (delay) can be characterized by the velocity $\mathbf{U}$. Vanderkooy (1989 p.127) states, "physically, for an applied voltage step (i.e., $\underline{\mathrm{E}}$ in Eq. 2.51), the coil will try to create a magnetic field [i.e., $\underline{\mathrm{H}}$ in Eq. 2.51] which takes a while to diffuse into the iron. Hence there will be no back emf for the first instant, and the current waveform will rise sharply at the leading edge." The words "takes a while," may be interpreted as the delay resulting from the velocity $\mathbf{U}$. Thus the voltage lags behind the current. When $U = 0$, there is no back emf. Note that $\Phi = -B_0 l U$ is the anti-reciprocal equation of the gyrator. Detailed discussion may be found in Section 2.5.3, Eq. 2.81.

When the velocity U is zero, there is no magnetic force ($q\mathbf{U} \times \mathbf{B} = q\mu\mathbf{U} \times \mathbf{H} = 0$ in Eq. 2.49). Because the magnetic force is defined, when, and only when, a charge is moving. However, the electric force ($q\mathbf{E} = 0$ in Eq. 2.49) exists with a stationary charge q (charge is not moving, zero velocity). Therefore the denominator in Eq. 2.51 lags behind the numerator,

[6]The current $I = \int \mathbf{J} \cdot \mathbf{dS}$. Based on Eq. 2.49, $\mathbf{J}$ can be defined in two different ways, $\mathbf{J}_e = \sigma\mathbf{E}$ and $\mathbf{J}_m = q\mathbf{U}$. The zero current specified in $F_{I=0}$ is relevant to $\mathbf{J}_e = 0$, as the condition of U is still unspecified; therefore $F_{I=0}$ indicates the magnetostatic force, $q\mathbf{U} \times \mathbf{B}$.

and this phase shift can make a part of Z_{mot}'s real parts negative.

2.4.3 Z_{mot} interpretation with Eq. 2.43

In this section, we search for a realizable (simple) circuit such that Z_{mot} has a negative real part. Figure 2.9 demonstrates a case where a difference of two input impedances (Z_{in} with different boundary conditions) goes negative.

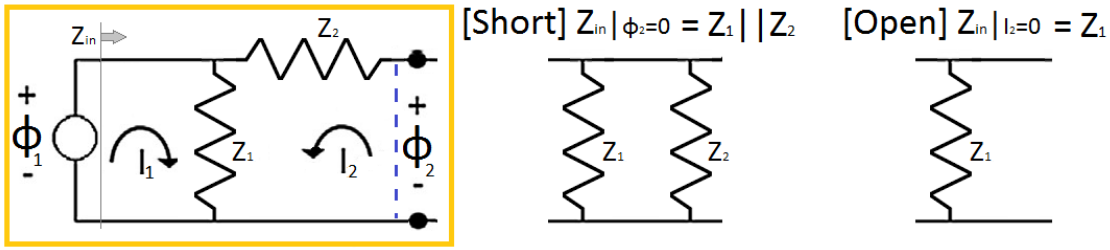

Figure 2.9: Demonstration of Z_{mot}'s negative real part using a simple circuit example

For example, taking $Z_1 = Z_2 = 100$ [Ω]. Based on the definition of Z_{mot} (Eq. 2.43), subtracting the open circuit impedance from the short circuit impedance results in -50 [Ω] ($Z_{in}|_{\Phi_2=0} - Z_{in}|_{I_2=0} = Z_1||Z_2 - Z_1 = 50$ [Ω] -100 [Ω]). This simplest example tells us a lot about the nature of Z_{mot}, as well as modeling the electromechanic system.

Let us consider a real example, an electromechanic system. If there is no SHUNT resistance (i.e., Z_1) in a system, Z_{mot} cannot have the negative real part, as may be seen from Fig. 2.9. The physical meaning of the shunt is this: any current through the shunted component cannot be seen from the other components. The only physical place for this (shunt component) loss is in the eddy current, the diffusing current into the magnetic core. It has been shown experimentally since Kennelly and Pierce (1912), that Z_{mot} has negative real parts. This fact supports the view that a shunt loss in the electrical side of the system must contribute to this loss (semi-inductor) when modeling the system (Kim and Allen, 2013).

In the results (Section 4.3), we study Z_{mot} from the physically based, simplified electromechanic system. The real part of Z_{mot} (Eq. 2.43, Eq. 2.46) from the suggested two-port network is the target of our investigation. Also in Appendix D, we reconsider the Z_{mot} formula based on each parameter's spatial relationship.

2.5 Hidden, quasi-static assumptions in classic circuit theories

We revisit classic theories related to the anti-reciprocal circuit networks, such as KCL, KVL, the gyrator, and the semi-inductor. The purpose is to clarify quasi-static limitations in each well-known formula with derivations starting with Maxwell's equations.

2.5.1 Arguments about quasi-static approximation

The objective of this section is to devise another working definition of the quasi-static assumption. Starting from a physical example, such as the human ear, we claim that the key feature of the QS approximation is the absence of accuracy to describe a pure delay. To deal with this pure delay, one must use the reflectance Γ.

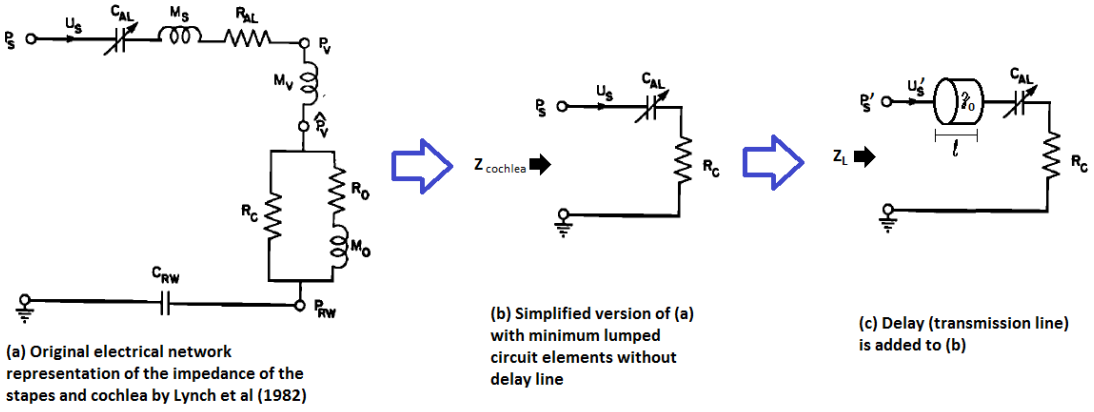

Figure 2.10: Electrical lumped circuit representations of the cochlea (adapted from Lynch et al. (1982)). (a) and (b) employ the quasi-static assumption where (b) is a simplified version of (a). A transmission line (length l and characteristic resistance r_0) is used in (c), which introduces the pure delay $\tau = l/c$ forcing Z_L to be non-quasi-static.

Figure 2.10 represents the acoustic impedance of the human ear in terms of electrical elements. Figure 2.10(a) is the network representations of the impedance of the stapes and cochlea (Lynch et al., 1982). In Fig. 2.10(b), we simplified this original model by considering only the significant components, the cochlear resistance R_c and nonlinear stiffness of the annular ligament C_{AL}. For this simplified version, the cochlear impedance is

$$Z_{cochlea} = R_C + \frac{1}{sC_{AL}}. \tag{2.52}$$

Note that both Fig. 2.10(a) and Fig. 2.10(b) use lumped (Brune's) circuit elements constituting a QS approximation, having a band-limited system delay, not a pure delay.

To include the effect of the ear canal and ear drum delay (that is a pure delay) (Puria and Allen, 1998), a transmission line (i.e., ear canal) is added, as shown in Fig. 2.10(c), with two extra parameters, length l and characteristic impedance $r_0 = \frac{\rho c}{A}$. Note that ρ, c, and A are the air density, speed of sound, and area of ear canal, respectively. When $l \to 0$, the reflectance of this network is

$$\Gamma_0 = \frac{Z_{cochlea} - r_0}{Z_{cochlea} + r_0} = \frac{Z_0 - 1}{Z_0 + 1}, \tag{2.53}$$

where $Z_0 = Z_{cochlea}/r_0 = \frac{R_c}{r_0} + \frac{1}{sC_{AL}r_0}$ is the normalized cochlear input impedance. Then reflectance at the measurement location L (Γ_L) is

$$\Gamma_L = \Gamma_0 e^{-s\tau} = \Gamma_0 e^{-j\omega 2L/c}, \tag{2.54}$$

where $s = \sigma + j\omega$ is the Laplace frequency and $2L/c$ is the pure delay, τ. Thus, the impedance at the measured point L becomes

$$Z_L = r_0 \frac{1 + \Gamma_L}{1 - \Gamma_L}. \tag{2.55}$$

This model has been verified many times (Lynch et al., 1982; Puria and Allen, 1998; Parent and Allen, 2010)

The final impedance does not obey the QS assumption (i.e., it is non-QS) due to the delay τ. It would require an infinite number of poles and zeros to form a QS approximation of this model, due to the delay. Note that the difference between Eq. 2.52 and Eq. 2.55 is in the delay $\tau = 2L/c$.

The simulation comparison between Eq. 2.52 (QS) and Eq. 2.55 (non-QS) is shown in Fig. 2.11. The very simple distinction between non-QS and QS is the number of poles and zeros. In the case of QS ($Z_{cochlea}$, red line), there is 1 pole and 1 zero, while in the non-QS case (Z_L, blue line), the system has an infinite number of poles and zeros.

Next, we will show how this example is equivalent to the traditional quasi-static description, namely, the low-frequency or long-wave approximations.

Quasi-static in electromanetism

The origin of QS approximation is not clear. However, the QS assumption has been widely used in classic circuit analysis, such as Kirchhoff's circuit laws (Kirchhoffs voltage and current laws). Efforts to search for the beginning of the QS in history can be found in Appendix A.

In 1865, James Clerk Maxwell completed his full mathematical description of electromag-

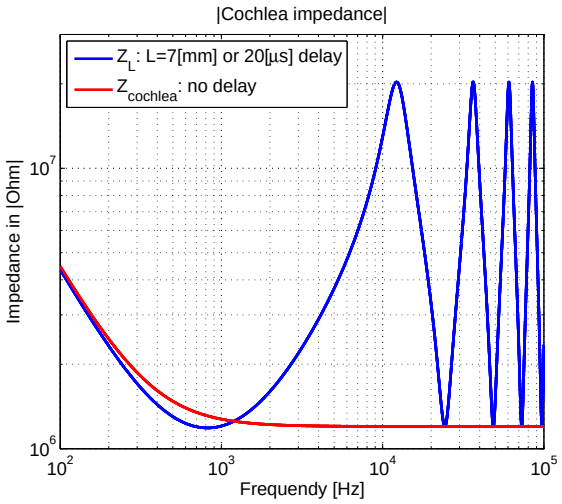

Figure 2.11: Input impedance simulation based on Fig. 2.10. Values for the simulation are as follows: Cochlea resistance $R_c = 1.2 \times 10^6$ [dyn-s/cm^5], stiffness of the annular ligament $C_{al} = 0.37 \times 10^{-9}$ [cm^5/dyn], air density $\rho = 1.14$ [kg/m^3], speed of sound in room temperature $c = 340$ [m/s], area of ear canal $A = r^2\pi$ [m^2] with $r = 0.5$ [cm], and length of ear canal $L = 0.7$ [cm].

netic fields using Michael Faraday's theory,[7]

$$\nabla \cdot \mathbf{D} = \rho \tag{2.56a}$$

$$\nabla \cdot \mathbf{B} = 0 \tag{2.56b}$$

$$\nabla \times \mathbf{E} = -\frac{\partial \mathbf{B}}{\partial t} \tag{2.56c}$$

$$\nabla \times \mathbf{H} = \mathbf{J} + \frac{\partial \mathbf{D}}{\partial t}. \tag{2.56d}$$

Regardless of the appreciation for the QS theorem in Maxwell's time, the concept of QS can be applied to Eq. 2.56 by disregarding either the magnetic induction $\dot{\mathbf{B}}$ (electroquasi-static, EQS) or the electric displacement current $\dot{\mathbf{D}}$ (magneto-quasi-static, MQS, Woodson and Melcher (1968)). With either of those terms removed, there can be no delay, since wave equation does not exist.

In EQS, $\mathbf{E}$ is irrotational since $\nabla \times \mathbf{E} = -\frac{\partial \mathbf{B}}{\partial t} \approx 0$ and $\nabla \cdot \mathbf{D} = \nabla \cdot \epsilon_0 \mathbf{E} = \rho$. Therefore, the curl and divergence of $\mathbf{E}$ specify the charge density ρ. In the case of MQS, $\mathbf{H}$ is rotational (solenoidal) as the divergence of $\mathbf{H}$ is zero ($\nabla \cdot \mu_0 \mathbf{H} = 0$) and $\nabla \times \mathbf{H} = \mathbf{J} + \frac{\partial \mathbf{D}}{\partial t} \approx \mathbf{J}$. Once the current density $\mathbf{J}$ is known, the curl and divergence of $\mathbf{H}$ can be solved in MQS.

[7]The original Maxwell's equations were written in 20 equations with 20 variables using quaternion. It was Oliver Heaviside who reformulated them into four vector equations having 4 variables by using curl and divergence vector operators

To illustrate this, one can imagine a source distribution in each case (EQS with ρ or MQS with $\mathbf{J}$). The solution for these equations ignores the delay between the source and measurement points (i.e., functionally, $c \to \infty$). Thus, each field (EQS with $\mathbf{E}$ or MQS with $\mathbf{H}$) at a certain instant will be governed by its source, ρ or $\mathbf{J}$.

One interesting comparison is that in both the EQS and MQS situations, similar to Kirchhoff's circuit laws, the time-derivative terms are not considered. EQS ignores the $\dot{\mathbf{B}}$ term (KVL) and MQS ignores the $\dot{\mathbf{D}}$ (KCL). Sommerfeld (1964) explained this as "neglecting retardation of fields."

However, the QS definition used for MQS and EQS does not mean setting $\frac{\partial}{\partial t} \to 0$. For instance, impedance of lumped circuit elements (i.e., capacitors or inductors) cannot be defined if $\frac{\partial}{\partial t} \to 0$. Such elements are also known as the QS Brune's impedance (Brune, 1931; Van Valkenburg, 1960, 1964). Therefore, it is critical to search for a precise way to define QS systems.

Quasi-static descriptions

The QS assumption is loosely defined via the long wave approximation

$$kl \ll 1, \tag{2.57}$$

where $k = \frac{2\pi}{\lambda} = \frac{2\pi f}{c}$ is the wave number (f is the frequency and c is the speed of sound or light) and l is the circuit dimension (Sommerfeld, 1964).

This QS description (Eq. 2.57) involves inequalities (i.e., $\gg$, or $\ll$ operator), which makes it confusing to specify each system's QS status. Moreover, when we deal with a physical system, such as the middle ear or a loudspeaker, it becomes even more difficult to properly characterize the QS system because of the relatively slow speed of sound. A more precise definition for QS is not based on inequalities. We shall deal with the proper definition depending on the delay. (The QS systems have no internal delay).

Transmission line and a pure delay

Ohm's law suggested in 1781 represents the ratio of the voltage over the current as an impedance.[8] The now classical definition of QS impedance was first stated by Brune (1931). He characterized a *point impedance* (Eq. 2.57) as a positive-real (PR) quantity (positive-definite operator in matrix version), meaning that an impedance cannot have a negative

[8] At that time, the theory of impedance was applied only to resistance. It was Arthur Edwin Kennelly in 1893 who first suggested using the impedance concept in AC circuits.

resistance as discussed in Section 2.2.1 (postulate B1), which is proved by Van Valkenburg (1960, 1964).

Brune's impedance is consistently studied with KCL and KVL under the QS condition because it assumes no delay ($\tau = 0$) in the system (Fig. 2.10 (a), (b)). For instance, wire delay in the system is ignored. A Brune impedance network is represented using lumped circuit elements such as resistors, inductors, and capacitors, but not delay. All Brune's impedances are minimum phase (MP), because every PR function must be MP. Thus a Brune impedance is QS, PR, and MP. We shall see that the more general wave impedance is PR but not QS (Section 2.2).

A transmission line is a natural element to represent delay. Under the QS assumption, we assume no delay (i.e., no transmission line). A transmission line is a two-port network, which can be interpreted as the physical cable connecting the circuit components. As shown in Fig. 2.10, a transmission line is required for physical modeling of the middle ear and electroacoustic transducers, especially where a delay plays a significant role in understanding the system (Kim and Allen, 2013; Parent and Allen, 2010). The transmission line becomes critical when the signal's wavelength is similar to or less than l. A delay (τ) is related to this l, defined as $\tau = l/c$, where c is the speed of sound or light. Note that any system exhibiting modes requires a delay.

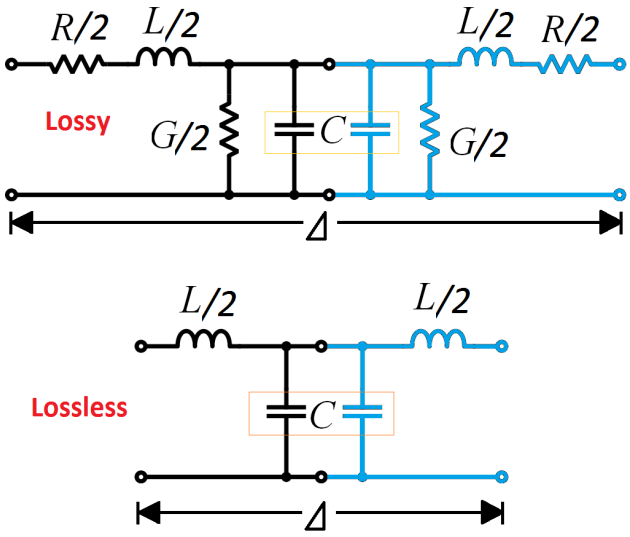

Figure 2.12: An infinitesimal unit of a transmission line (in the limit as $\Delta \to 0$) having primary line constants, L (series inductance or mass per unit length [H/m]), R (series resistance per unit length [Ω/m]), C (shunt capacitance or compliance per unit length [F/m]), and G (shunt conductance per unit length [S/m]). The upper figure represents a loss case while the lower figure is lossless case. Transmission segments are mirrored (shown in blue) to represent reversible transmission lines. By taking $\Delta \to \infty$, this goes from a QS to a true transmission line having a delay.

A low-frequency approximation of a transmission line, using lumped elements, is effectively a Brune approximation satisfying PR (postulate B1 in Section 2.2.1). A popular and simple loss-transmission line approximation uses four elements: L (series inductance per unit length), R (DC resistance per unit length), C (shunt capacitance between the two conductors per unit length), and G (shunt conductance per unit length). In the lossless case, R and G can be ignored.[9] The remaining circuit elements, L and C, represent an elementary unit of the lossless Brune (QS) transmission line. Usually, infinite numbers of these units are cascaded when defining a transmission line. In terms of the transmission line, per-length parameters (divided by the line length Δ), characteristic impedance r_0, and propagation constant κ are computed as

$$r_0 = \sqrt{\frac{\mathcal{Z}}{\mathcal{Y}}},\ \kappa = \sqrt{\mathcal{Z}\mathcal{Y}}, \tag{2.58}$$

where $\mathcal{Z}|_{\Delta\to 0} = R + sL$, $\mathcal{Y}_{\Delta\to 0} = G + sC$, and $s = j\omega$. Note that $\mathcal{Z}$ and $\mathcal{Y}$ are function of s (inverse Laplace transform exists, causal, analytic functions). In the lossless case $r_0 = \frac{L}{C}$, $\kappa = s\sqrt{LC}$. As shown in Fig. 2.12, the QS input impedance is

$$Z_{in,QS} = s(L/2) + \frac{1}{sC}\bigg|_{@low freq} \approx \frac{1}{sC}, \tag{2.59}$$

.

However, the model for a true transmission line having delay, such as a coaxial cable, will differ from this QS transmission line segment (Eq. 2.59). Cascading an infinite number of AS transmission line units and using Eq. 2.58, the input impedance of the transmission line becomes

$$Z_{in} = \frac{\Phi}{I}. \tag{2.60}$$

The voltage Φ (in frequency domain) and current I are composed with outbound $(+)$ and inbound $(-)$ waves as

$$\Phi(x,\omega) = \Phi^+ e^{-\kappa x} + \Phi^- e^{+\kappa x}, \tag{2.61}$$

$$I(x,\omega) = \frac{1}{r_0}(\Phi^+ e^{-\kappa x} - \Phi^- e^{+\kappa x}). \tag{2.62}$$

Note that waves travel between $x = 0$ and $x = l$ based on each direction (the $\pm$ signs).

When we short the transmission line ($\Phi = 0$ or $Z_L = 0$),

$$Z_{in,short}(x) = r_0 \tanh(\kappa x), \tag{2.63}$$

[9]This transmission line model was created by Oliver Heaviside based on Maxwell's equations.

and if it is opened ($I = 0$ or $Z_L = \infty$),

$$Z_{in,open}(x) = r_0 \coth(\kappa x). \tag{2.64}$$

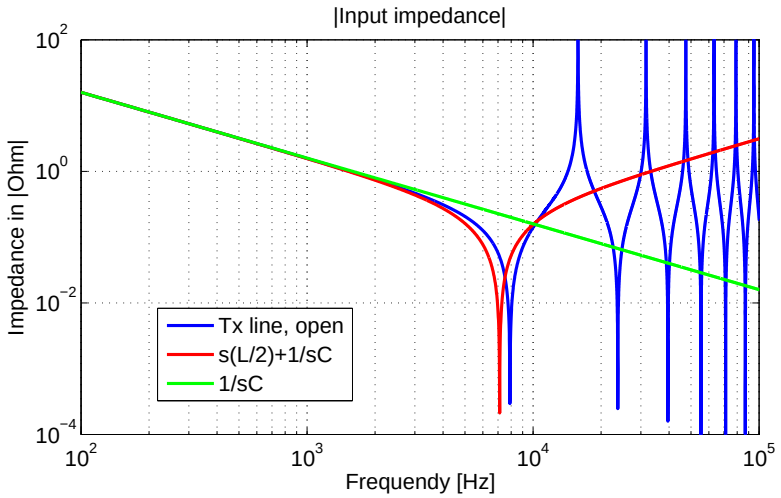

Figure 2.13: Simulation of transmission line input impedance from Eq. 2.59 and 2.63. Values for this specific example are $L = 1e-5$ [H/m], $C = 1e-4$ [F/m].

Input impedance (magnitude) simulation results based on Eq. 2.59 and 2.64 are shown in Fig. 2.13. In this figure,

1) Blue line: Infinite numbers of poles and zeros exist with the exact transmission line formula (Eq. 2.64). These poles and zeros (shown in impedance domain) come from delay (standing waves) based on the length of the line.[10]

2) Red line: Number of poles and zeros is limited. There is one zero and one pole in this approximation. Compared to the blue line, this approximation works out to 2000 [Hz].

3) Green line: One pole at the origin, and no zero is found. This approximation works under 2000 [Hz].

There is a finite number of poles and zeros in the QS (lumped circuit) approximation (red and green), while poles and zeros are infinite for the transmission line model (blue).

If a system is QS (having Brune-type impedance), a finite number of poles and zeros exists. If it is not QS (non-QS, having a pure delay), then the number of poles and zeros is infinite.

[10] $Z = \frac{1+\Gamma}{1-\Gamma}$, where the reflectance $\Gamma = e^{-s\frac{eL}{c}}$. When $\Gamma = \pm 1$, poles and zeros appear in impedance domain (magnitude), respectively. Note that L, c stand for the length of the line and speed of sound and the reflection of the wave relates to the standing wave.

It follows that any system having a pure delay will have infinite numbers of modes without any exception. This is especially applicable for acoustical and mechanical systems because of the relatively slow speed of sound compared to the speed of light.

Reinterpretation of quasi-static

Signals (usually in wave form) and systems are distinguished in terms of causality. Signals are defined over all time support, $|t| \leq \pm\infty$, whereas in systems, the support is restricted to $t \geq 0$. The forwarding waves are typically reflected back if the network has a finite length. A traveling time difference between the forward and backward waves represents the group delay $\tau(\omega)$. Regardless of the speed of the wave, there is a system delay given a finite system length l.

The QS approximation is a classic tool used to simulate and analyze electrical systems, assuming $\lambda \gg l$. However, this assumption does not always describe the physical reality. Critical examples include electroacoustic networks, where the system's speed transits from the speed of light to the speed of sound. The ED7045 receiver (Knowles balanced armature receiver) is a $4.29 \times 6.5 \times 3$ [mm]. Considering the frequency range of human hearing (20 [Hz] to 20 [kHz]) with the speed of sound (345 [m/s]), the wave length λ calculated at 20 [kHz] is 17 [mm], which is compatible with the width of the receiver ($l = 6.5$ [mm]). It does not, however, satisfy the rule of thumb for $\lambda \gg l$; the calculated λ is less than 10 times that of l.[11] Also, acoustic networks having a fairly slow system speed compared to their frequency regions of interest are another example, such as the speed of sound on the eardrum relative to the speed of sound in air.

Assume a train (1 mile in length, a very long train) has a speed of 60 mph and someone slowly moves inside the train at a speed of 1 mph for at least an hour. The QS approximation may be applied in this scene; an observer outside the train may think that the train and he are in the same border until he hits the end of the train. The observer feels that the speed is 60 mph for at least an hour. When he hits the train wall, the QS approximation breaks. After one hour (if he breaks out of the train wall), he and the train will be separated. The outside observer no longer thinks that he and the train are in the same location or have the same speed. The circumstance becomes non-QS when the two subjects are physically separated. Then, what is the meaning of relating the QS to delay? It means that the outside observer can discern his exact location inside the train at each time frame when he is moving around the train. This interpretation does not depend on the position of the person, whether

[11] In the classical way, to apply QS in a system, $ka \ll 1$ must satisfy. $ka = \frac{2\pi a}{\lambda} = \frac{2\pi 6.5}{17} \approx 2$ for our specific case, which does not satisfy the condition.

inside or outside the train. The previous portion on the train is similar to the phase across the object where the phase is due to the delay (i.e., 90° is $\lambda/4$ while 180° is $\lambda/2$, half way down the train).

In summary, we propose a more fundamental way to characterize the QS approximation. In describing a system as QS or non-QS, delay is the critical parameter as it determines the pole-zero frequency density. This definition does not violate the traditional descriptions of QS such as long-wave approximation; rather, it provides a precise analysis of the system.

2.5.2 Kirchhoff's voltage and current laws (KVL, KCL)

KVL Equation 2.65 is the classical definition of KVL,

$$\sum_{k=1}^{n} \phi_k = 0, \tag{2.65}$$

where ϕ_k is a voltage at each node k in a circuit.

Starting from Faraday's law

$$\nabla \times \mathbf{E} = -\frac{\partial \mathbf{B}}{\partial t}, \tag{2.66}$$

and applying Stoke's theorem, an electric potential (voltage) is defined as a line integral over an electric field.

$$\int (\nabla \times \mathbf{E}) \cdot \mathbf{dA} = -\frac{\partial}{\partial t} \int \mathbf{B} \cdot \mathbf{dA}, \tag{2.67}$$

is equal to

$$\oint \mathbf{E} \cdot \mathbf{dl} + \frac{\partial}{\partial t} \underbrace{\int \mathbf{B} \cdot \mathbf{dA}}_{\Psi,\ \text{flux}} = 0. \tag{2.68}$$

The first term in Eq. 2.68 represents emf, the direction is opposite to the voltage.

$$\text{emf} \equiv \oint \mathbf{E} \cdot \mathbf{dl} = \int_a^b \mathbf{E}' \cdot \mathbf{dl} = -\phi(t), \tag{2.69}$$

where E is the electric field intensity measured by an observer moving with the contour of the conductor and $\mathbf{E}' = \mathbf{E} - (\mathbf{u} \times \mathbf{B})$ (Woodson and Melcher, 1968) based on the quasi-static Lorenz force (Eq. 2.49). To arrive at the classical KVL, Eq. 2.65, the quasi-static assumption ($-\frac{\partial \mathbf{B}}{\partial t} = -\mu_0 \frac{\partial \mathbf{H}}{\partial t} = 0$) must be assumed. In other words, the classic KVL is valid when the magnetic field is not time-varying (i.e., a constant $\mathbf{B}_0$ or very slowly changing in time). The classic KVL equation deals with the quasi-static electric field with a stationary charge and thus assumes the electric field around a closed loop to be zero. Therefore Eq. 2.65 is a

special, quasi-static case of KVL. The general form of KVL is

$$-\sum_{k=1}^{n}\phi_k + \dot{\Psi} = 0, \tag{2.70}$$

where $\dot{\Psi}$ is time derivative of the magnetic flux Ψ. In a frequency domain Eq. 2.70 becomes

$$-\sum_{k=1}^{n}\Phi_k + j\omega\underline{\Psi} = 0, \tag{2.71}$$

where $\underline{\Psi} = L_m I$ represents the magnetic flux in frequency domain. Finally we have

$$\boxed{\sum_{k=1}^{n}\Phi_k = sL_m I}, \tag{2.72}$$

meaning that the sum of the Φ_k is the induced voltage (emf) in the right hand side is equal to the left hand side, which represents the mutual inductance (L_m). Typically the leakage flux is considered as an undesirable effect (mutual inductive leakage flux).

KCL To derive KCL, Gauss's law and Ampere's law (Eq. 2.73 and Eq. 2.74, respectively) must be used. Note that Eq. 2.74 and Eq. 2.102 are equivalent. Gauss's law is

$$\nabla \cdot \mathbf{D} = \rho, \tag{2.73}$$

and Ampere's law is

$$\nabla \times \mathbf{H} = \mathbf{J} + \frac{\partial \mathbf{D}}{\partial t}. \tag{2.74}$$

When we apply a divergence theorem on Eq. 2.74, the left term ($\nabla\cdot(\nabla\times\mathbf{H})$) becomes zero as the divergence of the curl is zero. Then assuming a quasi-static magnetic field, $\frac{\partial \mathbf{D}}{\partial t} = 0$ (Eq. 2.74),

$$\nabla \cdot \mathbf{J} + \frac{\partial(\nabla \cdot \mathbf{D})}{\partial t} = \nabla \cdot \mathbf{J} + \frac{\partial \rho}{\partial t} = 0. \tag{2.75}$$

Via the divergence theorem,

$$\int(\nabla \cdot \mathbf{J}) \cdot \mathbf{dV} + \frac{\partial}{\partial t}\int \rho \mathbf{dV} = \int(\nabla \cdot \mathbf{J}) \cdot \mathbf{dV} + \frac{\partial Q}{\partial t} = \underbrace{\int \mathbf{J} \cdot \mathbf{dA}}_{i(t)} + \dot{Q} = 0. \tag{2.76}$$

One can deduce the classical KCL from Eq. 2.76. The net flux of current at a point (node) is zero (the classic KCL assumption, no accumulating current at a node) when we ignore the

stray capacitance $\dot{Q}$. Therefore the correct KCL is

$$\sum_{k=1}^{n} i_k + \dot{Q} = 0, \tag{2.77}$$

and the frequency domain representation of Eq. 2.77 is

$$\sum_{k=1}^{n} I_k + sQ = 0. \tag{2.78}$$

Note that $Q = C\Phi$ is physically interpreted as stray capacitance (C) related to current between two adjacent inductors. Usually it is considered to be an undesirable effect (capacitive leakage current):

$$\boxed{\sum_{k=1}^{n} I_k = -sC\Phi}. \tag{2.79}$$

Note that the difference in the sign for Eq. 2.72 and Eq. 2.79 follows from Lenz's law.

Extension of KCL/KVL to include flux coupling and time delay When KVL and KCL are derived from Maxwell's equations, electrostatic and magnetostatic assumptions (i.e., quasi-static) are used, respectively, in Section 2.5.2. In the KCL derivation, the coupling of a charge, due to a stray capacitance ($\frac{\partial \mathbf{D}}{\partial t}$), is ignored, while for the KVL the magnetic flux coupling (stray mutual inductance, $-\frac{\partial \mathbf{B}}{\partial t}$ in Eq. 2.66) is ignored. That is, in both cases the time-dependent components in the Maxwell's equations are assumed to be negligible, since

$$\lambda \left(= \frac{c}{f} \right) \gg \text{circuit size}, \tag{2.80}$$

where c is the speed of light, and f is frequency of interest. This is a low-frequency approximation where the standard KVL and KCL apply under the quasi-static assumption.

However, the ignored terms in KVL or KCL have their own significance. For example, when current flows through a wire, there is a magnetic field created around the wire. The flux in a KVL loop has an induced flux (Ψ) that induces an emf ($\dot{\Psi}$). This term results in the anti-reciprocal coupling terms require the gyrator in the Hunt matrix (Eq. 2.88 and Eq. 2.89), and it has been ignored in the KCL/KVL analysis based on the time dependency of the magnetic field in the system. Also in terms of the wave equation, both $\dot{\mathbf{B}}$ and $\dot{\mathbf{D}}$ terms allow us to derive the wave equation describing delay, and without them we get diffusion equations.

This discussion can be extended to the limitation of general circuit theory, the quasi-static

assumption. Once we include time delay (elements that include the wires), we must consider the finite transit time when describing circuits. To clearly relate the delay to a dimension, we defined a term "Einstein causality" as a generalization of causality (B2 in Section 2.2.1).

2.5.3 Gyrator

A two-port network, such as an electromechanic system, has Φ, I, $\mathbf{F}$, and $\mathbf{U}$ as the system's variables. A gyrator exists to couple the electric and mechanical sides. Specifically, through the gyrator, the potential, Φ, maps to the velocity $-\mathbf{U}$ and the current I maps to the force F. To show this property, one can employee the impedance matrix of the gyrator

$$Z_{gyrator} = \begin{bmatrix} 0 & -G \\ G & 0 \end{bmatrix}, \tag{2.81}$$

where $G = B_0 l$ is the gyration coefficient, B_0 is the DC magnetic field, and l is the length of the wire. Thus

$$\begin{bmatrix} \Phi(\omega) \\ F(\omega) \end{bmatrix} = \begin{bmatrix} 0 & -B_0 l \\ B_0 l & 0 \end{bmatrix} \begin{bmatrix} I(\omega) \\ U(\omega) \end{bmatrix}, \tag{2.82}$$

namely,

$$\Phi(\omega) = -B_0 l U(\omega) \text{ and } F(\omega) = B_0 l I(\omega). \tag{2.83}$$

When defining an impedance, the flow direction is defined as into the terminals, thus U is defined as going into the network. Thus, the minus sign of U in Eq. 2.83 follows from Lenz's law. Note that Eq. 2.83 explains an ideal gyrator, considering only a DC magnetic field.

The non-ideal gyrator Here we derive the nature of the gyrator from the basics of electro magnetism. Ulaby (2007) described the induced emf (voltage ϕ) as the sum of a transformer component (ϕ_{tr}) and a motional component (ϕ_{mot}), namely,

$$\phi(t) = \phi_{tr} + \phi_{mot}. \tag{2.84}$$

The transformer voltage is $\phi_{tr} = -(-\int \frac{\partial \mathbf{B}}{\partial t} \cdot \mathbf{dA}) = \frac{\partial \psi}{\partial t}$, where ψ is magnetic flux. In the static case ($\frac{d}{dt} = 0$), the time-varying term is zero.

The ϕ_{mot} represents the motion of electrical voltage (Ulaby, 2007)[12] as observed from the mechanical side (motional voltage due to u). Derivation of ϕ_{mot} starts from the Lorentz magnetic force ($\mathbf{f}_m$), acting on a moving charge q inside a magnetic field $\mathbf{B}$ with a velocity

[12]The (electrical) voltage which is associated from the motion from the other port (i.e., mechanical). Note that this concept can be applied only in two-port (or higher order) systems.

$\mathbf{U}$,

$$\mathbf{f}_m = q(\mathbf{U} \times \mathbf{B}). \tag{2.85}$$

Then the motion of magnetic force from the electrical field $\mathbf{E}_{mot}$ is $\mathbf{f}_m = q\mathbf{E}_{mot}$.[13] Therefore,

$$\mathbf{E}_{mot} = \frac{\mathbf{f}_m}{q} = \mathbf{U} \times \mathbf{B}, \tag{2.86}$$

where $\mathbf{E}_{mot}$ is the motional electric field seen by the charged particle q and its direction is perpendicular to both $\mathbf{U}$ and $\mathbf{B}$.

Thus the voltage Φ_{mot} is defined as the line integral of the corresponding electric field, which is $\mathbf{E}_{mot}$ in this case,

$$\phi_{mot} = -\oint_C \mathbf{E}_{mot} \cdot \mathbf{dl} = -\oint_C (\mathbf{U} \times \mathbf{B}) \cdot \mathbf{dl}. \tag{2.87}$$

Note that only this term has been considered in an ideal gyrator.

Finally, the total voltage is

$$\phi = \phi_{tr} + \phi_{mot} = \int \frac{\partial \mathbf{B}}{\partial t} \cdot \mathbf{dA} - \oint_C (\mathbf{U} \times \mathbf{B}) \cdot \mathbf{dl}. \tag{2.88}$$

In the frequency domain with scalars, Eq. 2.88 is rewritten as

$$\Phi = s\Psi - BlU = sL_eI - BlU, \tag{2.89}$$

where L_e is a leakage inductance due to the leakage flux of a self-inductance in the electrical side, $\Psi = L_eI$.

Assuming a static DC magnetic field (B_0), then $s\Psi = 0$ and we find the ideal gyrator definition $\Phi = \Phi_{mot} = -UB_0l$ (Eq. 2.83). Note that the frequency dependant term shown in Eq. 2.89 ($j\omega\Psi$ and $j\omega L_eI$) is a non-QS term that is not considered in an ideal gyrator. The minus sign for the other term $-UBl$ is related to Lenz's law.

Figure 2.14 shows a simple experiment to demonstrate Lenz's law, using a magnet and an ammeter. Moving the north pole of a magnet towards the coil causes positive current I. The motion that the magnet is pushed into the coil reveals the negative direction of the Ψ or emf. If the magnet is pulled out from the coil (positive Ψ or emf), the direction (sign) of the current is reversed. When there is no motion of the magnet, then the current does not

[13]The unit of q is in coulombs [C], $\mathbf{E}_{mot}$ is in [V/m] = [N/C] as 1 [V] $\equiv$ 1 [J/C] and 1 [N] = 1 [J/m]. Therefore $q\mathbf{E}$ stands for force with a unit of [N]. A positive charge ($q > 0$, proton) is 1.602×10^{19} [C]; thus the charge of an electron (negative charge) is -1.602×10^{19} [C]. One coulomb of charge equals to the charge which can light a 120-watt-bulb for one second.

flow. A faster moving magnet creates a larger induced current.

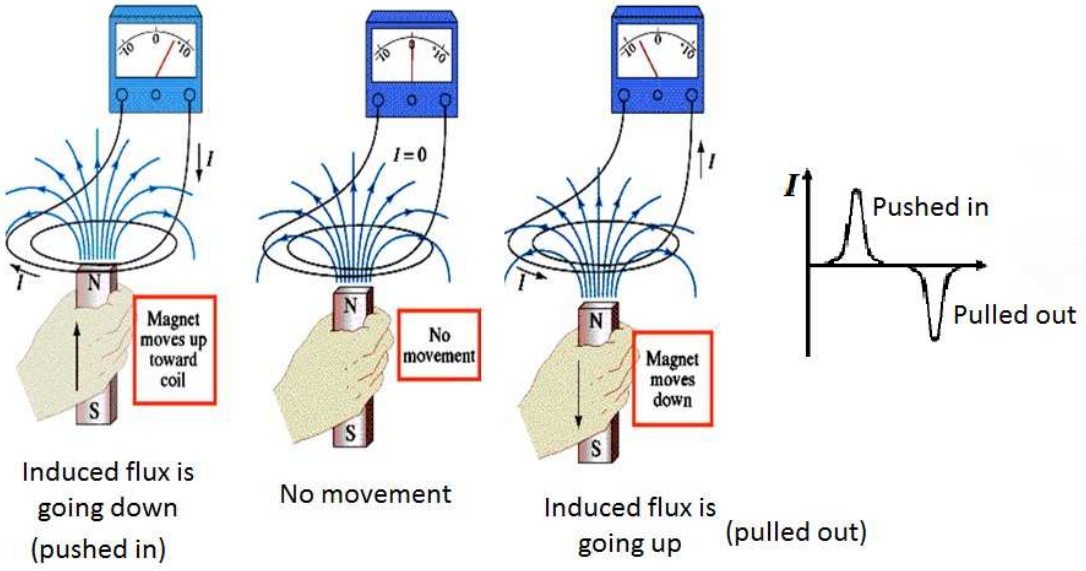

Figure 2.14: A simple experiment to display Lenz's law. The induced flux, Ψ (or emf), gives rise to a current I whose direction opposes the direction of the Ψ. Moving the north pole of a magnet towards the coil causes positive current I. The motion that the magnet is "pushed into the coil" reveals the negative direction of the Ψ or emf. If the magnet is "pulled out from the coil" (positive Ψ or emf), the direction (sign) of the current is reversed. When there is no motion of the magnet, then the current does not flow. The image is retrieved and modified from https://bearspace.baylor.edu/Walter_Wilcox/www/courses/phy2435/chap29xxa.pdf

Consider a simple circuit of a moving coil loudspeaker, with a resistor R across the terminal, voltage $-UBl$ (the induced emf grounded to zero), and current I which is moving across the R. By Ohm's law, the current satisfies

$$I(\omega) = \frac{0-(-UBl)}{R} = \frac{UBl}{R} = \frac{U}{R}\frac{l}{A}\Psi, \tag{2.90}$$

where $\Psi = BA$, and l, A are length and area of wire, respectively. The direction of current is always opposite of the induced emf. This explains Lenz's law.[14] Note the minus signs in Eq. 2.89 requires anti-reciprocity, Carlin's postulate C6.

Similar to Eq. 2.88, one can examine the relation between the force and the current in Eq. 2.83. This force term also needs two parts: transformer force and motional force,

$$f(t) = f_{tr} + f_{mot}. \tag{2.91}$$

Reconsidering the magnetic force density in Eq. 2.85, the motion of force in the electrical

[14]If we consider the emf with its positive sign (UBl), indicating the fixed positive direction in the circuit, we will have $-I$.

side, f_{mot} [N], is

$$\mathbf{f_{mot}} = i(t) \oint_C \mathbf{dl} \times \mathbf{B}, \tag{2.92}$$

where $i(t)$ stands for the current.

Assuming that the magnetic field is uniform and the conducting wire is not closed, starting from a ending at b (if it is closed then the net magnetic force is zero; in Eq. 2.93 a equals b.), then Eq. 2.92 becomes

$$\mathbf{f_{mot}} = i(\int_a^b \mathbf{dl}) \times \mathbf{B}_0 = i\mathbf{l} \times \mathbf{B}_0, \tag{2.93}$$

where $\mathbf{l}$ is a vector, a piece of wire directing from a to b. In frequency domain, Eq. 2.93 is $F = B_0 l$, it is the ideal gyrator's equation discussed in Eq. 2.83 which only considers motional behavior of the network.

Based on the Lorentz force, the transformer force on the mechanical side is defined as

$$f_{tr} = m_B \times a = m_B \frac{dU}{dt}, \tag{2.94}$$

where m_B is the leakage mass due to imperfect (frequency dependent) mass coupling on the mechanical side, and $a = \frac{dU}{dt}$ is acceleration. In frequency domain, this term becomes $F_{tr} = sm_B U$, where $s = j\omega$.

The final force for the non-ideal gyrator is

$$f = f_{tr} + f_{mot} = m_B \frac{dU}{dt} + i\mathbf{l} \times \mathbf{B}. \tag{2.95}$$

In frequency domain with scalars, Eq. 2.95 is reconsidered as

$$F = sm_B U + B_0 l I. \tag{2.96}$$

In conclusion, two types of magnetic fields exist in an electromechanic network; one is a DC magnetic field and the other is an AC magnetic field. In the ideal gyrator formula, only the motional parts (or the DC magnetic field) of the variables (voltage and force) are considered. The two modalities in the network (electrical and mechanical) share this DC magnetic field which is shown in the motional part of each variable. For the non-gyrator case, one must use the transduction parts (or AC magnetic field) of variables along with the motional parts, which do not contribute to the opposite modality.

One can convert the impedance matrix form of the ideal gyrator in Eq. 2.81 into an ABCD

matrix form using Eq. 2.8,

$$T_{i-gyrator} = \begin{bmatrix} 0 & G \\ G^{-1} & 0 \end{bmatrix}, \tag{2.97}$$

where $G = B_0 l$. The ABCD matrix for of the non-ideal gyrator is,

$$T_{noni-gyrator} = \frac{1}{G} \begin{bmatrix} sL_e & s^2 L_e m_B + G^2 \\ 1 & sm_B \end{bmatrix}. \tag{2.98}$$

The determinants (Δ) of both Eq. 2.97 and Eq. 2.98 are minus one, which define the anti-reciprocal network. When Δ is one, the network is reciprocal. Note that all of these relationships are in the Laplace complex frequency domain $s = j\omega$.

Finally the suggested non-ideal gyrator's impedance matrix formula is

$$Z_{noni-gyrator} = \begin{bmatrix} sL_e & -G \\ G & sm_B \end{bmatrix}, \tag{2.99}$$

a non-reversible and anti-reciprocal network (if $L_e \neq m_B$).

What provides the coupling between the electrical and mechanical sides? The only thing that matters in the electromechanic coupling is the magnetic field, $\dot{\mathbf{H}}$. This variable is hidden in terms of input and output variables of the system (voltage, current, force, and velocity). The $\dot{\mathbf{H}}$ generated by the conducting current from the coil affects the armature by inducing magnetic polarity on the armature surface. This induced $\dot{\mathbf{H}}$ and the permanent magnet define the net force on the armature. Thus the armature moves based on the experienced total net force.

It is intuitive that the electrical current leads to a force, because the system transforms the current signal into a force on the diaphragm, creating sound pressure waves. According to this logic, a gyrator equation relates the electrical current to the force, $F = B_0 l I$.[15] Therefore, we can conclude that the gyrator is a more physically intuitive convention.

[15] We may can relate the current to the velocity (transformer and mobility), which seems to be less intuitive.

2.5.4 Eddy currents and diffusion waves

Along with the gyrator, the semi-inductor (due to the eddy current[16]) is one of the key components to describe an electromechanic system (Kim and Allen, 2013). If a magnetic field near a conductor is changing in time, the traveling magnetic field is described in terms of the diffusion equation. This is a physical phenomenon which can be observed in our daily life.

There are two ways to examine the eddy current, (1) the direct way and (2) indirect ways: In the direct way, a magnet traveling inside of a copper pipe can be affected by this diffusive eddy current. The magnet falling outside of a conductor does a free fall, while falling inside of the conducting pipe it experiences a significant delay, due to the opposite force caused by the eddy current. Figure 2.15 describes this phenomenon.

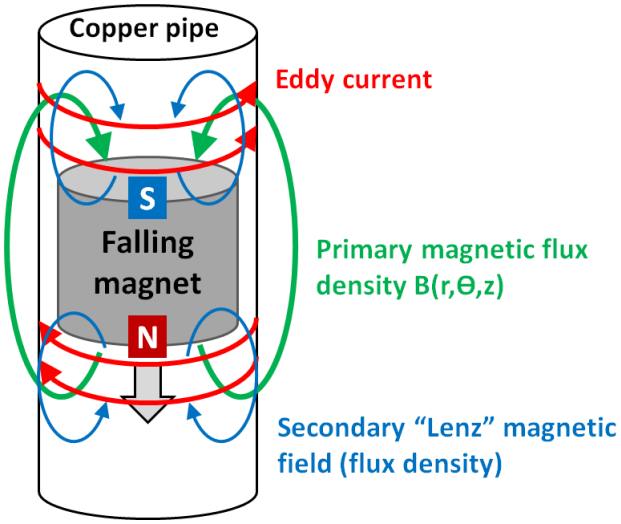

Figure 2.15: Eddy current with a falling magnet inside a conductor (falling from south to north). When the magnetic field is changed in time in a closed electric field (a falling magnet in a copper pipe), an eddy current is induced on the copper pipe (red). The direction of the eddy current is perpendicular to the primary magnetic field (green; when velocity is zero, the primary magnetic field is static and is not a function of θ) followed by right hand rule (thumb, 1^{st} finger, and 2^{nd} finger indicate the direction of force, electric field, and magnetic field, respectively). The eddy current creates the secondary magnetic loop (blue) whose force is opposite to the force of gravity. At the terminal velocity, the force of gravity equals the Lenz reactive force.

[16]There are three types of currents in an electromagnetic system

1) Conducting current is created by the moving charge in the conducting medium (J term in Ampere's law, i.e., current through wire).

2) Displacement current is current due to changing electric field (E) ($\dot{D}$ term in Ampere's law, i.e., capacitors).

3) Eddy current is current due to changing magnetic field (H). It is directly related to Faraday's (induction) law.

In the indirect way, starting from Ampere's law, the current in the wire, namely driven (or conducting) current, induces magnetic field **H**. Then, similar to the direct way, based on the Faraday's law, the **H** creates the eddy current (induced current via **H** on the surface of the adjacent ferromagnetic material). Note that the magnitude of the eddy currents is a function of the drive current with in the opposite direction.

Vanderkooy (1989) modeled the electrical impedance representation of the semi-inductor based on this concept (indirect way to examine the eddy current). Impedance of the semi-inductor is proportional to $\sqrt{s}$, to realize a diffusive element in the circuits. A simple impedance formula of the semi-inductor is derived with the assumption that the length of a coil sheet is infinite. Neglecting the radius of the coil and the air gap between the magnetic material and the wire,

$$Z_{semi} = n^2\sqrt{\frac{\mu s}{\sigma}} = K\sqrt{s}, \tag{2.100}$$

where K is semi-inductance per unit length in semi-Henrys, n is the number of coil winding turns of wire, μ is the iron's permeability, and and σ is the conductivity of the iron armature.

Semi-inductors, which result from magnetic diffusion, are not commonly found in circuit analysis. However, they are a key element in characterizing the eddy current (skin effect) in electromagnetic models, such as loudspeakers. In a BAR, the eddy current is distributed through the surface of the armature, as well as in the cross section of the laminated iron box which surrounds the magnets (Fig. 1.2). In a dynamic loudspeaker, the coil is directly connected to the diaphragm and the eddy current is distributed through the surface of an iron core (a pole-piece structure).

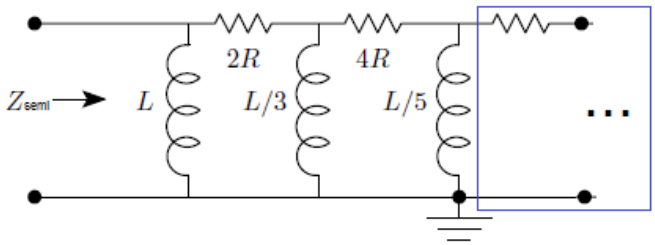

Figure 2.16: The semi-inductor is approximated by a truncated ladder network using lumped circuits. It is defined by the ladder network resistance factor R and shunt inductance factor L (Weece and Allen, 2010). This circuit follows from a continued fraction expansion of $\sqrt{s}$.

Warren and LoPresti (2006) noted that the Bessel function ratio in the Vanderkooy model (1989) can be expanded as a continued fraction expansion, into a diffusion ladder network, so that the electrical impedance can be represented by the circuit shown in Fig. 2.16. The semi-inductor model includes two parameters: the diffusion resistance R, and the shunt diffusive inductance L, which can be represented by the physical characteristics of the transducer.

The R and L are given by

$$R = \frac{4\pi n^2 l}{\sigma},\ L = \mu l n^2 \pi r_0^2, \tag{2.101}$$

where n is the number of coil windings, l is the coil length, σ is the conductivity of the pole structure, μ is the permeability of the pole structure, and r_0 the coil radius.

Although the combination of the resistor and the inductor should extend to infinity (more resistor-inductor pairs), these can only affect higher frequencies (i.e., Fig. 2.16 is a sufficient low-frequency approximation). As shown in Fig. 2.16, Weece and Allen (2010) determined only five elements (L, 2R, L/3, 4R, and L/5), and compared the network to the demagnetized condition of their bone driver transducer. Demagnetizing the transducer ($T = B_0 l = 0$) is mathematically equivalent to the open circuit condition (i.e., $V = 0$).

Starting from Maxwell's equation, we derive two types of wave equations, normal and diffusive cases.

Equation 2.102 has two terms, current from the source, and displacement current:

$$\nabla \times \mathbf{H} = \epsilon \frac{\partial \mathbf{E}}{\partial t} + \sigma \mathbf{E}, \tag{2.102}$$

where $\mathbf{D} = \epsilon \mathbf{E}$ and $\mathbf{J} = \sigma \mathbf{E}$. Via $\mathbf{B} = \mu \mathbf{H}$, Faraday's law (Eq. 2.66) for free space written as,

$$\nabla \times \mathbf{E} = -\mu \frac{\partial \mathbf{H}}{\partial t} = -\dot{\mathbf{B}}. \tag{2.103}$$

Also since monopole magnetic charge does not exist, and μ is independent of x (i.e.,$\nabla \mu = 0$),

$$\nabla \cdot \mathbf{B} = \nabla \cdot \mathbf{H} = 0. \tag{2.104}$$

Taking a curl of Eq. 2.102 using the following vector identity,

$$\nabla \times (\nabla \times \mathbf{H}) = \nabla(\nabla \cdot \mathbf{H}) - \nabla^2 \mathbf{H}, \tag{2.105}$$

then using Eq. 2.103 and Eq. 2.104, Eq. 2.105 becomes

$$\nabla \times (\nabla \times \mathbf{H}) = \epsilon \frac{\partial (\nabla \times \mathbf{E})}{\partial t} + \nabla \times (\sigma \mathbf{E}) = -\mu\epsilon \frac{\partial}{\partial t}\frac{\partial \mathbf{H}}{\partial t} - \mu\sigma \frac{\partial \mathbf{H}}{\partial t} = 0 - \nabla^2 \mathbf{H}. \tag{2.106}$$

Finally we have,

$$\nabla^2 \mathbf{H} = \underbrace{\mu\epsilon \frac{\partial^2 \mathbf{H}}{\partial t^2}}_{loseless\ wave} + \underbrace{\mu\sigma \frac{\partial \mathbf{H}}{\partial t}}_{lossy\ wave} \leftrightarrow (\frac{s^2}{c^2} + \mu\sigma s)\underline{\mathbf{H}} = \mu\sigma s(s\epsilon/\sigma + 1)\underline{\mathbf{H}}, \tag{2.107}$$

where $\underline{\mathbf{H}}$ is the frequency variable of $\mathbf{H}$, and $s = j\omega$. When $\omega \ll \sigma/\epsilon = \omega_c$ the wave is dominated by diffusion; otherwise we have lossy waves. Since the two waves satisfy superposition, we can separate the two solutions.

Lossless wave equation ($\mathbf{J} = 0$ or $\sigma = 0$) When there is zero conductive current density ($\mathbf{J} = 0$),

$$\nabla \times \mathbf{H} = \frac{\partial \mathbf{D}}{\partial t} + \cancelto{0}{\mathbf{J}} = \epsilon \frac{\partial \mathbf{E}}{\partial t}. \tag{2.108}$$

Going through the same algebra from Eq. 2.103 to Eq. 2.106, we have the wave equation,

$$\nabla^2 \mathbf{H} = \mu\epsilon \frac{\partial^2 \mathbf{H}}{\partial t^2} = \frac{1}{c^2} \frac{\partial^2 \mathbf{H}}{\partial t^2}. \tag{2.109}$$

Lossy wave equation: diffusion equation (semi-inductor basics) A similar step is used to derive the diffusion equation via Maxwell's equation. The fundamental difference is in the first step. When the medium is a conductor, we can ignore the displacement current term in Eq. 2.102 as it is small compared to the conducting current term. Therefore in this case we can set $\frac{\partial \mathbf{D}}{\partial t}$ to zero,

$$\nabla \times \mathbf{H} = \mathbf{J} + \cancelto{0}{\frac{\partial \mathbf{D}}{\partial t}} = \sigma \mathbf{E}. \tag{2.110}$$

Based on Eq. 2.103 to Eq. 2.106, finally the diffusion wave equation is derived,

$$\nabla^2 \mathbf{H} = \mu\sigma \frac{\partial \mathbf{H}}{\partial t}. \tag{2.111}$$

The normal wave equation in 3D wave form (Eq. 2.109) describes the propagation of electromagnetic (EM) waves through a medium, whereas the diffusion wave equation (Eq. 2.111) describes the propagation of EM waves in a conducting magnetic medium. For both equations, the Laplacian on the left-hand side is the same. A diffusion case has a single time-derivative term, whereas a normal wave equation has a double time-derivative term. Let us define $\mathbf{H}(x, t)$ assuming a simple geometry,

$$\mathbf{H}(x, t) = H_0 e^{j(\omega t - kx)}, \tag{2.112}$$

where H_0 is the $\mathbf{H}$, $\mathbf{E}$ propagated in y, z directions, respectively. Note that k is the wave number. Then Eq. 2.111 in frequency domain

$$(jk)^2 = \mu\sigma j\omega. \tag{2.113}$$

Then the wave number k is

$$k = \sqrt{\mu\sigma\omega}(\cos 45^o - j \sin 45^o). \tag{2.114}$$

Thus the wave propagation is proportional to the square-root frequency ($\sqrt{s}$).

To derive the exact impedance formula of a semi-inductor:

1) Substitute Eq. 2.114 into Eq. 2.112

$$\mathbf{H}(x,t) = H_0 e^{j(\omega t - \sqrt{\mu\sigma\omega}x(1-j)/\sqrt{2})}. \tag{2.115}$$

2) Calculate the magnetic flux Ψ per unit area, where $\Psi = \int \mathbf{B} \cdot \mathbf{dS} = \mu \int \mathbf{H} \cdot \mathbf{dS}$.

3) Then the inductance L per unit length with n numbers of turn with current I is

$$L = \frac{n}{I}\Psi = n^2 \frac{\mu}{1+j}\sqrt{\frac{2}{\mu\sigma\omega}}. \tag{2.116}$$

4) The impedance of an inductor is $Z(s) = sL$, where $s = j\omega$. Therefore

$$Z_{semi}(s) = n^2\sqrt{\frac{\mu s}{\sigma}} = K\sqrt{s}, \tag{2.117}$$

where K is the semi-inductance.

The semi-inductor's impedance is proportional to the square-root of frequency. More details considering different geometries are discussed in Vanderkooy (1989).

One can calculate a propagation cutoff frequency of two waves (diffusion and normal) in a medium. Convert Eq. 2.109 and Eq. 2.111 into frequency domain representation via Laplace transform, and set them equal to each other. If

$$\mu\sigma\frac{\partial \mathbf{H}}{\partial t} = \mu\epsilon\frac{\partial^2 \mathbf{H}}{\partial t^2} \tag{2.118}$$

$$\mu\sigma(j\omega)\mathbf{H} = \mu\epsilon(j\omega)^2\mathbf{H} \tag{2.119}$$

$$\sigma = \epsilon(j\omega), \tag{2.120}$$

the cutoff frequency(f_c) is

$$f_c = \frac{\sigma}{2\pi\epsilon}. \tag{2.121}$$

The f_c of copper, for example, is about 4300 [GHz] ($\sigma = 5.96 \times 10^7$, $\epsilon_r = 250,000$, $\epsilon_0 = 8.854 \times 10^{-12}$), meaning that the wave below this frequency is diffusive. The corresponding

wave length (λ_c) can be calculated as

$$\lambda_c = \frac{c_{copper}}{f_c} = \frac{3 \times 10^8}{4.3 \times 10^{12}\sqrt{250,000}} \approx 0.14\mu \text{ [m]}, \tag{2.122}$$

where $c_{copper} = \frac{c_0}{\sqrt{\epsilon_r}}$.

CHAPTER 3

EXPERIMENTAL METHODS

3.1 Measurements for BAR modeling

Three different experiments were conducted for modeling the BAR. First, we calculate the Hunt parameters of a BAR from electrical input impedance measurements (Appendix E). The calculation of Hunt parameters may be considered as a two-port Thevenin calibration of the receiver, since Z_e, T, and Z_a characterize the initial electrical, acoustical, and transfer properties of the unloaded receiver. Second, we measure the receiver's diaphragm velocity in the vacuum using a laser. This procedure was needed to verify the mechanical and electrical parts of the model. The last step is the pressure measurement of the receiver using an ER7C probe microphone (Etymotic Research). The resulting Thevenin pressure of the receiver from our transducer model and Hunt parameters is compared with this experimental pressure data. The details of this result are discussed in Chapter 4 (model verification).

3.1.1 Electrical input impedance measurements for the Hunt parameter calculation

Step 1 of calculating the Hunt parameters of the receiver requires a system for measuring electrical impedance as a function of frequency. As shown in Fig. 3.1, all stimulus signals

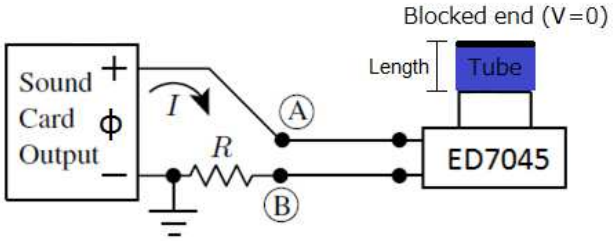

Figure 3.1: Experimental setup for the electrical input impedance measurement, where Φ is the voltage, I is the current, and R is a reference resistance. We varied the experimental acoustical load impedance by changing the length of a blocked tube and measured the voltage at two points (A, B) denoted as Φ_A and Φ_B.

were generated using a laptop sound card so that voltages could be recorded. The stimulus waveform was a 24-bit, 2048-point frequency-swept chirp with a sampling rate of 48 [kHz] (bandwidth is 24 [kHz]). The signal-to-noise ratio (SNR) was improved by looping the chirp and averaging between 10 and 1000 consecutive frames, depending on the required SNR. The $\leqq$1 volt chirp signal from an Indigo sound card (Echo Audio) was sent to the receiver, which was in series with a known reference resistor R (1000 [Ω], Fig. 3.1). The resistor was located between one of the receiver's terminals and the sound source ground. The measured electrical input impedance is expressed as

$$Z_{in} = \frac{\Phi_A - \Phi_B}{I} = \frac{\Phi_A - \Phi_B}{\Phi_B / R} = R\left(\frac{\Phi_A}{\Phi_B} - 1\right). \tag{3.1}$$

As shown in Fig. 3.2, eight different acoustic loads were attached to the end of the receiver

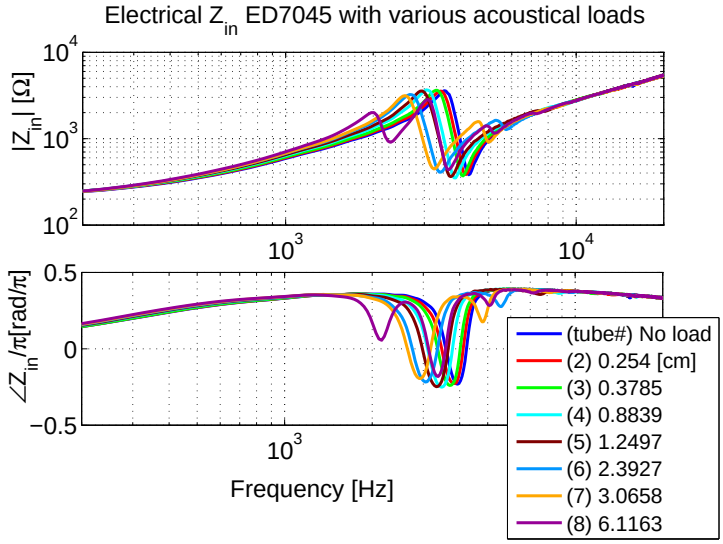

Figure 3.2: Measured Z_{in} of ED7045 with the eight acoustical load conditions, blocked cavities. Different lengths of the tubes are used to vary the acoustical load. Three different known electrical input impedances are selected to calculate Hunt parameters.

output and eight corresponding electrical input impedances were recorded. Six of the seven tubes (excluding the longest length 6.11 [cm], which has the largest delay among the tubes, due to minimizing the discrepancy in the Hunt parameter calculation) were used in the experiments: 0.25, 0.37, 0.88, 1.24, 2.39 and 3.06 [cm]. The inner diameter of the tested tubes (with uniform area) was approximately measured as 1.5 [mm], which is similar to the outer diameter of the ED receiver port. As three different measurements were required to calculate the three unknown Hunt parameters (Z_e, Z_a, T_a) (Weece and Allen, 2010), three out of six tubes with different lengths were selected, resulting in ${}_6C_3 = 20$ possible

combinations of the Hunt parameters. The results from every possible combination are not discussed in this paper; rather, we focus on the four calculated sets of Hunt parameters. We categorized our testing tube lengths into short, medium and long tubes, and picked one of each to make a set of three tubes. An open circuit condition (the volume velocity, V, is zero, rigid termination) was applied, as the ends of the tubes were blocked for the experiment. The characteristics of the resulting derived Hunt parameters are discussed in Section 2.1.1.

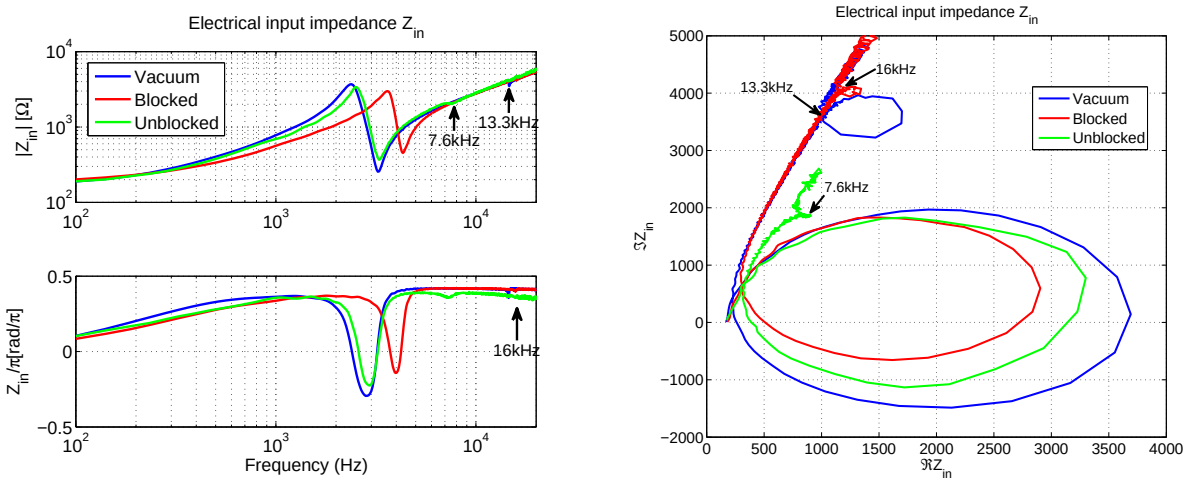

(a) Magnitude and phase of Z_{in} of the ED7045 receiver

(b) Z_{in} polar plot

Figure 3.3: This plot shows the electrical input impedance of the ED7045 receiver in blocked/unblocked port, and vacuum conditions. In the unblocked receiver port case, the FR moves to the lower frequency (2.5 [kHz]) compared to the blocked case, 3.8 [kHz]. The FR in vacuum is at the lowest frequency, 2.3 [kHz]. The frequency locations of SR for each curve are indicated by arrows in the figures. (a) Magnitude and phase of the electrical input impedance; (b) polar plot of the electrical input impedance ($\Re Z_{in}$ vs $\Im Z_{in}$). Note that above 5 [kHz], the phase of Z_{in} in (a) approaches $\approx .4\pi$ [rad]. Thus in (b), the curves merge at a fixed angle as $\omega \to \infty$.

When the acoustic load impedance is unblocked, a small second resonance (SR)[1] appears around 7.6 [kHz], following the first resonance (FR)[2] at 2.5 [kHz], as shown in Fig. 3.3 (a) (green). In fact, a very small SR appears in *every* case in the figure, as clearly seen in the polar plot, Fig. 3.3 (b). The SR of the blocked case (red) is not obvious in the magnitude plot, but one sees the SR location from the phase in the polar data. Note that a loop in the polar data corresponds to the SR in the magnitude data. The vacuum data (blue) shows the biggest FR in magnitude (the largest circle in the polar plot), and the FR is located at the lowest frequency among all the other cases. Compared to the unblocked case (red), the SR frequency of the other two cases (blocked and vacuum) is above the frequency range of reliable measurements. In detail, it has almost an octave difference

[1]SR: Second resonance
[2]FR: First resonance

($SR_{unblocked} \approx 7.6$ [kHz], $SR_{vacuum} \approx 13.3$ [kHz], $SR_{blocked} \approx 15.7$ [kHz]). In addition, the size of $SR_{blocked}$ is insignificant. For these reasons, we have ignored the SR effect in our model analysis of the BAR model.

In fact, the SR is due to the non-linear flux of the system. In unblocked case, the frequency of the anti-FR (zero) is twice of the the anti-SR. The anti-resonance relates to the resonance across a gyrator; therefore the anti-SR gives an account of second harmonic in the acoustic side followed by the first harmonic (anti-FR).

3.1.2 Laser vacuum measurements

Figure 3.4 shows the experimental setup of the laser mechanical velocity measurement in the vacuum environment. In preparation for the laser measurement, a portion of the transducer's case was carefully removed using a dental drill, to expose the diaphragm. A thin plastic window was glued on, to reseal the case. The laser beam is finely focused on the diaphragm

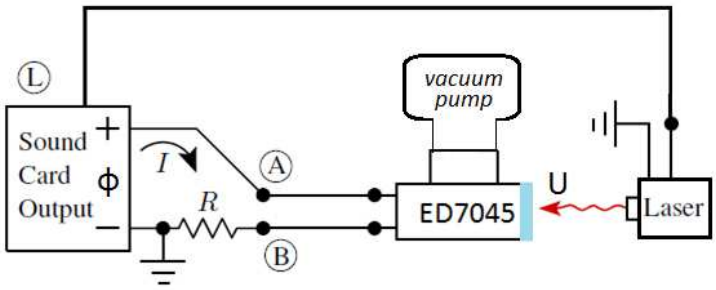

Figure 3.4: Experiment setup for the laser mechanical velocity measurement in vacuum. The circled L means an input from the laser system. The laser beam is focusing on the plastic window of the transducer to measure the diaphragm velocity (U).

through the window. The measurement was made where the driver rod (Fig. 1.2) connects to the diaphragm. For the vacuum condition, air inside the receiver was evacuated prior to measurement. The ambient pressure was maintained at less than 0.003 [atm] during these measurements. The custom-built vacuum system was used with a Sergeant Welch vacuum pump and a 10-inch bell-shaped jar. A Polytec OFV-5000 Vibrometer controller was used with a 10× lens on the laser. The calibration factor for the laser velocity was 125 [mm/sec/volt]. As before, a chirp was used to measure the complex velocity frequency response.

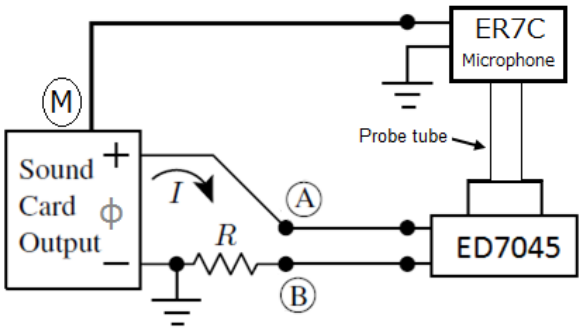

Figure 3.5: Experiment setup for pressure measurement. The circled M means an input from the ER7C microphone. The ER7C microphone system is factory-calibrated as 50 [mV/Pa]. It consists of an amplifier box, a microphone, and a probe tube. Note that the ER7C microphone and the ED7045 receiver are connected carefully to minimize the space between the probe tube's end and the receiver's port.

3.1.3 Pressure measurements

The purpose of experiment three is to compare the output pressure to the model with $V = 0$ (rigid termination). An ER-7C probe microphone (Etymotic Research) was used for the transducer pressure measurement (Fig. 3.5). The ER7C microphone has an attached probe tube whose dimension was .95 OD × .58 ID × 76 [mm], and made of medical grade silicon rubber. In fact, it is impossible to connect the microphone probe tube with a blocked receiver ($V = 0$, the condition that we want to make a comparison with our modeling data) due to the finite load impedance of the microphone. The space between the microphone's tube and the port of the receiver is minimized, so the microphone's tube and the receiver's port do not touch each other. The real part of the characteristic impedance of a tube, Zc_{tube}, (without loss) is given by

$$Zc_{tube} = \frac{\rho c}{Area_{tube}}, \tag{3.2}$$

where ρ is the air density and c is the speed of sound (1.21 [kg/m^3] and 342 [m/s] at 20 [^{o}C], respectively). The diameter, d, of the receiver's port and the microphone's tube are $d_{receiver} = 1.4$ [mm] and $d_{mic} = 0.58$ [mm], thus the area of the receiver's port is about 5.8 times larger than the microphone's. Regarding the length of both cases, Zc_{mic_tube} is much greater than $Zc_{recever\_port}$. Thus we assume that Zc_{mic_tube} has a negligible loading effect on the source impedance of the receiver. Recognizing these experimental limitations prior to comparing the measurement data to theoretical results should give us better understanding of the Thevenin pressure of the BAR.

Utilization of this experiment can be found in Section 4.2.4 for comparing the model-calculated Thevenin pressure (per voltage) to the experimental pressure measurement.

3.2 Technical analysis of an OAE hearing measurement probe

In this section, we introduce several experimental methods to investigate an existing hearing measurement probe system, the ER10C by Etymotic Research, for otoacoustic emission (OAE) measurements. The ER10C system consists of two parts: a probe and an amplifier box (Fig. 3.6(a)). The ER10C probe has built-in sound sources (receivers), which eliminate the need for having external speakers (Fig. 3.6(b)). The amplifier box contains special circuits for each probe to meet the unified and standard performance specification of the ER10C system.

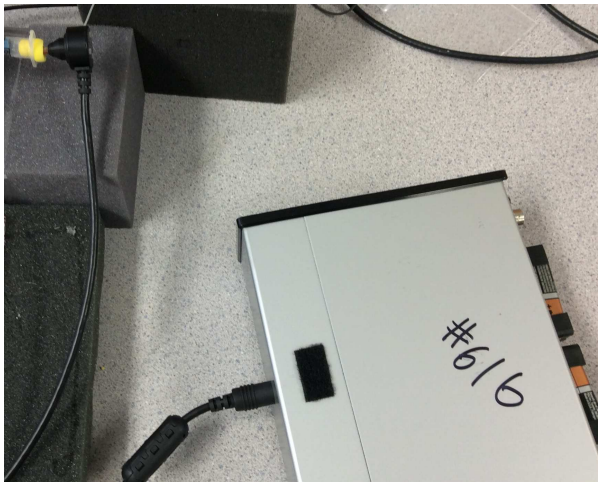

(a)ER10C with its amplifier box

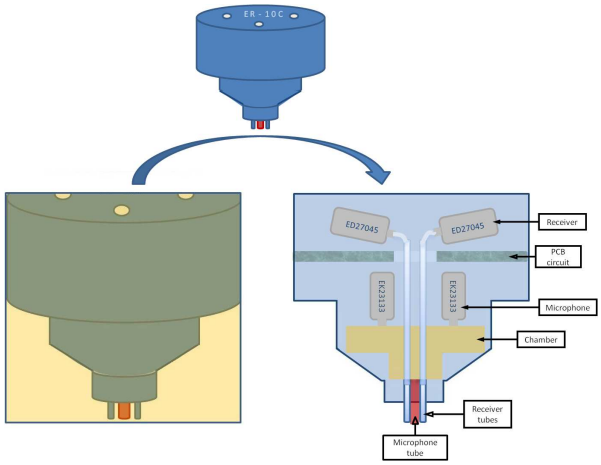

(b) The cross-sectional view of ER10C probe

Figure 3.6: (a) A yellow foam tip (14A) is attached to the probe's head. Note that numbers on the box indicates the system's serial number. (b) Schematic representation of the ER10C probe. Two speakers and microphones are separated internally across the PCB circuit; microphones are placed ahead of the receivers (speakers).

For the last decade, the system (or the probe alone with other software such as HearID or OtoStat by Mimosa Acoustics) has been widely used in clinics for hearing screening and diagnostics by measuring DPOAEs (distortion-product otoacoustic emissions), and middle ear reflectance. Following the probe's Thevenin calibration, OAE stimuli may be calibrated to have constant forward pressure levels (FPL).

Because of the small number of competitors in the market, users have not had many alternatives to the system, even though the ER10C has several drawbacks. First, the size of the probe is too big for infants. Second, because the probe is such a delicate device, handling it without extreme caution may lead to malfunction of the probe. Finally, the result of the measurement depends too much on the condition of the foam tip that is inserted in the subject's ear canal.

Appreciating these facts, we believe that investigation of the properties of the ER10C will

provide fundamental and operational understanding of not only the ER10C system but also hearing measurement devices in general.

3.2.1 Physical structure of ER10C

In this section, we report detailed observations of the ER10C by opening up the device. Figure 3.7 shows the internal structure of the ER10C probe, which has been carefully disassembled into two parts: a holder with microphones (Fig. 3.7(a)) and a printed circuit board (PCB) with speakers (Fig. 3.7(b)). The microphone holder part has a chamber in the middle, holding steel tubes to construct the input (microphone) and the output (speakers) sound paths to each transducer. The microphones are firmly attached to the chamber while the speakers are attached to steel tubes via a soft rubber tubes, floated in the air. Because air acts as the best damper, in this way, any vibrational nonlinear effect (crosstalk) from the speakers can be reduced.

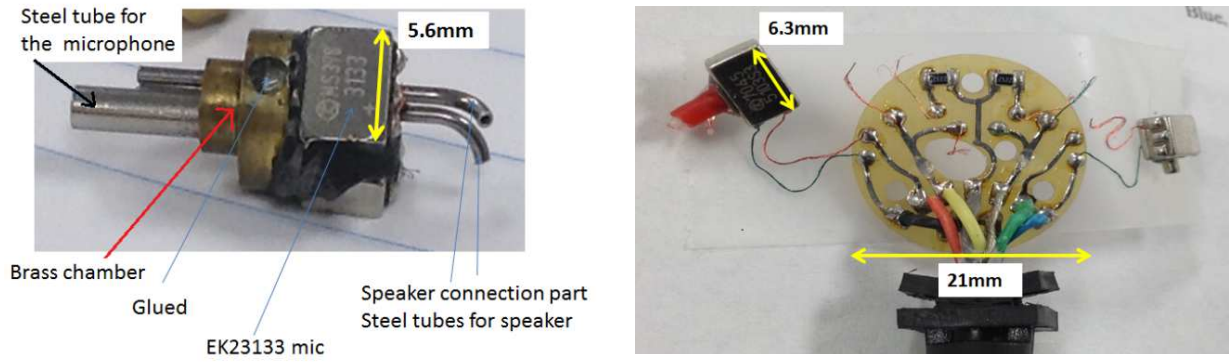

(a) ER10C microphone holder

(b) ER10C circuit board part

Figure 3.7: Disassembled ER10C. Two parts are inside: (a) microphone holder and (b) circuit board parts. Note that much care was needed to see the part (a), as it was permanently attached to the probe's case.

The shape of the chamber (alone) is shown in Fig. 3.8. The front side of the chamber has three holes: two small holes are for the two outputs, and one large hole is for the input. The back side has four holes: two microphone ports are directly plugged into the larger two upper holes, and thin steel tubes (for the speakers) are passing through the small two lower holes.

It may be noted from the structure of the brass cavity (Fig. 3.8) that a unique point about the input structure of the ER10C (compared to the other hearing measurement probes) is that it has two internal microphones, which act as one input. The electrical terminals of two microphones are connected with a two-diode package (i.e., MMBD7000), but only one

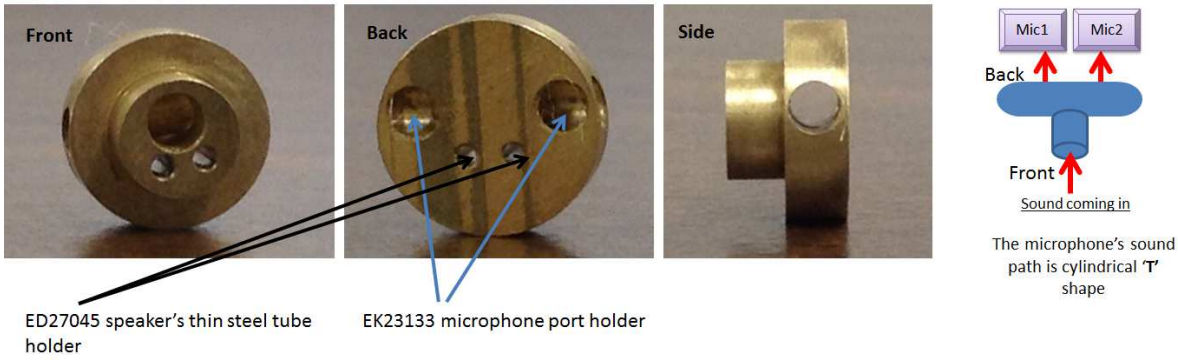

Figure 3.8: Details of the brass chamber in Fig. 3.7. The recent design of ER10C, an aluminum material chamber is used, maintaining the same shape.

diode is used, set up to be reverse biased in series with a capacitor (between the nominal microphone's output and the ground terminals, Fig. 3.9). This is a traditional approach in the hearing aid industry, to protect the input from spark discharge. The capacitor is to filter out the very large spark discharge, and take it out (clip it) with the diode. There are two parallel 22k [Ω] resistors for two microphones as shown in Fig. 3.7 (black squares with 2122 written on them). But as this system has a single input (this input channel may be separated as two inputs externally), the resistance of the input channel reads 11k [Ω].

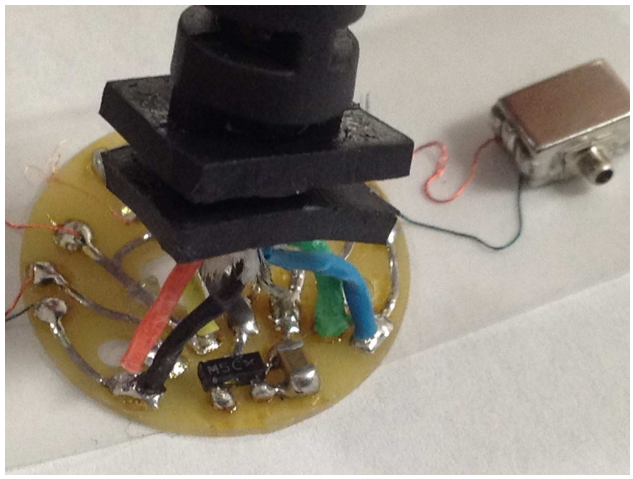

Figure 3.9: ER10C circuit board details. A diode package and a capacitor are shown under the wire soldering ends. Only one diode is used to set up to be reverse biased, in series with a capacitor between the microphone's output and the ground terminals. It is a traditional approach in the hearing aid industry, to protect the input from spark discharge.

Figure 3.10 shows the connection details of the two probe parts shown in Fig. 3.7. The speakers are connected to the curved steel tubes (right side of the upper right picture) via red rubber tubes attached on speaker port (upper left).

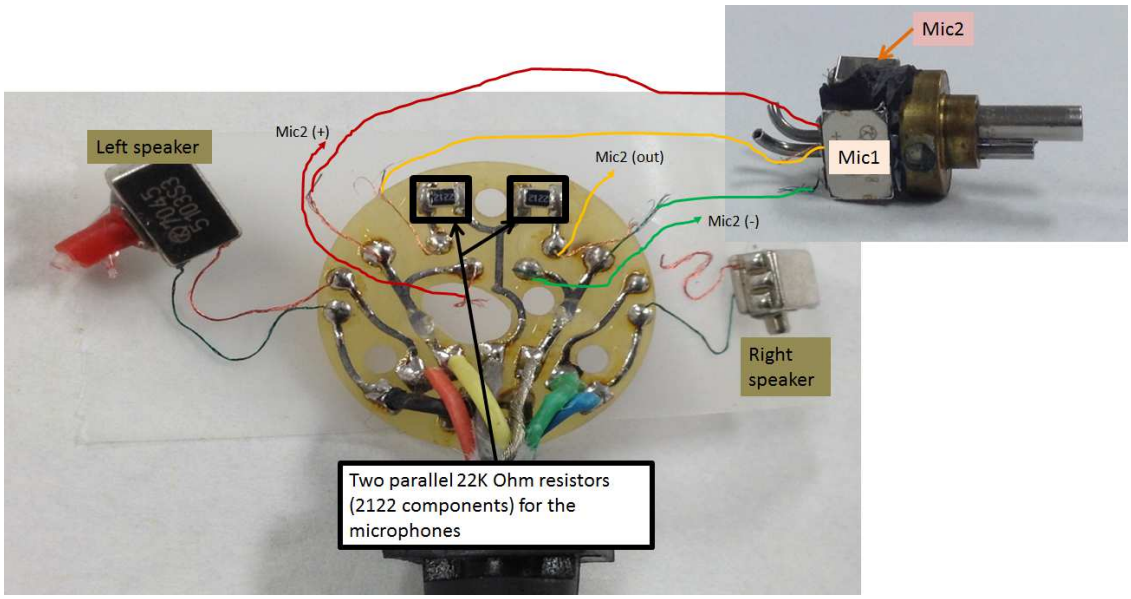

Figure 3.10: ER10C circuit board (Fig. 3.7(b)) and connection derails with microphone holder part in Fig. 3.7(a). Note that the speakers are connected to the curved steel tubes via red rubber tubes.

3.2.2 Crosstalk measurement

In this part, we investigate a critical topic to design a hearing measurement probe: crosstalk. Starting from categorizing various types of crosstalk, we describe each crosstalk measurement.

In an electroacoustic system, crosstalk is undesired signal that is observed in the system's response. It may contaminate a system's signal to and from both the speaker and the microphone. Our main concern is the crosstalk in the microphone, which may be categorized into three types:

1) Electrical: Coupling of the input signals via the electrical wires, usually affecting the output at high frequencies. To measure this, we may block the probe's microphone and generate a signal from the speaker, then measure the probe's microphone response. Ideally, as we blocked the microphone, the signal from the probe's microphone should be similar to the noise floor. If any signal is greater than the noise floor, it is the electrical crosstalk.

2) Mechanical: Vibrational coupling to the microphone's diaphragm. Any physical vibration through the probe's body, not through the main input path, the port of the microphone (i.e., touching the probe' head during measurement can affect the microphone's diaphragm). To prevent this crosstalk, the probe should be placed with a "hands-free" condition during experiments.

3) Acoustical: Any signal coming into the system from outside the region of measurement (i.e., noise). Typically this is related to poor acoustic seals in the system, and affects low-frequency measurements, increasing the noise floor. To measure this acoustic crosstalk, we may stimulate output channel 1 (connected to input channel 1) with a signal and measure the input of channel 2. Ideally, input channel 2 should have no signal, if the device has zero crosstalk (or similar to noise floor). However, if the acoustic crosstalk is present, some signal that corresponds to the output of channel 1 will be observed at the channel 2 input.

3.2.3 Calibration issues

Figure 3.11 shows calibration details of the ER10C. The ER10C probes may be categorized into three types based on their calibration pass/fail frequency range.

With careful investigation to find out the reason of the calibration failure both physically and theoretically, we hypothesized that the problem is in the electrical crosstalk based on the experimental data shown in Fig. 3.12 and Fig. 3.13. When we blocked the ER10C microphone, sound signal cannot pass through the acoustic sound path of the microphone. Therefore the acquired data from the microphone should be similar to noise floor. The result that we had in Fig. 3.12 does not agree with this fact, meaning that it is experiencing electrical crosstalk. One might assume that imperfectly blocking the hole may cause this result, but the signal would have been shown in low-frequency, not in high-frequency.

The long electric wire attached on ER10C probe head is the source of the electrical crosstalk. One ER10C was specially modified as requested to eliminate the capacitive coupling in blocked ER10Cs microphone response which was approximately 20 [dB] per octave or 60 [dB] per decade curve in high-frequency (Fig. 3.12). To remove the capacitive coupling caused by the ER10Cs long wire, we put the amplifier near the probe head. (The improved crosstalk result is introduced in Fig. 3.13.) A theoretical explanation of this can be found in Eq. 2.74, $\frac{\partial \mathbf{D}}{\partial t}$ term in Ampere's law, which is underestimated in the probe's design process.

3.3 A new probe design

Motivated by the published transducer model (Kim and Allen, 2013) as well as the experimental investigation of ER10C, we have designed improved measurement probes to extend middle ear diagnostics. These new acoustic probes, the MA16 and MA17, have been considered to enhance characteristics of the ER10C, such as sensitivity, frequency response, noise

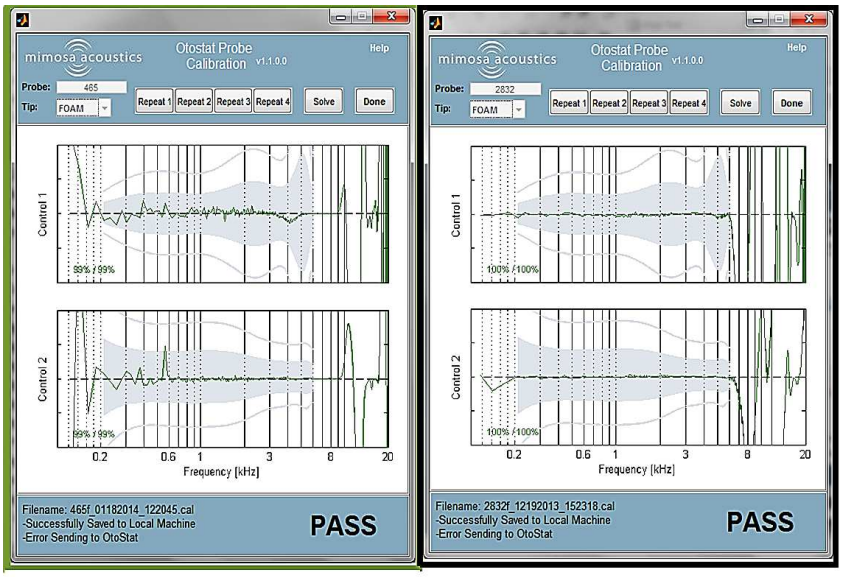

(a) Old good ER10C

(b) New good ER10C

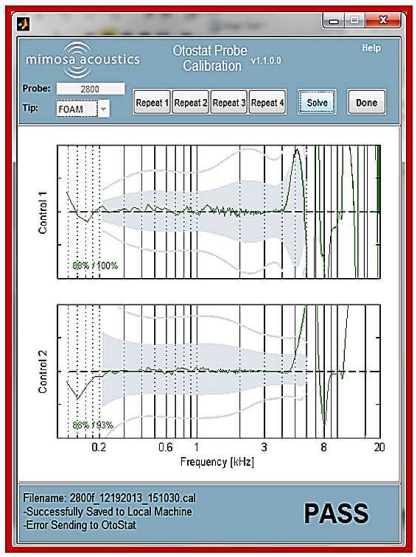

(c) New bad ER10C

Figure 3.11: (a) Brass material for the middle tube holder part (the brass holder). RTV silicon is used to block the holder's side hole. Calibration passes up to 9-10 [kHz] (ER10C with 3 digits serial number). (b) Aluminum material for the chamber. RTV silicon is not used to block the holder's side hole, but some of black material seals the side hole. Calibration passes up to 6 [kHz] (ER10C with 4 digits serial number). (c) Aluminum chamber is used. None of material seals the holder's side hole, a portion of the hole could be sealed randomly. Calibration totally fails or sometimes it passes but is unstable usually above 4 [kHz] (ER10C with 4 digits serial number). Also (based on the manufacturer), the type of wire used in ER10C has been changed.

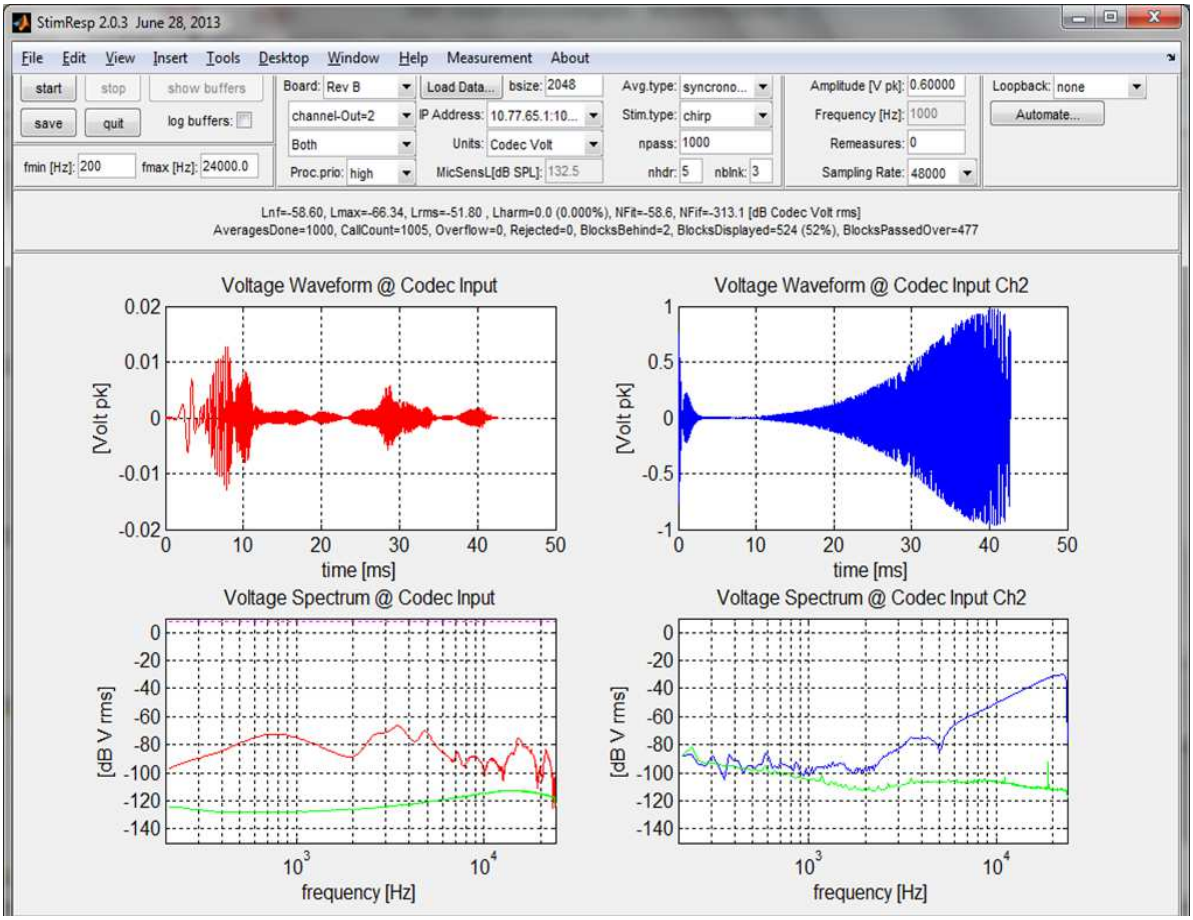

Figure 3.12: Original ER10C crosstalk (blue) with ER7C response (red): The sound (0.6 [V] chirp, zero to peak, not RMS) was generated by one of the internal ER10C speakers. The right (blue, channel 2) shows the blocked ER10C (serial: 2928) microphone response, and the left (red, channel 1) shows the E7C microphone response as a reference of the sound level. Note that we used a small cut syringe with a tiny volume to connect both ER7C microphone and ER10C probe. We blocked the microphone hole on the attached ER10C foam tip for decoupling the microphone path from the sound in the cavity generated by the internal ER10C speaker. Physically and theoretically, internal ER10C's sound paths for the microphones and the receivers are separated. Therefore if the microphone hole is blocked, none of the acoustic signal can go thorough the microphone's diaphragm. Any signal that is shown on the right side of this figure (blue) is internal crosstalk of the probe. We read that in high-frequency, the slope is approximately increased in proportion to 20 [dB] per an octave. Based on this observation, we hypothesize the source of this crosstalk is in wire of ER10C. This was the motivation of modifying ER10C, including the preamp on the ER10Cs head. Note that this measurement was made on May 14 2014 at Mimosa Acoustics by NK using Stimresp software (Mimosa Acoustics).

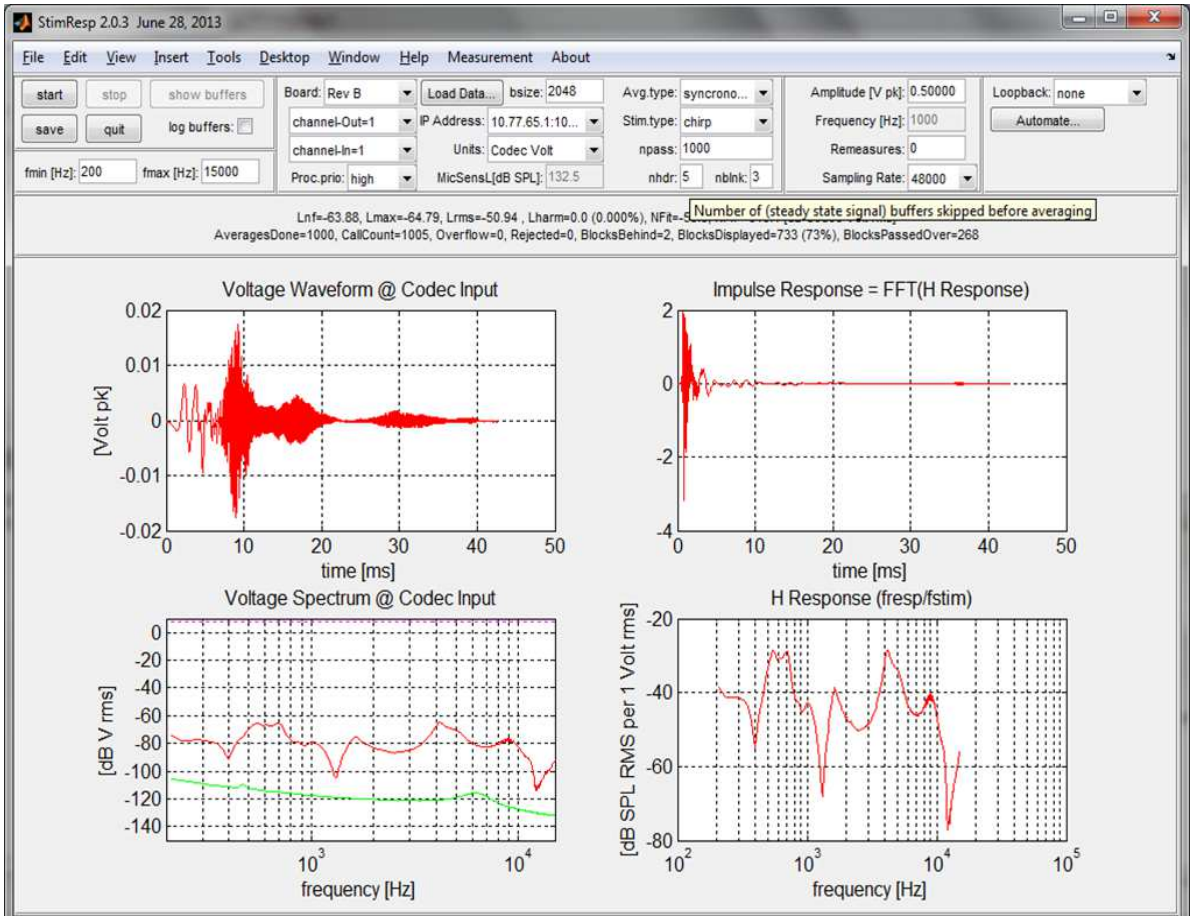

Figure 3.13: ER10C crosstalk (blue) after the modification; Crosstalk measurement after the modification, the rising crosstalk behavior in the high frequencies is apparently reduced. The modified ER10C is inserted in a short cavity with the blocked microphone. The probe is connected to the specially modified APU for the modified ER10C.

floor, and linearity.

We explain how we designed our hearing measurement probe based on the theoretical understanding of the probe's functions as well as trials and errors from experiments.

3.3.1 Choice of transducers

Two kinds of transducers are needed, a microphone and receiver. Based on the linearity of the receiver, (usually) we may need two receivers in a probe to measure, such as DPOAE.

Using a factory-calibrated microphone (i.e., BK2137 or ER7C), the sensitivities of both microphone and receivers should be measured in [mV/Pa] and [Pa/mV]. The industry standard for the microphone sensitivity is 50 [mV/Pa] at 1 [kHz].

Dynamic range (or linearity) of the probe defines the usable range of the probe in terms of both frequency range and the level of the signal.

Based on the all of the above, we can choose the right combination of microphone and receiver.

3.3.2 Sound delivery path for the microphone

The microphone picks up the sound inside a space such as a testing cavity, ear canal, or artificial ear. Though there are many modes in the spreading waves, namely higher order modes (HOMs) in the space, what we really consider is the plane wave, which is easy to analyze, especially for the source calibration procedure; the HOMs may be ignored if there is a sufficiently large distance in the system over which they will die out exponentially. Here are experimental technicalities for performing a simple calibration procedure, assuming the microphone is used to measure an ideal cylindrical cavity.

1) Center the microphone port, pointing the cavity end.

2) About 3 [mm] of tube is needed in front of the microphone's port to pick up the plane wave. Note that the HOMs die out within a few millimeter once the wave starts to spread from the source.

3) When the frequency response of the microphone is not flat (dividing the microphone response to an ideal microphone), introducing peaks, it usually means the microphone tube is too long. One may use a loosely packed cotton or acoustic resistor to minimize the tube effect.

3.3.3 Sound delivery path for the receiver

When sound is generated from a receiver, it is guided by its port and then spreads out. An ideal speaker has a flat frequency response regardless of the signal level, maintaining a constant level across all frequencies. But the reality is that distortions are observed due to high peaks (in pressure) at certain frequencies if we drive high voltage level to the receiver. There is not a linear relationship between the level of the distortion and the level of signal, due to the hysteresis effect of a electromagnetic system. Indeed the BAR is a really noisy device to deal with. Here are systematic procedures to handle this device when we make a probe.

1) Finding out the linear region of this transducer (dynamic range) based on the given sensitivity is critical.

2) Instead of acoustic resistors, a small piece of cotton (loosely packed) can be applied to the sound spreading area inside the probe. This will help not only to damp out the pressure peak at the certain frequency point but also to design the wave spreading space close to the ideal shape (i.e., cylinder).

3.3.4 Probe evaluation

The following is a list of specifications to evaluate a hearing measurement probe:

1) Frequency responses of both microphone and speaker should be as flat as possible, especially within the frequency range of human hearing (ideally up to 20 [kHz] for the microphone and up to 16 [kHz] for the speaker).

2) Thevenin parameters must be stable over time. This can be evaluated via source calibration (i.e., four-cavity calibration, Allen (1986)).

3) Output levels for loudspeakers should be higher for amplification of the signal, especially for measuring hearing impaired ears. (i.e., 85 [dBSPL] is desirable).

4) Dynamic range as large as possible. Dynamic range is defined as the subtraction between the first harmonic level and the total harmonic level at each frequency (i.e., 50-60 [dB] is acceptable).

5) Linearity superior to current probes. Dynamic range should be linear across the frequency range of interest.

6) Impulse response should be short and exact. The duration of impulse ringing should be less than 1 [ms]. This result is critical to TEOAE (transiently evoked otoacoustic emissions) measurement.

7) Crosstalk issues including all noise sources must be addressed, such as a microphone and a loudspeaker.

8) Good seal and stability in the ear canal. This needs good earplug design to fit a range of adult ear-canal sizes and shapes easily.

The size of the probe is an especially critical factor in the clinic for measurements of infant ears, due to their very small ear canals. There are other serious issues relevant to manufacturing a probe, such as handling ear tips, removing ear wax, etc., which must be taken into account in the probe design.

A general acoustic measurement setup (to test the itemized evaluation categories) is found in Fig. 3.14.

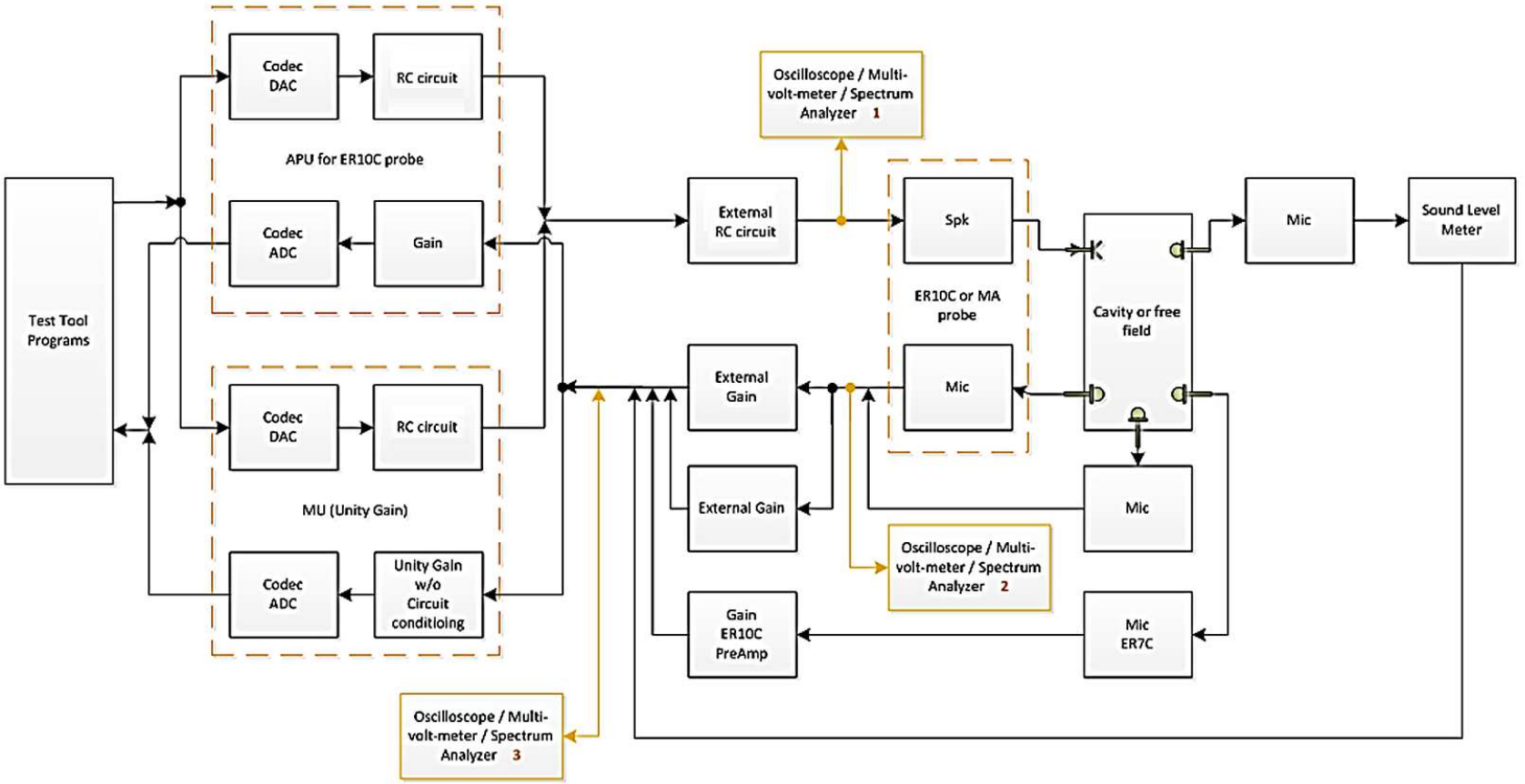

Figure 3.14: Basic acoustic testing setup.

The cavity or free field block can be the DB100 or B&K4157 artificial ear coupler, a cut-off syringe, any tube, or any rigid cavity in which the probe may be sealed. The probe block can be any probe containing a loudspeaker and a microphone (or two microphones). The probes we have used include the ER10C and MA probes. We also use a probe simulator[3] to evaluate the electronic part of the system, in order to provide a baseline for the probe's performance characteristics.

In our specific experiments, two audio processing units were used, an APU and MU (Audio Processing Unit and Modified Unit by Mimosa Acoustics). The APU is built for use with the ER10C probe. The other, the MU, is built to by-pass the internal RC (a parallel combination of a resistor R and a capacitor C to boost up the signal level in the high-frequency region) of the ER10C probe, setting the gain to unity. The MU is used for the other probes, such as the MA probes and ILO probe from Otodynamics. When using the MU with these other probes, an external RC circuit and preamp can be added for evaluation.

Several microphones can be used for calibration of the transducers used in the probe, to measure the receiver and microphone sensitivities, frequency responses, and other characteristics. The microphone (Mic, the previous stage of the Sound Level Meter in Fig. 3.14) and ER7C microphone (Mic ER7C in Fig. 3.14) are reference microphones, which have wide and flat frequency responses. When both the reference microphones and the tested probe microphone pick up the response from the test cavity, the tested microphone's response is divided by the reference microphone's response to obtain the test microphone frequency response.

An oscilloscope, spectrum analyzer, or multi-meter can be used to monitor the voltage at various points of the setup. In this setup, the specific points of interest are at

1) the input to the tested probe speaker for computing the receiver sensitivity,

2) the output of the tested probe microphone, and

3) the output of the external gain for computing the microphone sensitivity.

To check the frequency response of the transducers, it is necessary to calibrate the transducers (receivers and microphone inside the probe). Once we calculate the sensitivity of the transducer, we can compute the frequency response of the probe by applying a chirp signal and normalizing the response with the sensitivity at 1 [kHz].

[3]A package of circuit elements to simulate the electrical part of the probe excluding the acoustic elements.

CHAPTER 4

RESULTS

In this section, we represent key results based on our theoretical and experimental study (Chapters 2 and 3). Details of modeling BAR and its calibration results using Hunt parameters are discussed. Then, we reduce the BAR model to a simple electromechanic system, only involving essential circuit components for composing the system. This minimized model is used for Z_{mot} simulations to justify our theory discussed in Chapter 2.

4.1 Hunt parameter calibration

The calculated Hunt parameters of the BAR derived from various Z_{in} (Fig. 3.2) are shown in Fig. 4.1. Some considerations for the Hunt parameters of the BAR are as follows:

1) $\mathbf{Z_e}$: Compared to $Z_a(s)$ and $T_a(s)$, $Z_e(s)$ has the smallest dependency on the choice of load cavities (the three of six chosen load impedances: loads (2)-(7) in Fig. 3.2). Below 200 [Hz], $Z_e(s)$ converges to a fixed resistance (ED7045: $\approx$ 195 [Ω]). The frequency range between 0.5 and 2.5 [kHz] is proportional to s (Z_e shows a slope of 1 in this frequency range). It is not clearly shown at frequencies below 10 [kHz]; however when the frequency increases, the slope of Z_e approaches that of $\sqrt{s}$. More precise evidence of $\sqrt{s}$ domination at high-frequency is shown in Fig. 3.3 in the polar plot. This frequency dependant impedance behavior (e.g., proportional to a constant, s and $\sqrt{s}$) is determined by the coil properties, which are closely related to the DC resistance, inductance and the semi-inductance. Note that Z_{in} (measured) $\rightarrow$ Z_e (calculated) as $V \rightarrow 0$.

2) $\mathbf{Z_a}$: For frequencies below 2.5 [kHz], Z_a is stiffness dominated (i.e., a capacitance), and between 2.5 and 4 [kHz] it is dominated by the mass of the diaphragm and armature. Those properties determine the first anti-resonance (zero, near 2.5 [kHz]). The resonance (pole) at 3.7 [kHz] is the frequency where the transfer impedance, T_a, is maximum. The pole of Z_e is also introduced in this same frequency. As T_a and Z_a are tied more closely, they move together when the set of Hunt parameter is changed while

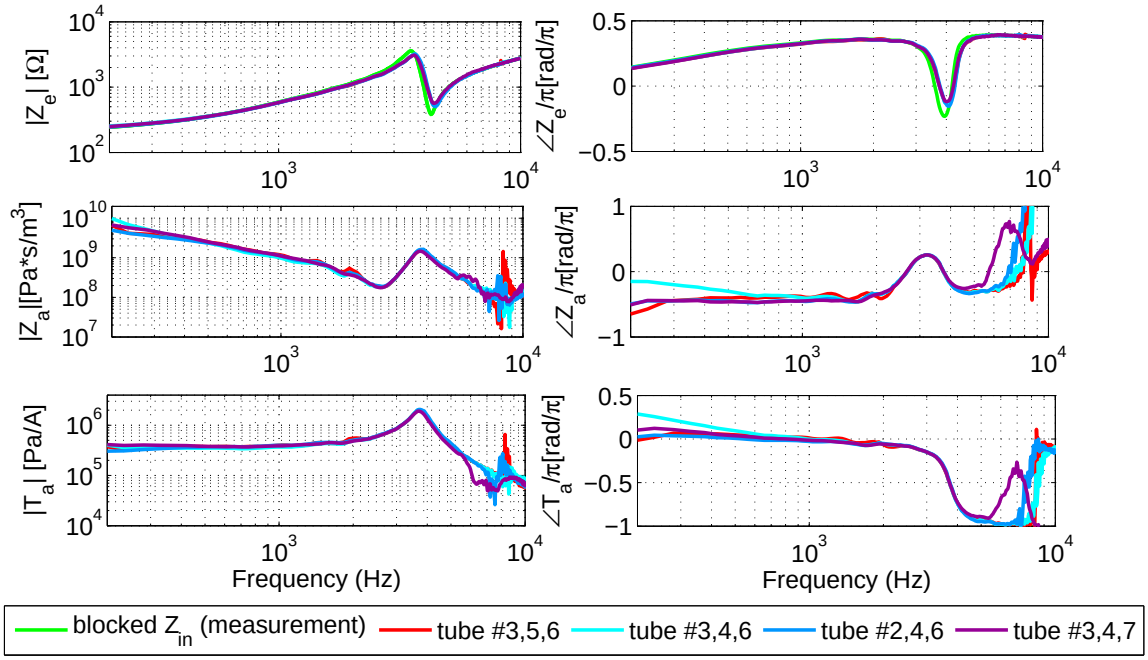

Figure 4.1: Calculated Hunt parameters (Z_e, Z_a, and T_a) of the ED7045. Three measurements of Z_{in} with acoustic loads (indicated by number as shown in the legend) are required to find one set of the three Hunt parameters. The length of each numbered tube is shown in Fig. 3.2. Z_{in}, which is measured by blocking the receiver's port ($V = 0$), is plotted with Z_e (green line).

Z_e is almost identical over every set of the Hunt parameters (Fig. 4.2). Above 4 [kHz] the transmission line and acoustic properties dominates given the small volume inside the receiver. The error above 6 to 7 [kHz] is primarily caused by the experimental limitations, such as the manual manipulation of the tubes.

3) $\mathbf{T_a}$: It is nearly constant below 2 to 3 [kHz] and is 4×10^5 [Pa/A] at 1 [kHz]. The phase shift in T_a is due to acoustic delay. Although the frequencies above 6 [kHz] are obscured by the noise, T_a behaves as an all-pole function, which depends on the system delay τ. To account for this delay, a transmission line (Tx line) is added to the acoustic model, as shown in Fig. 1.1.

4.2 Receiver model

In this section, we discuss details of our refined BAR model introduced in Fig. 1.1. The electrical circuit elements are shown to the left of the gyrator. R_e is approximated to the DC resistance. The source of the armature movement is the Lorentz force ($F = \int J \times BdA$) due to the interaction of the current in the coil and the static magnetic field B_0 of the magnets. The current in the coil and the core of the E-shaped armature give rise to the inductance L_{em}, while the penetration of the magnetic field into the core induces an eddy current, depicted by a semi-inductor element K_1 (see, Fig. 1.1 in Chapter 1). The L_e represents any leakage flux, in an air gap, which explains an additional small stored energy. The specific values for the BAR model is shown in Table 4.1.

There should be a transition frequency, $f_t = \frac{1}{2\pi}\left(\frac{K_0}{L_0}\right)^2$, between the inductor ($L_0$) and the semi-inductor (K_0). Since we used two inductors and one semi-inductor (total of 3) for our receiver model, it is unclear exactly how to calculate the f_t from these components as we discussed in Section 4.1. However as shown in Fig. 4.3 (polar plot), the slope of the impedance is approaching $\sqrt{s}$ (45^o) as ω increases. Based on Thorborg et al. (2007), the f_t of a dynamic loudspeaker is 100 to 200 [Hz], which means the f_t for the balanced armature receiver is much higher than for the moving coil loudspeaker.

The gyrator relates the electrical and the mechanical sections with parameter $T = B_0 l$. The wire inside the ED7045 receiver is made of 49 AWG copper, which has a resistivity of 26.5 [Ω/m]. Since the measured DC resistance of the receiver is around 190 [Ω], we can calculate the length of the wire is approximately 7.1 [m]. In general, the dynamic moving-coil speaker's length is shorter than the BAR's. Therefore we can expect a larger T value for the BAR ($n \propto l$, $1/d_{coil}$).

To the right of the gyrator are the mechanical and acoustical sections of the transducer.

Table 4.1: Specific parameters that are used for the suggested model (Knowles BAR ED7045). where c is the speed of sound in the air (334.8 [m/s]), $j\omega/c$, z_0, and l_t are the propagation function, specific characteristic resistance and length of the transmission line, respectively. GYR and TRF stand for the gyrator and the transformer. All model parameters were found by minimizing the RMS error between the model and electrical input impedance measurements of the receiver.

Electrical elements
$R_e = 195$ [Ω],
$L_e = 9$ [mH],
$K_1 = 27.5$ [Semi-Henry], $L_{em} = 52$ [mH]
GYR $= 7.5$
Mechanical elements
$C_m =$ 1.25e-3 [F], $L_m =$ 4.3e-6 [H], $R_m = 0.003$ [Ω]
TRF (1/Area) $= 1/(2.4e^{-6})$
Acoustical elements
$C_a =$ 4.3e-15 [F]
Tx Line: $z_0 =$ 1e9 [kg/sec], $l_t =$ 1e-4 [m]
Radiation impedance
$L_{rad} = 10^{10}$ [Acoustic-Henry], $R_{rad} = 10^{11}$ [Acoustic-Ohm]

We can simply describe the mechanical section as composed of a series combination of the armature and the diaphragm's stiffness, mass, and damping. The transformer's coupling ratio of the acoustic side to the mechanical side is related to the diaphragm's area. The capacitor (C_a) and a transmission line in the acoustical part account for the back (rear) volume and sound delay. Because we are using a gyrator, the mobility analogy method is not used (Beranek, 1954; Hunt, 1954).

The Thevenin pressure of the BAR is defined given that the volume velocity (V) at the port is zero (blocked port), meaning the load impedance is set to ∞.

Several comparisons are made to verify the transducer model. First, the Hunt parameters are calculated from the model to support the transfer relation between electrical and acoustical parts (Section 3.1.1). The mechanical part of the transducer model was verified by conducting laser mechanical velocity measurements in a vacuum condition (Section 3.1.2). Along with these results, we simulated the Thevenin pressure of the transducer from our model and compared the result to the pressure measurement (when $V = 0$) (Section 3.1.3). These three comparisons (electrical, mechanical, and acoustical) justify and verify the transducer model (Fig. 1.1).

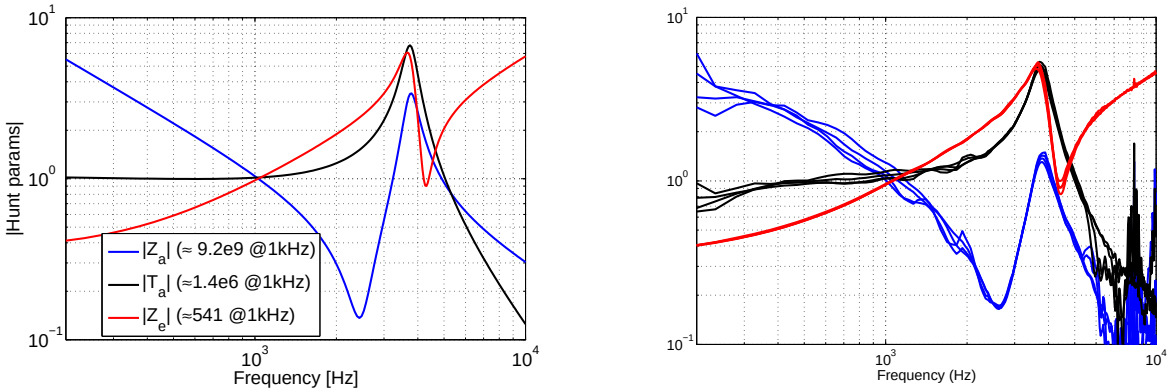

(a) Hunt parameters from the model

(b) Hunt parameters from measurement

Figure 4.2: Comparison of Hunt parameters (Z_e (red), T_a (black), and Z_a (blue)) from the model (a) and the measurements (b). Any significant differences between the model and the data occur above 6 [kHz]. All parameters are normalized to their 1 [kHz] values.

4.2.1 Hunt parameters comparison

The Hunt parameters, from the model and the experimental calculation, are compared in Fig. 4.2. The discrepancies of Z_a above 6 to 7 [kHz] are presumably caused by the manual adjustment of the experimental conditions. This error is insignificant in Z_e. However, the small noise in electrical impedance impacts the parameter estimation far from the electrical side. In other words, we can see the largest variation in acoustical parameter (Z_a), as the transition order goes from $Z_e \rightarrow T_a \rightarrow Z_a$.

Another interesting parameter is the resonant frequency (3 to 4kHz). The frequency of the pole (f_p) in Fig. 4.2 looks almost identical to each parameter: Z_e. Z_a and T_a slightly differ by the set, but the f_p of the three parameters occurs at the same location for the same set of Hunt parameters. The three parameters assume the zero-loaded condition, which means, in theory, the f_p should be identical for all cases. Because of small measurement differences, this is not exactly the case. This resonant frequency can thus be interpreted as one of the most fundamental characteristics (eigenmode) of an electromagnetic transducer.

4.2.2 Verification 1: Electrical impedance *in vacuo*

The acoustical part in the transducer model is removed for the vacuum case, while all the electrical and mechanical parameters in Fig. 1.1 during the experiments remain the same as the no-vacuum condition.

In Fig. 4.3, the simulated electrical input impedance results are expressed in two ways: the magnitude-phase and the polar plot (real vs. imaginary parts). For both the vacuum

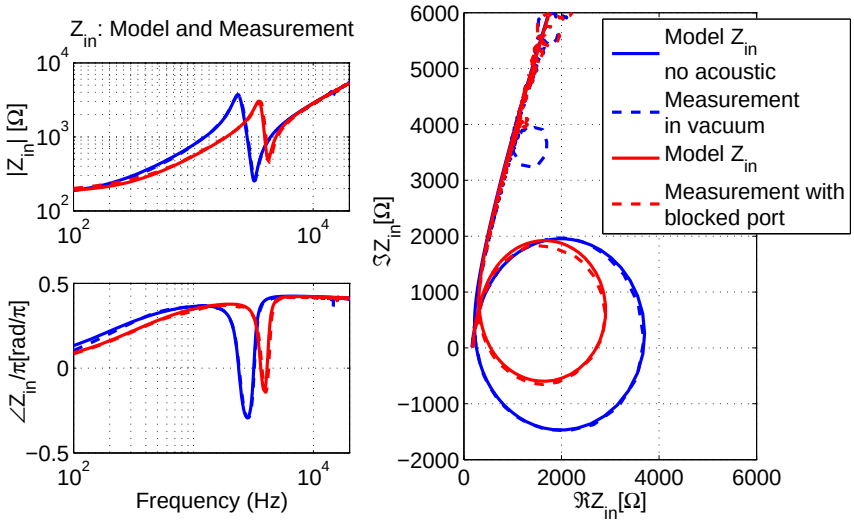

Figure 4.3: Comparison of the suggested model of Fig. 1.1 and real electrical input impedance measurement of a balanced armature hearing-aid receiver (Knowles, ED7045). Blue and red colors represent vacuum and non-vacuum (ambient) conditions, respectively. The dashed lines represent the experimental result, whereas the single lines show the model results. For the vacuum experiment, the static pressure is less than 0.003 [atm]. The left panel shows the magnitude and the phase of each condition while the real and imaginary parts of the same data are plotted in the right panel. Up to 23 [kHz], the experimental data is in good agreement with the modeling result. (The sampling rate is 48 [kHz]; therefore the maximum measured frequency is 24 [kHz].) In the polar plot, above 8 [kHz], the impedance behaves as $\sqrt{s}$.

and the blocked port condition, the model (solid lines) and the experiment result (dashed lines) show reasonable agreement below $\approx$ 12 [kHz].

The transducer model, including acoustical elements (blocked output port) is in red, and the model excluding acoustical elements (vacuum condition) is in blue. Both cases give the similar shape, a pole, followed by a zero, with increasing frequency ($\approx$890 [Hz] in vacuum, $\approx$750 [Hz] in blocked case). We conclude that the trapped air (between the diaphragm and the port of the receiver) influences the resonance by pushing it to higher frequencies due to the increased stiffness-to-mass ratio. Also because of the acoustical properties (including mechanical-acoustical coupling), the magnitude of the vacuum resonance is reduced by 1.9 [dB] compared to the blocking the receiver's output port (in air).

By looking at the polar plot (the right panel in Fig. 4.3), we can clearly see that the high-frequency impedance is dominated by $\sqrt{s}$, clear evidence of the eddy current, in the BAR. The many small loops appearing above 16 [kHz] may be a measurement artifact; however, the second resonance at 15 [kHz] is real.

4.2.3 Verification 2: Mechanical velocity measurement using laser *in vacuo*

As shown in Fig. 4.4, the mechanical velocity is also calculated from the transducer model and compared with the laser velocity measurement result. The model and the experiment are well matched below 10 [kHz].

However, a small magnitude difference is observed; the laser measured data has about 1 [dB] higher velocity at the FR and the low-frequency area. There are some possible solutions to improve the model. First, as explained in Section 3.1.2, when we make the measurement, we put the laser's focus near at the rod (where the armature and the diaphragm is connected). And secondly, when modeling the data, we could add or remove mechanical damping in the transducer model (i.e., increasing or decreasing the value of R_m in our model Fig. 1.1) relative to the present value. The problem below 200 [Hz] is due to a very small hole that is burned into the diaphragm, to act as a very low-frequency leak.

The mechanical velocity is calculated by assuming the force (F) *in vacuo* is zero. In reality, it is impossible to reach an absolute vacuum condition. Our experimental condition of 0.003 [atm] seems adequate to understand the nature of the mechanical velocity of the transducer, as the measurement gives a reasonable agreement with the model.

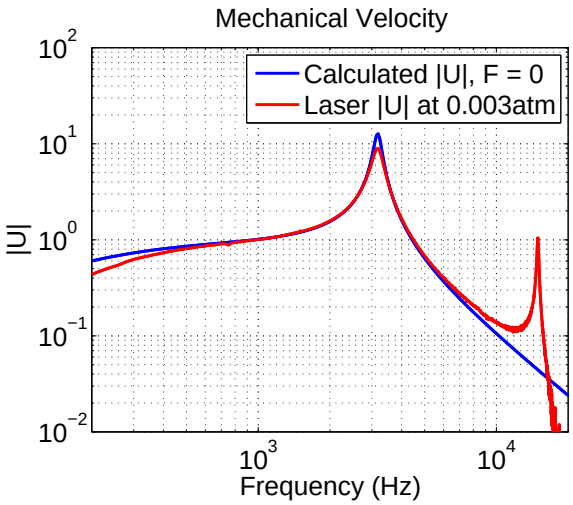

Figure 4.4: Comparison of the diaphragm (mechanical) velocity between the transducer model and the laser measurement *in vacuo*; the pressure P is zero. For the model simulation, the acoustical part in Fig. 1.1 is not included. The laser measurement was performed after pumping out the air in the receiver. All values are normalized to one at 1 [kHz].

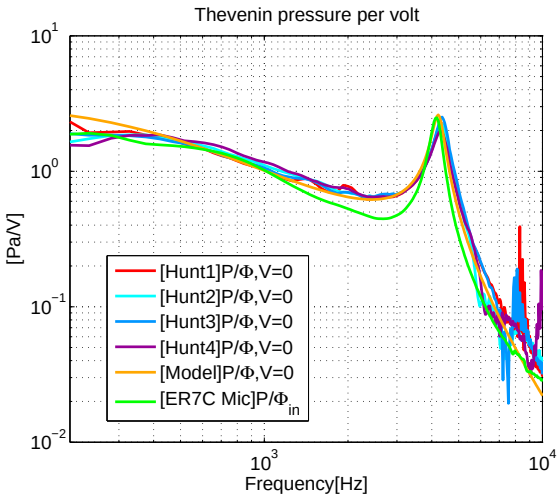

Figure 4.5: Comparison of Thevenin pressure (per voltage) data from various sources. There are six different lines; the first four lines are calculated from the electrical experiments (Hunt parameters), and the orange colored line is estimated from the model. The last pressure data (in light green) are taken from the pressure measurement and are divided by the electrical input voltage of the receiver. All data assume the blocked condition, V=0 (see text). Every value is normalized to one at 1 [kHz].

4.2.4 Verification 3: Thevenin pressure comparison

The model and measured Thevenin pressure are plotted in Fig. 4.5. Two indirect pressure estimation methods are used: one using the Hunt parameters, and the other using the simulation of our transducer model. There is a reasonable agreement among these measures up to 6 to 7 [kHz]. The mathematical definition of these data is the Thevenin pressure per unit voltage (P/Φ), with a zero volume velocity ($V = 0$),

$$\left.\frac{P}{\Phi}\right|_{V=0} = \left.\frac{T_a}{Z_e}\right|_{V=0}. \tag{4.1}$$

Note that $\frac{P}{I}$ and $\frac{P}{\Phi}$ differ in the theoretical meaning as well as in the definition; $T_a \equiv \left.\frac{P}{I}\right|_{V=0}$ is one of the Hunt parameters, while the Thevenin pressure (per volt) in Eq. 4.1 is a more realistic experimental function, when one uses a voltage drive. For the comparison, the pressure data is divided by the voltage (Φ_{in}) across the two electrical terminals of ED7045 (see the circled A and B in Fig. 3.5 in Chapter 3) when $V = 0$. The data from Section 3.1.1 is imported for Φ_{in}, assuming $V = 0$ at the port in the pressure measurement.

The green line in Fig. 4.5 shows the Thevenin pressure data derived from the ER-7C probe microphone. Other than the direct pressure measurement (green), all responses are derived from the Hunt parameter calculation introduced in Appendix E, using the electrical input impedance measurements for acoustical loads.

4.3 Z_{mot} simulation of simplified electromechanic systems

For further application, we will investigate a simple electromechanic network model including a semi-inductor. The goal is to demonstrate some condition that $\Re Z_{mot} < 0$ based on the simplified electromechanic model. The simple electromechanic model has been reduced from Kim and Allen's original work (Fig. 1.1: the electroacoustic network model; Kim and Allen (2013)). Related theories are discussed in Section 2.4 and Appendix B.

The left side figure in Fig. 4.6 shows a oversimplified two-port network from Fig. 1.1 containing only essential components for better and easier understanding of the physical electromechanic system. In this simple model, any acoustic or resistive components are eliminated.

In this figure, we have four components: a semi-inductor, an inductor in the electrical port, a mass in the mechanical port, and a gyrator that links the two ports.

The two circuits in Fig. 4.6 represent equivalent circuits via the mobility (dual) analogy. In both, at very low and high frequencies the capacitor m is opened. The parallel relation

of semi-inductor and inductor enables the semi-inductor's high-frequency dominance (Vanderkooy, 1989). The mid frequency is governed by the inductor L and the capacitor m. If we ignore the semi-inductor in Fig. 4.6, the system looks like a Helmholtz resonator with neck mass L and barrel compliance m. Therefore these two components act like a resonator in the system.

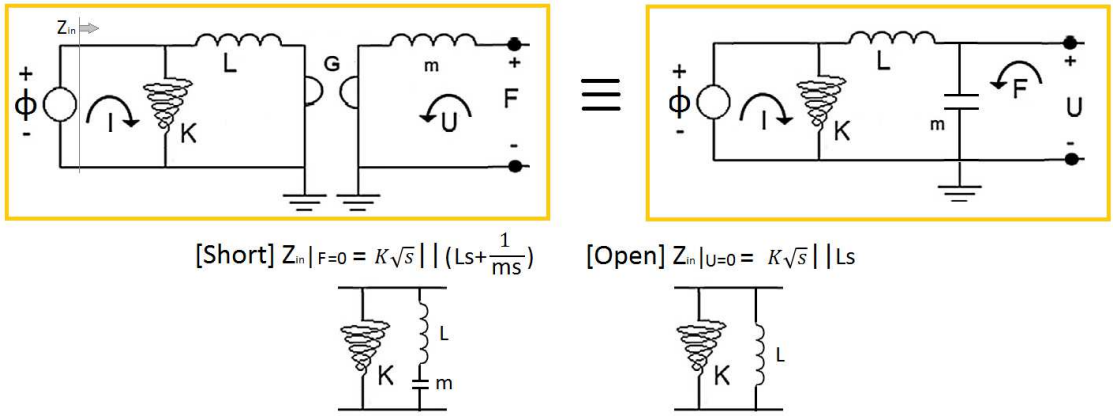

Figure 4.6: The top left circuit: A simple anti-reciprocal network with a semi-inductor presence. The top right circuit: The dual representation of the left circuit (equivalent) by applying the mobility analogy beyond the gyrator. Z_{mot} is reconsidered based on Eq. 2.43. The frequency dependent real parts (shunt loss) of the semi-inductor in $Z_{in}|_{F=0}$ (short) experience positive phase shift when the open condition impedance ($Z_{in}|_{U=0}$) is subtracted from it.

To realize this system into a matrix form, we can use the ABCD matrix cascading method, which results in Eq. 4.2.

$$\begin{bmatrix} \Phi(\omega) \\ I(\omega) \end{bmatrix} = \begin{bmatrix} 1 & 0 \\ \frac{1}{K\sqrt{s}} & 1 \end{bmatrix} \begin{bmatrix} 1 & sL \\ 0 & 1 \end{bmatrix} \begin{bmatrix} 0 & G \\ \frac{1}{G} & 0 \end{bmatrix} \begin{bmatrix} 1 & sm \\ 0 & 1 \end{bmatrix} \begin{bmatrix} F(\omega) \\ -U(\omega) \end{bmatrix}, \tag{4.2}$$

where s is the Laplace frequency ($\sigma + j\omega$) and L, K, G, and m are the inductance, the semi-inductance, the gyration coefficient, and the mass of the system respectively.

Let us isolate the ABCD matrix part in Eq. 4.2 and set L, K, G, and m to be 1 to make the algebra a simple calculation. Then the equation is reduced to

$$\begin{bmatrix} 1 & 0 \\ \frac{1}{\sqrt{s}} & 1 \end{bmatrix} \begin{bmatrix} 1 & s \\ 0 & 1 \end{bmatrix} \begin{bmatrix} 0 & 1 \\ 1 & 0 \end{bmatrix} \begin{bmatrix} 1 & s \\ 0 & 1 \end{bmatrix} = \begin{bmatrix} 1 & s \\ \frac{1}{\sqrt{s}} & \frac{s}{\sqrt{s}} + 1 \end{bmatrix} \begin{bmatrix} 0 & 1 \\ 1 & s \end{bmatrix}. \tag{4.3}$$

Finally the ABCD matrix of the system in Fig. 4.6 is

$$\begin{bmatrix}\Phi(\omega)\\ I(\omega)\end{bmatrix} = \begin{bmatrix}T_1\end{bmatrix}\begin{bmatrix}F(\omega)\\ -U(\omega)\end{bmatrix} = \begin{bmatrix}A(s) & B(s)\\ C(s) & D(s)\end{bmatrix}\begin{bmatrix}F(\omega)\\ -U(\omega)\end{bmatrix}$$
$$= \begin{bmatrix}s & 1+s^2\\ \frac{s}{\sqrt{s}}+1 & \frac{1}{\sqrt{s}}+\frac{s^2}{\sqrt{s}}+s\end{bmatrix}\begin{bmatrix}F(\omega)\\ -U(\omega)\end{bmatrix}, \quad (4.4)$$

where $\Delta_{T1} = -1$. Converting Eq. 4.4 into an impedance matrix, Eq. 2.7 is used to give us

$$Z_1 = \begin{bmatrix}z_{11} & z_{12}\\ z_{21} & z_{22}\end{bmatrix}, \quad (4.5)$$

where

$$z_{11} = \frac{s}{\frac{s}{\sqrt{s}}+1} = \frac{s\sqrt{s}}{s+\sqrt{s}} \ (\equiv s||\sqrt{s}) \ , \quad (4.6)$$

$$z_{12} = \frac{-1}{\frac{s}{\sqrt{s}}+1} = -\frac{\sqrt{s}}{s+\sqrt{s}}, \quad (4.7)$$

$$z_{21} = \frac{1}{\frac{s}{\sqrt{s}}+1} = \frac{\sqrt{s}}{s+\sqrt{s}}, \quad (4.8)$$

$$z_{22} = \frac{\frac{1}{\sqrt{s}}+\frac{s^2}{\sqrt{s}}+s}{\frac{s}{\sqrt{s}}+1} = \frac{1+s^2+s\sqrt{s}}{s+\sqrt{s}}. \quad (4.9)$$

By substituting s with $j\omega$ one can easily find that all impedances of this system (Eq. 4.6, 4.7, 4.8, and 4.9) are complex quantities, meaning that all have both real and imaginary parts in each frequency point. The results shown in Eq. 4.6 to Eq. 4.9 are a counter example that does not follow the traditional approach of a lossless LC network. In the other words, a lossy network has been realized without having a resistor in a system. We will show in the next section that this is due to the existence of the semi-inductor in a system by comparing a case where the semi-inductor does not exist.

Using Eq. 2.46, Z_{mot} of this system can be calculated as

$$Z_{mot1} = \frac{1}{(\frac{s}{\sqrt{s}}+1)(\frac{1}{\sqrt{s}}+\frac{s^2}{\sqrt{s}}+s)} = \frac{s}{\sqrt{s}+s+s^2+2s^2\sqrt{s}+s^3}. \quad (4.10)$$

For computational benefits, we can convert Eq. 4.10 to an admittance (Y_{mot}) to investigate

the real part of Z_{mot},

$$Y_{mot1} = 1 + (\sqrt{s})^{-1} + s + 2s\sqrt{s} + s^2 = 1 + (\sqrt{j\omega})^{-1} + j\omega + 2j\omega\sqrt{j\omega} + (j\omega)^2$$
$$= (1 - \omega^2 - \frac{2\omega\sqrt{\omega}}{\sqrt{2}} + \frac{\sqrt{\omega}}{\sqrt{2}\omega}) + j(\frac{2\omega\sqrt{\omega}}{\sqrt{2}} - \frac{\sqrt{\omega}}{\sqrt{2}\omega} + \omega). \quad (4.11)$$

Since ω is always greater than 0, the real part of Eq. 4.11 can have negative real parts if the equation satisfies

$$1 - \omega^2 - \frac{2\omega\sqrt{\omega}}{\sqrt{2}} + \frac{\sqrt{\omega}}{\sqrt{2}\omega} < 0. \quad (4.12)$$

For example, if we have an angular frequency ω=1 [rad/sec], Eq. 4.12 is satisfied ($1 - 1 - \sqrt{2} - \frac{\sqrt{2}}{2} = -\frac{1}{\sqrt{2}} < 0$). We can generalize if Y_{mot} is not positive then Z_{mot} is also not positive. In this specific example, any angular frequency (ω) which satisfies Eq. 4.12 can have negative resistance in Z_{mot} (Fig. 4.9). This Z_{mot} is not a positive definite quantity, which means it does not conserve the energy of the network.

Figure 4.7 represents the simulated Hunt parameters (Eq. 4.6 to Eq. 4.9). All impedances are complex, meaning both real and imaginary parts have frequency dependance. The two transfer impedances have the same magnitude but have 180^o angle difference in the complex domain. The input impedance is inductive, but as frequency increases the angle approaches 45^o . The output impedance behaves like a resonator with damping. Figure 4.8 shows the motional impedance and input impedances with both open and short circuit conditions. To help us understand better, one can think of the open circuit impedance when a system is demagnetized, and the short circuit condition when the system's free oscillation is in a vacuum.

4.4 Calibration results from both the modified and the manufactured probes

The probe's source calibration is the first and perhaps most critical step to characterize the probe system. Stable and accurate source parameters enable precise computation of the impedance of the acoustic load (impedance of a human ear). In the previous experiment section, we discussed several issues about existing probes and found the most common reason for calibration failure was crosstalk. Based on a solid understanding of the problem in the system, we physically modified and manufactured the probes to minimize the crosstalk effect in the system to calibrate the system above 6 [kHz]. As a result, the modified system can pass four-cavity (4C) calibration (Allen, 1986) above 10 [kHz]. The 4C calibration computes

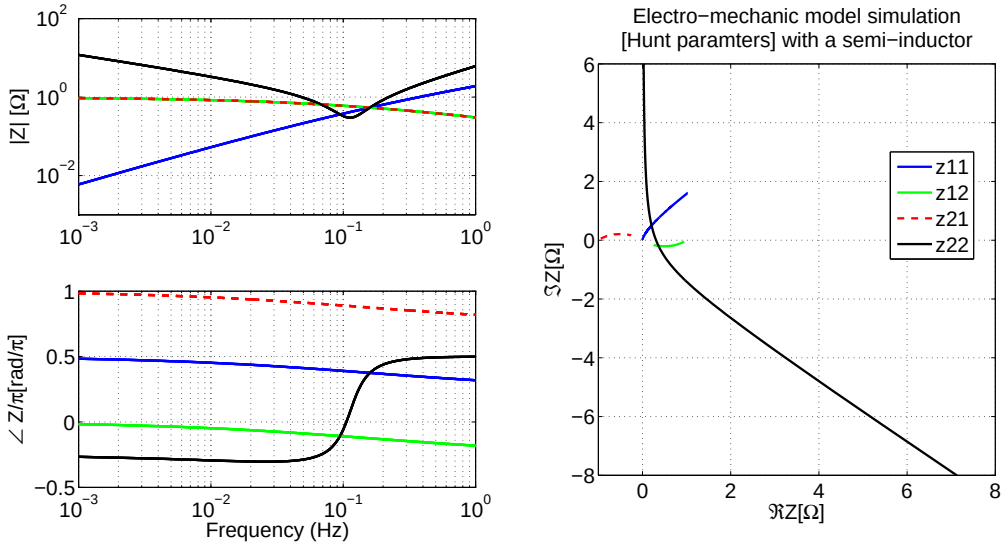

Figure 4.7: Computed Hunt parameters based on a simple electromechanic network shown in Fig. 4.6 (Eq. 4.6 to Eq. 4.9). All parameters K, L, G, and m are set to be 1 for a simple computation.

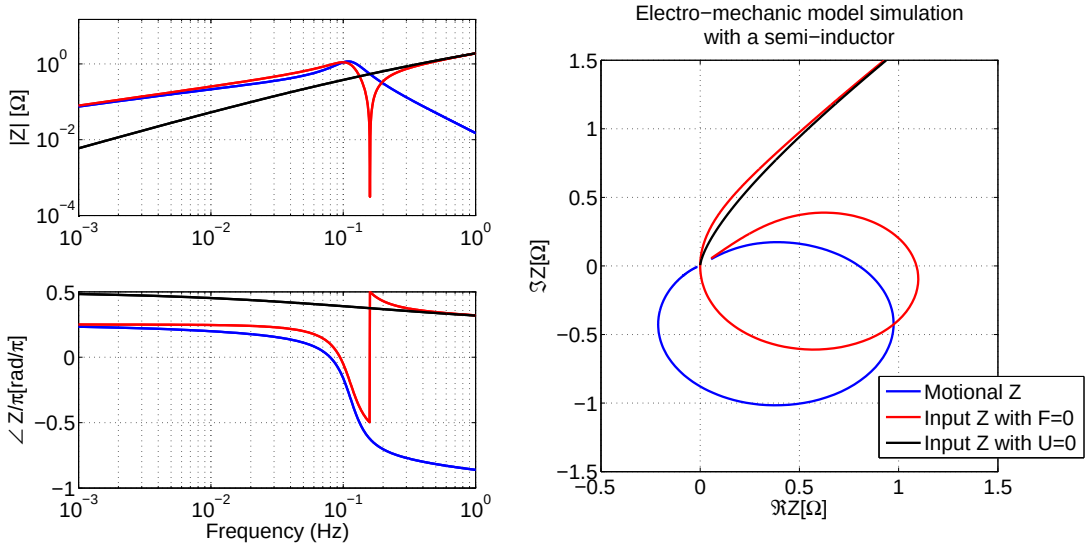

Figure 4.8: Computed motional impedance (Eq. 4.10), and input impedances with both open (Eq. 4.6) and short circuit conditions (Eq. 4.10 and Eq. 4.6) based on a simple electromechanic network shown in Fig. 4.6.

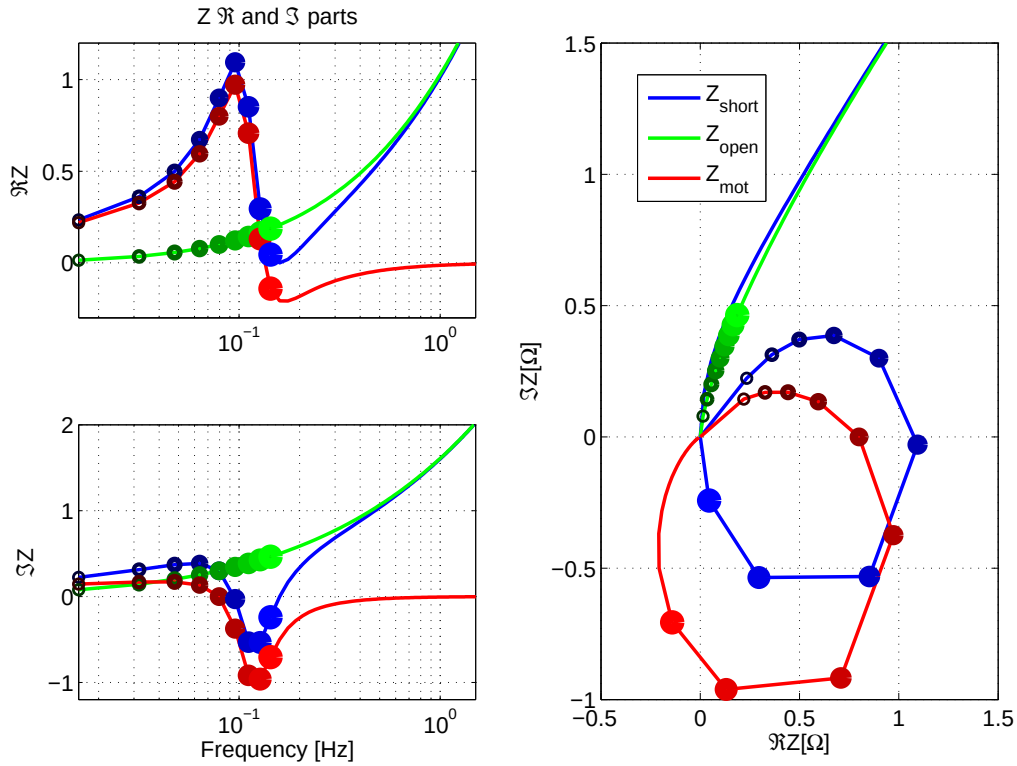

Figure 4.9: Real and imaginary parts of a simple electromechanic network shown in Fig. 4.6. The marker's size indicates increments in frequency. Between the 8^{th} and 9^{th} frequency points, the real parts of Z_{mot} goes negative.

the 4C lengths (L_k) and Norton parameters $P_s(f)$, $Y_s(f)$ based on the measured four cavity pressures, using a least-squares procedure.

Also the MA16 and the MA17 (our manufactured prototype probes) have comparable performance to the modified ER10C as shown in Fig. 4.10.

We believe that this study shows the electrical crosstalk may be a general problem for OAE hearing probe devices, which needs to be carefully addressed in the design process. This solution supports the importance of the $\dot{\mathbf{D}}$ neglected in classical KCL, as discussed in Section 2.5.2, the displacement current due to time varying electrical field. The capacitive coupling in the wire should be carefully considered when designing a probe.

4.4.1 The modified ER10C

The modification includes the modified ER10C containing a +14 [dB] differential amplifier, and a modified APU (Mimosa Acoustics) with a +20 [dB] differential amplifier whose output is fed directly into the APU's codec buffer amplifier. This modified system is shown in Fig. 4.11.

Compared to the original ER10C, this modified probe showed better performance as demonstrated in Fig. 4.12. This figure shows before and after characteristics of the ER10C modification compared to the theoretical values, particularly the change in sharpness of the acoustic null in each cavity (raw pressure data in a cavity with four different lengths). For example, if crosstalk is present at high frequencies, the pressure data around its corresponding null for the shortest cavity will be contaminated as shown (noisy notch in Fig. 4.12), the pressure null is hard to be matched to the theoretical result. With the low crosstalk probe, cleaner and sharper pressure acoustic nulls are detected, especially for the shortest cavity. One can also calculate the reflectance Γ of each cavity theoretically (Keefe, 1984), assuming that the load cavities have a perfect cylindrical shape.

This result will provide fundamental and operational understanding of not only the ER10C system but also hearing measurement devices in general.

4.4.2 Prototype probes: MA16 and MA17

Some efforts to make our own probe substitute for the ER10C can be found in the series of prototype probes that were made (i.e., MA4-8,6,12,13,14,16,17 series). Each series has four to six probes to demonstrate the strategy or idea highlighted at each stage. Finally we have demonstrated that our manufactured MA16 probe has a compatible performance to the modified ER10C probe, which has the best performance on the market. Design of

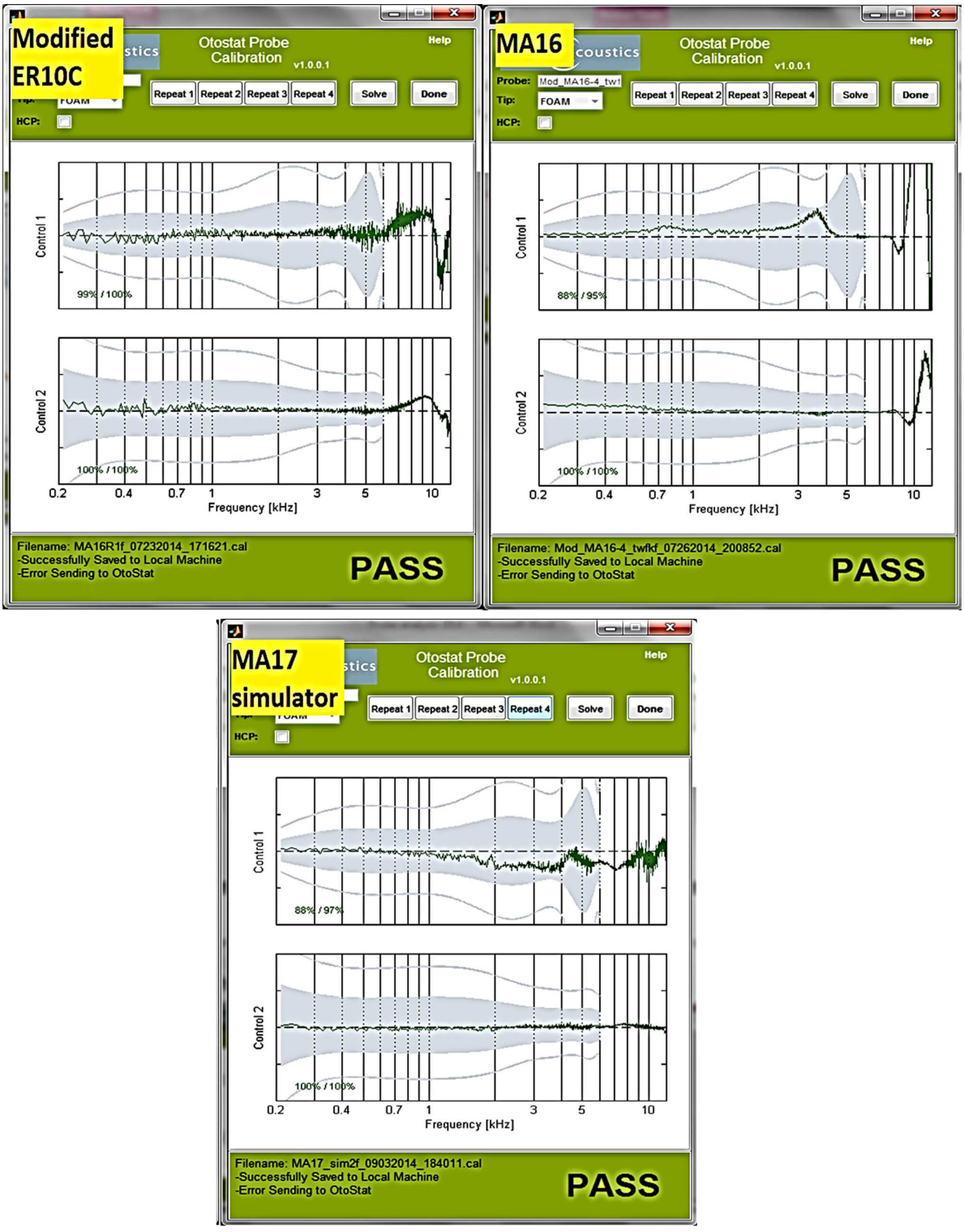

Figure 4.10: (Top left figure) Source parameter calibration result from the modified ER10C to diminish the crosstalk effect. The probe can be calibrated above 10 [kHz]. Based on this result, we concluded that the crosstalk was interfering with the calibration procedure. (Top right figure) MA16 calibration result. This result demonstrates that we made our own system which can pass the 4C calibration above 10 [kHz] as well, for the first time. (Bottom figure) MA17 simulator calibration result. To overcome some drawbacks of the MA16, especially the size, we have proposed a new probe design, namely MA17. Before manufacturing the probe, we simulated acoustics of the probe's structure to support the basic idea of the suggested design.

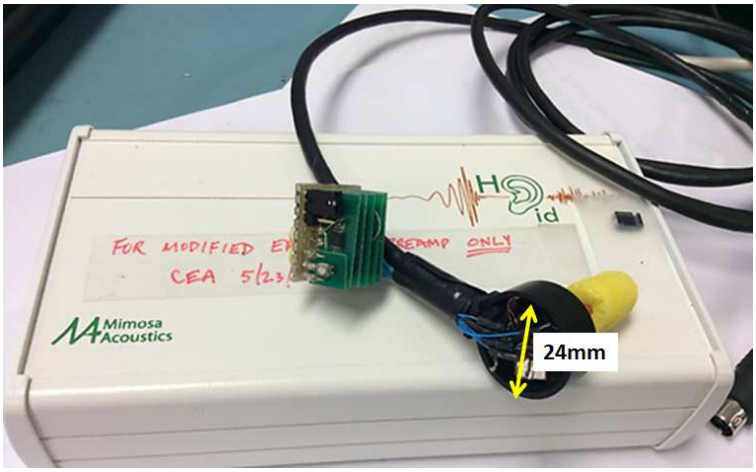

Figure 4.11: The purpose of this modification is to reduce crosstalk due to the long wire of the ER10C probe. This reveals that small changes in the wire may lead significant property changes of the probe. The key idea is to amplify the microphone signal before it passes through the long wire. Near the probe's head we placed amplifier as shown in this picture.

the MA17 is currently in progress to overcome drawbacks observed in the previous series, MA16. Compared to our target size specification, the size of MA16 is too large. Figure 4.13 (a) shows the MA16 probe when it is inserted in the MA cavity. The inside structure of the MA16 head is shown in Fig. 4.13 (b).

Based on appreciation of the fundamental theories relevant to the design of a hearing measurement probe, we proposed the MA17. Before manufacturing the probe, the probe's acoustic characteristics were simulated using the MA17 simulator (Fig. 4.14). The Knowles FG23652 microphone and ED27045 receiver were used for the simulator. The ER7C was used as a reference microphone. To hold the transducers in a syringe, a piece of cut-foam was used, and cotton was used to center the microphones. The key idea of this structure is to line up all transducers inside of the probe. Also for the 4C calibration, when we change cavity lengths, the junction between probe's head and the cavity entry is smooth. Therefore the acoustic load (cavity) can be more similar to the ideal cylinder shape. To change the length using a piston, we need to open and close a small hole (using a piece of putty) to adjust the pressure inside the syringe every time we change the cavity length.

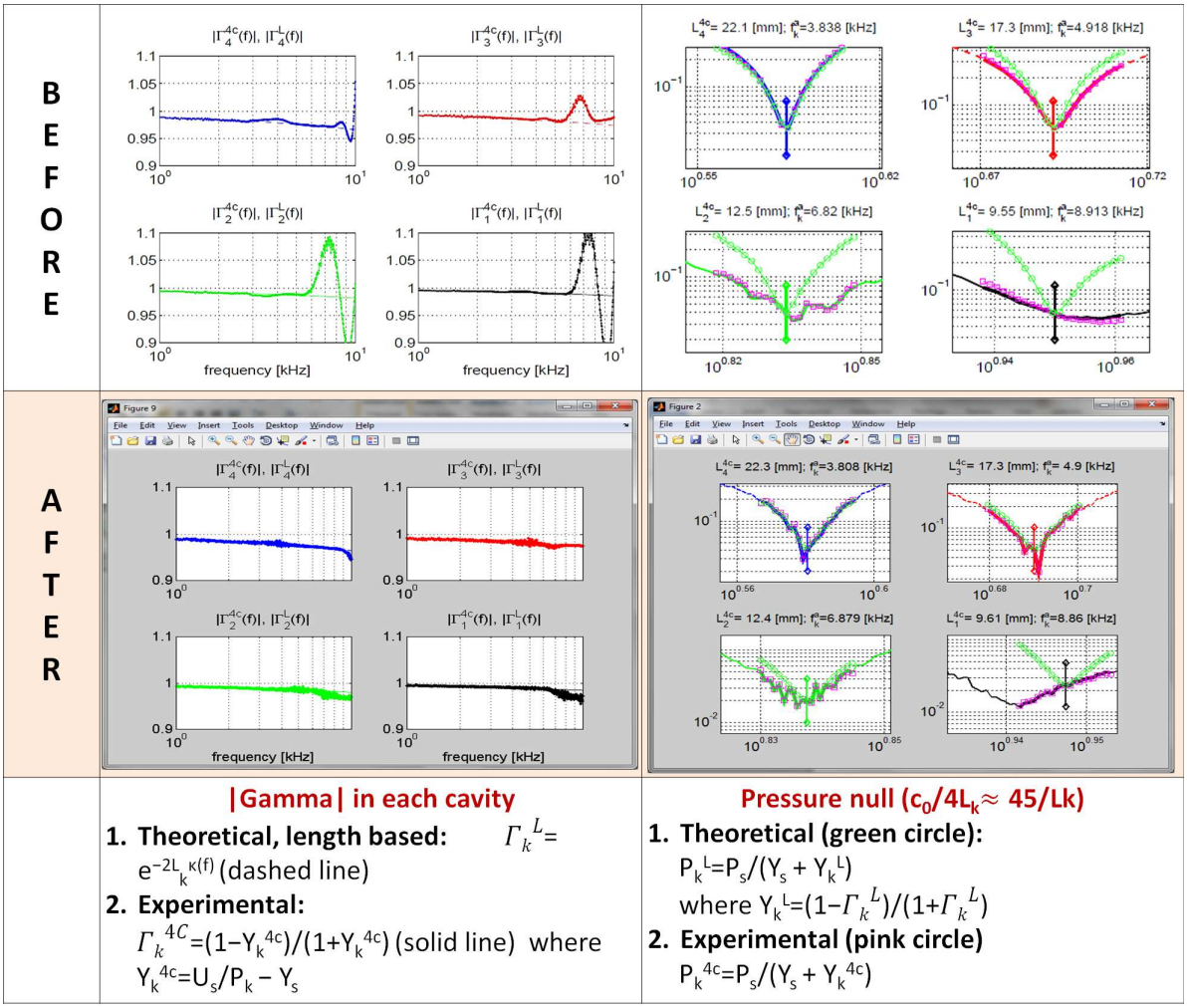

Figure 4.12: This figure shows improvement caused by the ER10C modification before and after. It gives clear evidence that crosstalk was the source of the problem in the ER10C, which has kept users from calibrating the probe above 6 [kHz]. Now the system can pass 4C calibration above 10 [kHz]. Note that all data and results are from preliminary tests. Some of the details are Mimosa Acoustics confidential information which will not be addressed here.

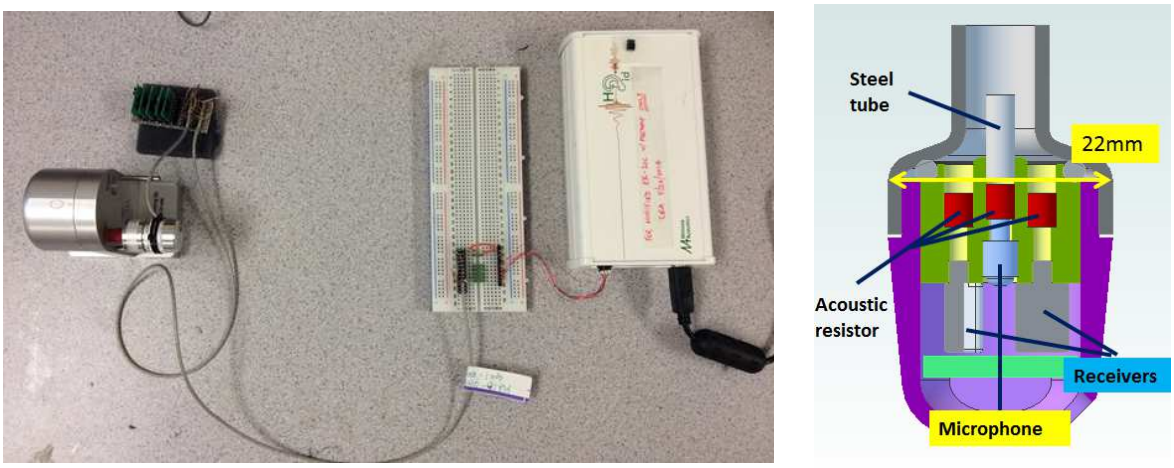

(a) The MA16 inserted in MA cavity

(b) Schematic representation of MA16

Figure 4.13: (a) MA16 is used with the modified APU (right side, white box) which is used for audio processing. (b) Two receivers and one microphone (in the middle) are used. The red parts represent acoustic resistors.

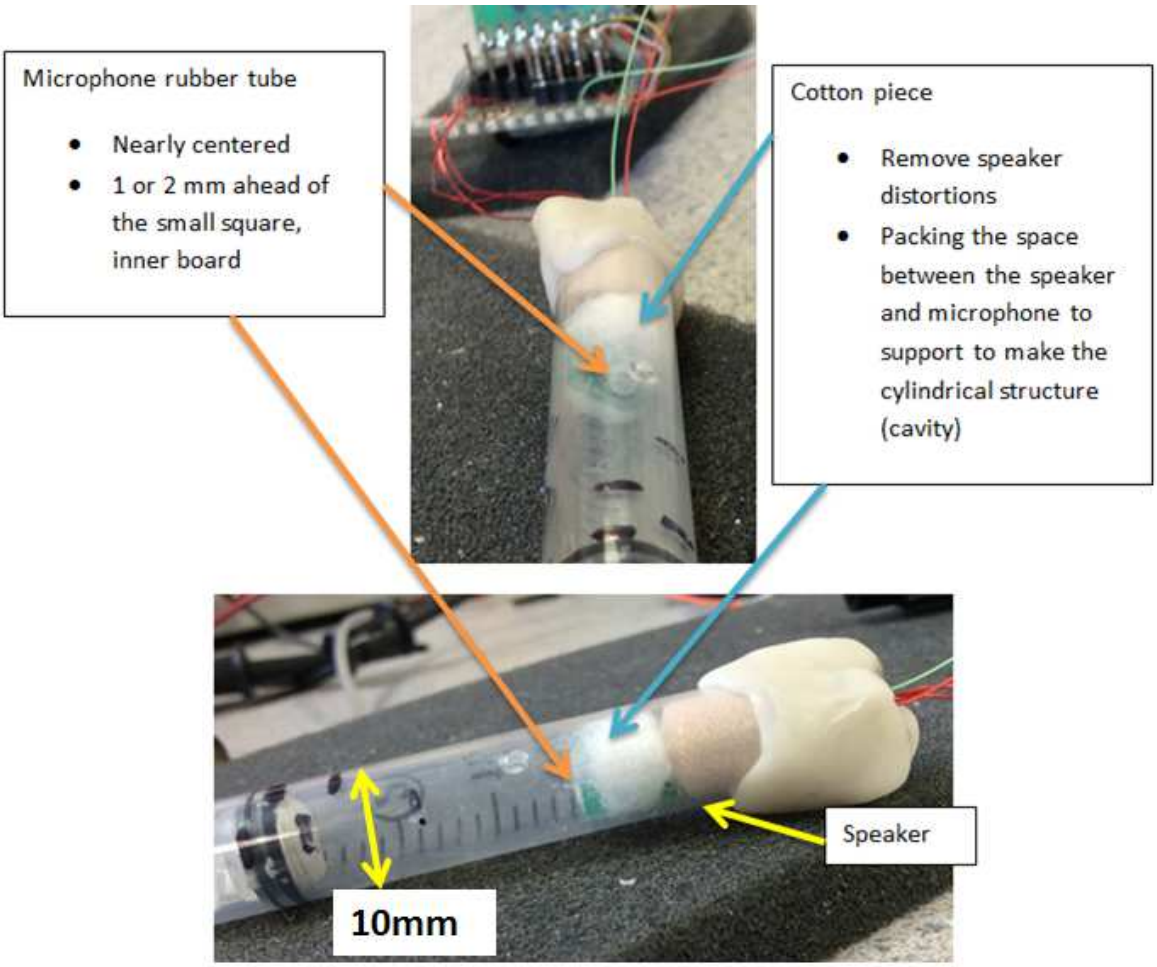

Figure 4.14: The MA17 simulator was made to simulate the proposed design of the MA17. Due to the lined up transducers, the size of the probe can be greatly minimized.

CHAPTER 5

CONCLUSIONS AND CONTRIBUTIONS

In this study, we have discussed the critical elements of a BAR including a gyrator and a semi-inductor, along with the two-port network properties. Starting by solving for the Hunt parameters of the receiver, we have proposed a new circuit model which contains these elements, the gyrator and the semi-inductor. An intuitive design of an electromagnetic transducer has been enabled by using the gyrator, thereby avoiding the mobility method, which can be confusing to explain or teach. Moreover, we have shown an improved high-frequency matching by using the semi-inductors, especially for the electrical impedance, $Z_{in}(s)$.

The model has been verified by comparing the experimental data (obtained from laser, vacuum, and pressure measurements) to theoretical data (obtained through model simulations). All the comparisons are in excellent agreement with the experimental results. The electrical input impedance data matches up to 23 [kHz] (Fig. 4.3). A major advantage of the proposed receiver model is that the acoustic Thevenin pressure can be calculated directly from electrical input impedance measurements.

To summarize the actual contributions from this study beyond the BAR model:

1) The uniqueness of our BAR model includes a) extending the circuit theory to include anti-reciprocal networks, b) semi-inductor networks, and c) non quasi-static networks by means of the transmission line in the refined circuit model (Fig. 1.1). These are uniquely necessary components of the BAR transducer.

2) In-depth investigation of the gyrator's impedance matrix form. Reinterpreting the formula via electromagnetic basics and explaining the anti-reciprocal characteristic due to Lenz's law.

3) Explaining the matrix composition method, which is characterized by the Möbius transformation. This appears to be a generalization of the ABCD (Transmission) matrix cascading method, one of the most powerful computational analysis tools in circuit theory.

4) A demonstration that Z_{mot} is not a physically realizable PR impedance, which is supported by PR property, using a simplified electromechanic model simulation. Historical analysis of the concept of impedance, such as development of AC impedance by Kennelly, also contributes to understanding the nature of the Z_{mot}.

5) The derivation of KCL, KVL from Maxwell's equations. This follows from a Galilean transformation of ME, which is an approximation to Einstein's theory of special relativity.

In summary, this analysis puts the electromagnetic transducer's theory on a firm theoretical basis since its invention by A. G. Bell in 1876.

APPENDIX A

DEFINITION OF ENERGY CONSERVATION, STARTING FROM MODALITY

In the field of engineering or physics, each field has an analogy to the other. If someone asks the meaning of the field in this context, the answer would be "an area with a specific way of how a particle feels a force." This means that there is a generalization with differences in each area. At this point, we can define the difference as a modality which refers a status of having characteristics in a given condition.

Two general variables are used to describe a modality by their product and their ratio. The two conjugate variables come in pairs: a generalized force and a flow. They could be either a **vector** (v, in bold) or a scaler (s), and also can vary spatially. And a product of these two variables defines the power, while a ratio of them defines the impedance, which is usually defined in the frequency domain.

Some examples of the conjugate variables in each modality are described in Table A.1, and examples of power and impedance are described in Table A.2. An frequency (phasor

Table A.1: Example of modalities and their conjugate variables. Upper case symbols are used for the frequency domain variables. The time domain representation of each variable can be described using the lower case of the same character, except in the EM case. But general electromagnetic (EM) theories consider the time domain, and its traditional notation uses capital letter for the time domain analysis. Note that in the electric field, $\mathbf{E} = -\nabla\Phi$, where Φ is scaler potential, the voltage.

Modality	Conjugate variables (vector in bold)	
	Generalized force [unit]	Flow [unit]
Electric	Voltage (Φ) [V]	Current (I) [A]
Mechanic	Force ($\mathbf{F}$) [N]	Particle velocity ($\mathbf{U}$) [m/s]
Acoustic	Pressure (P) [N/m^2]	Volume velocity ($\mathbf{V}$) [1/ms]
Electromagnetic	Electric field ($\mathbf{E}$) [V/m]	Magnetic field ($\mathbf{H}$) [A/m]

or time-harmonic) domain of EM expressions is also common. In this case, a different notation (i.e., *underline* or *italic*) is used based on the author's choice. The EM wave can be decomposed into the sum of the sinusoidal waves. The EM wave phasor form analyzes the waves' propagation if they are oscillating at a single frequency.

One can define a system using a single modality or a combination of them. For the combination of the modalities, the n-port network concept is required. Independent of how

Table A.2: Power and impedance definitions for each modalities in Table A.1. In general, the power concept (a product of conjugate variables) can be used in the time domain, however the impedance (a ratio) is thought of in the frequency domain. Assuming causality, the Laplace transformation can be applied to convert the impedance to the time domain.

Modality	Product in time domain	Ratio (Impedance Z) in frequency domain
Electric	$\phi(t)i(t)$	$Z_e = \Phi/I$
Mechanic	$\mathbf{f}(t) \cdot \mathbf{u}(t)$ (inner product)	$Z_m = F/U$
Acoustic	$p(t)\mathbf{v}(t)$ (intensity)	$Z_a = P/V$
Electromagnetic (EM)	$\mathcal{P} = \mathbf{E} \times \mathbf{H}$ (Poynting vector)	$\eta = \underline{\mathbf{E}}/\underline{\mathbf{H}}$

many modalities exist in a system, there is a well-known law that one can apply to every system. The law of the energy conservation (Van Valkenburg, 1960; Cheng and Arnold, 2013) is expressed as

$$e(t) \equiv \int_{-\infty}^{t} power(t)dt \geq 0, \tag{A.1}$$

where the total delivered energy e(t), which is an integration of the power over time, should be than greater than (or equal to) zero, and $power(t)$ is work done per unit time defined as a potential times a net flow. Simply speaking, Eq. A.1 means we can not have more energy than we supply.

Let us take an example of an electric modality case in the time domain power ($power_e$).

$$power_e(t) = \phi(t)i(t) = (i(t) \star z(t))i(t), \tag{A.2}$$

where $i(t)$ is the net current (the current flow integrated by its affected area therefore it is a scalar) in the time domain, which is not zero, $z(t)$ is an inverse Laplace transform of an impedance (Z=Φ/I) in frequency domain, $e(t)$ is a voltage in time, and $\star$ denotes a convolution operator.

In EM, a Poynting vector ($\mathcal{P}$), represents the power density, a rate of energy transfer per unit area,

$$\mathcal{P} = \mathbf{E} \times \mathbf{H}. \tag{A.3}$$

Note that a cross product is used to consider the spatial variation of each variable. The units for $\mathcal{P}$, $\mathbf{E}$, and $\mathbf{H}$ are [W/m^2], [V/m], and [A/m] respectively. The directions of the P, $\mathbf{E}$, and $\mathbf{H}$ vectors follow the Fleming's right-hand rule. By integration of this Poynting vector over the effective surface area A, we have a scalar power in units of [W] in the electromagnetic field ($power_{EM}$),

$$power_{EM} = \int_s \mathcal{P} \cdot \mathbf{dA} = \int_{\mathbf{s}} (\mathbf{E} \times \mathbf{H}) \cdot \mathbf{dA}. \tag{A.4}$$

In the field of acoustics, power is a measure of sound energy per unit time, which is defined as intensity times area $\mathbf{A}[\mathrm{m}^2]$ ($power_a$),

$$power_a = p(t)\mathbf{u}(\mathbf{t}) \cdot \mathbf{A}, \tag{A.5}$$

where $p(t)\mathbf{u}(\mathbf{t})$ defines the intensity.

To take into account the power concept in the frequency domain, one must use the Laplace transform ($\mathfrak{L}$)'s convolution theorem. Therefore a proper way to describe the instantaneous power in the Laplace frequency domain extending from Eq. A.2 is

$$power_e(t) = \phi(t)i(t) \overset{\mathfrak{L}}{\longleftrightarrow} Power(s)|_{s=j\omega} = \Phi(\omega) \star I(\omega), \tag{A.6}$$

where $j = \sqrt{-1}$, ω is the angular frequency and s is the Laplace frequency. Compared to an usual power definition $P = \Phi I$, this is an unusual expression. However based on Eq. A.2, a product relationship becomes a convolution via Laplace transform.[1]

[1] If it is not true, then more explanation should be followed to make that point clear.

APPENDIX B

TELLEGEN'S THEOREM AND KCL/KVL

Tellegen's theorem (Eq. B.1) states that the complex power, **S**, dissipated in any circuit's components (or branches) sums to zero,

$$\sum \mathcal{S}_{\mathrm{i}} = 0, \tag{B.1}$$

where i is branches in a circuit and, $\mathcal{S}$=$\Phi I^* = R + jQ$ is complex power measured. The $\mathcal{S}$ has both real (R) and imaginary (Q) parts.

$$R = \Re\mathcal{S} = \Re(\Phi I^*), \tag{B.2a}$$

$$Q = \Im\mathcal{S} = \Im(\Phi I^*) \tag{B.2b}$$

where R represents the average power measured in watts [W], and Q shows the reactive power measured in volt-amps reactive [VAR].

Therefore the total power (P_{total}) of the electromechanic system (Fig. 2.1) can be described as

$$P_{total} = \Phi I^* + FU^* = \Re(\Phi I^*) + \Re(FU^*) + j\Im(\Phi I^*) + j\Im(FU^*) = P_{avg} + jP_{reactive}, \tag{B.3}$$

where

$$P_{avg} = \Re\Phi I^* + \Re FU^* = \frac{1}{2}(\Phi I^* + \Phi^* I) + \frac{1}{2}(FU^* + F^* U) \tag{B.4a}$$

$$P_{reactive} = \Im\Phi I^* + \Im FU^* = \frac{1}{2}(\Phi I^* - \Phi^* I) + \frac{1}{2}(FU^* - F^* U). \tag{B.4b}$$

For any lossless network, the P_{avg} goes to zero. McMillan (1946) describes an elementary two-port network to generalize the system's total power using the impedance components of the system. Here, we revisit the steps using the Hunt parameters introduced in 1954.

The total averaged input power (P_{avg}) of an electromechanic system can be calculated

from Eq. 2.1,

$$\begin{aligned} P_{avg} &= \frac{1}{2}[\Phi I^* + \Phi^* I + F U^* + F^* U] \\ &= \frac{1}{2}[(Z_e I + T_{em} U) I^* + (Z_e I + T_{em} U)^* I + (T_{em} I + Z_m U) U^* + (T_{me} I + Z_m U)^* U] \\ &= \frac{1}{2}[(Z_e + Z_e^*) I I^* + (Z_m + Z_m^*) U U^* + (T_{em} + T_{me}^*) I^* U + (T_{em}^* + T_{me}) I U^*], \end{aligned} \quad \text{(B.5)}$$

where * is the complex conjugation operator. In the lossless network, the real part of the power, P_{avg}, is zero. Therefore Eq. B.5 vanishes for all I and U, and then we have the following conditions on the Hunt parameters,

$$Z_e = -Z_e^*, \quad \text{(B.6)}$$

$$Z_m = -Z_m^*, \quad \text{(B.7)}$$

$$T_{em} = -T_{me}^*. \quad \text{(B.8)}$$

Equation B.6 and Eq. B.7 show Z_e and Z_m are purely imaginary in the lossless system. If any loss is added to the system, Z_e and Z_m cannot have negative real part (resistance) to obey the conservation of energy law. Only positive resistance is allowed.

Equation B.5 gives us a general idea about reciprocity. If F is 90^o out of phase with I, then T_{em} and T_{me} should be imaginary; therefore we have $T_{em} = T_{me}$ (Eqs. 2.3, 2.4). A condenser transducer is a real-world example of this reciprocal case.

In an electromagnetic transducer, on the other hand, F is in phase with I; therefore, the F is proportional to the I. In this case, T_{em} is real, therefore to satisfy Eq. B.8, T_{me}=-T_{em}. This is the definition of the anti-reciprocity, the two transfer impedances are real and have different signs. These specific conditions are also discussed in Tellegen (1948). It is a lossless LC network with the anti-reciprocity characteristics considering only Brune's impedances (except resistors).

Two-port network without a semi-inductor

Simlar to Eq. 4.2, Eq. B.9 is a corresponding ABCD matrix representation of a simple two-port network depicted in Fig. B.1. In this figure, the semi-inductor is excluded from the

electrical side.

$$\begin{bmatrix}\Phi(\omega)\\ I(\omega)\end{bmatrix} = \begin{bmatrix}1 & 0\\ \frac{1}{sL_2} & 1\end{bmatrix}\begin{bmatrix}1 & sL_1\\ 0 & 1\end{bmatrix}\begin{bmatrix}0 & G\\ \frac{1}{G} & 0\end{bmatrix}\begin{bmatrix}1 & 0\\ \frac{1}{sm} & 1\end{bmatrix}\begin{bmatrix}F(\omega)\\ -U(\omega)\end{bmatrix}, \tag{B.9}$$

where s is the Laplace frequency $(\sigma + j\omega)$ and L_1, L_2, G, and m are the inductance 1 and 2, the gyration coefficient, and the mass of the system respectively.

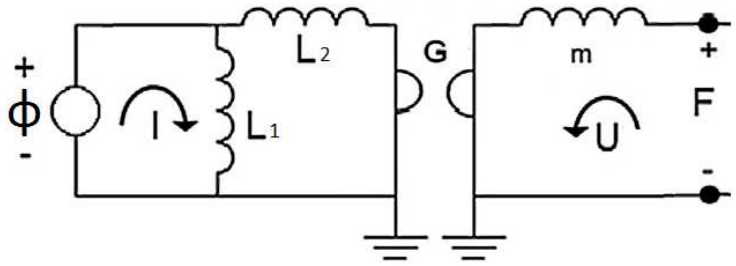

Figure B.1: A simple anti-reciprocal network without a semi-inductor.

For a simple analysis, the ABCD matrix part in Eq. B.9 is separated, and L_1, L_2, G, and m are set to be 1. The whole equation is rewritten as

$$\begin{bmatrix}1 & 0\\ \frac{1}{s} & 1\end{bmatrix}\begin{bmatrix}1 & s\\ 0 & 1\end{bmatrix}\begin{bmatrix}0 & 1\\ 1 & 0\end{bmatrix}\begin{bmatrix}1 & 0\\ \frac{1}{s} & 1\end{bmatrix} = \begin{bmatrix}1 & s\\ s & s^2+1\end{bmatrix}\begin{bmatrix}\frac{1}{s} & 1\\ 1 & 0\end{bmatrix} \tag{B.10}$$

Finally we have the second large ABCD matrix to represent the system in Fig. B.1.

$$\begin{bmatrix}\Phi(\omega)\\ I(\omega)\end{bmatrix} = \begin{bmatrix}T_2\end{bmatrix}\begin{bmatrix}F(\omega)\\ -U(\omega)\end{bmatrix} = \begin{bmatrix}A(s)' & B(s)'\\ C(s)' & D(s)'\end{bmatrix}\begin{bmatrix}F(\omega)\\ -U(\omega)\end{bmatrix} = \begin{bmatrix}\frac{1}{s}+s & 1\\ 2+s^2 & s\end{bmatrix}\begin{bmatrix}F(\omega)\\ -U(\omega)\end{bmatrix}, \tag{B.11}$$

where $\Delta_{T2} = -1$. Converting Eq. B.11 into an impedance matrix, Eq. 2.7 is used to give us

$$Z_2 = \begin{bmatrix}z'_{11} & z'_{12}\\ z'_{21} & z'_{22}\end{bmatrix}, \tag{B.12}$$

where

$$z'_{11} = \frac{\frac{1}{s}+s}{2+s^2} = \frac{1+s^2}{2s+s^3}, \tag{B.13}$$

$$z'_{12} = -\frac{1}{2+s^2}, \tag{B.14}$$

$$z'_{21} = \frac{1}{2+s^2}, \tag{B.15}$$

$$z'_{22} = \frac{s}{2+s^2}. \tag{B.16}$$

Note that this network is a typical lossless LC network which contains only Brune's impedances. Therefore z'_{11} are z'_{22} purely imaginary while z'_{12} and z'_{21} are purely real.

Based on Eq. 2.46, Z_{mot} of this system can be computed as follows,

$$Z_{mot2} = \frac{1}{s(2+s^2)} = \frac{1}{2s+s^3}. \tag{B.17}$$

Substituting the Laplace frequency s to be $j\omega$ in Eq. B.17,

$$Z_{mot2}|_{s=j\omega} = \frac{1}{2j\omega + (j\omega)^3} = j\frac{1}{\omega^3 - 2\omega}. \tag{B.18}$$

There is no real part in Eq. B.18. In this specific case, any angular frequencies (ω) cannot have the real part. Z_{mot} is always purely imaginary.

Figure B.2 represents the simulated Hunt parameters (Eq. B.13 to B.16). The two transfer impedances are real, and they are equal in magnitude but different in signs. The input impedance is purely inductive, and the output impedance behaves like a resonator. Figure B.3 shows the motional impedance and input impedances with both open and short circuit conditions. Compared to Fig. 4.8, all are purely imaginary, with no loss in this system (real part is zero).

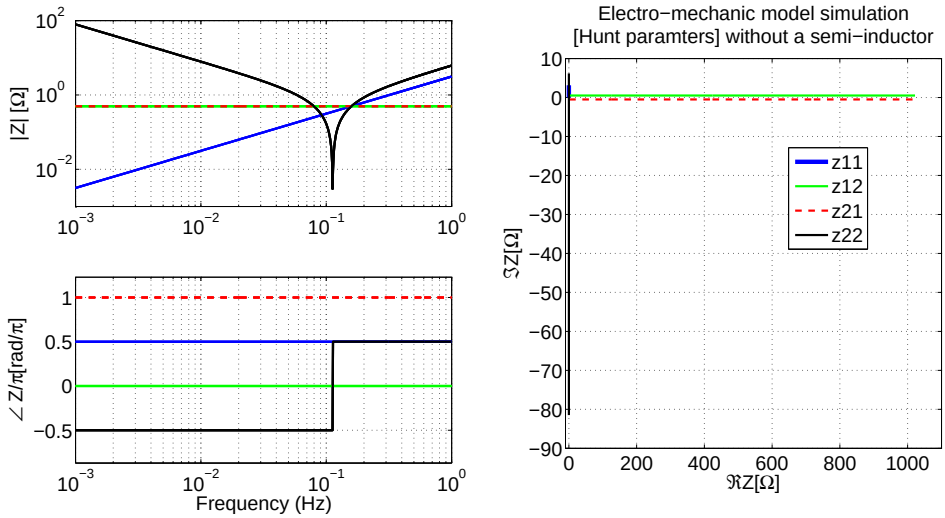

Figure B.2: Computed Hunt parameters based on a simple electromechanic network shown in Fig. B.1 (Eq. B.13 to B.16). All parameters $L1$, $L2$, G, and m are set to be 1 for simple computation.

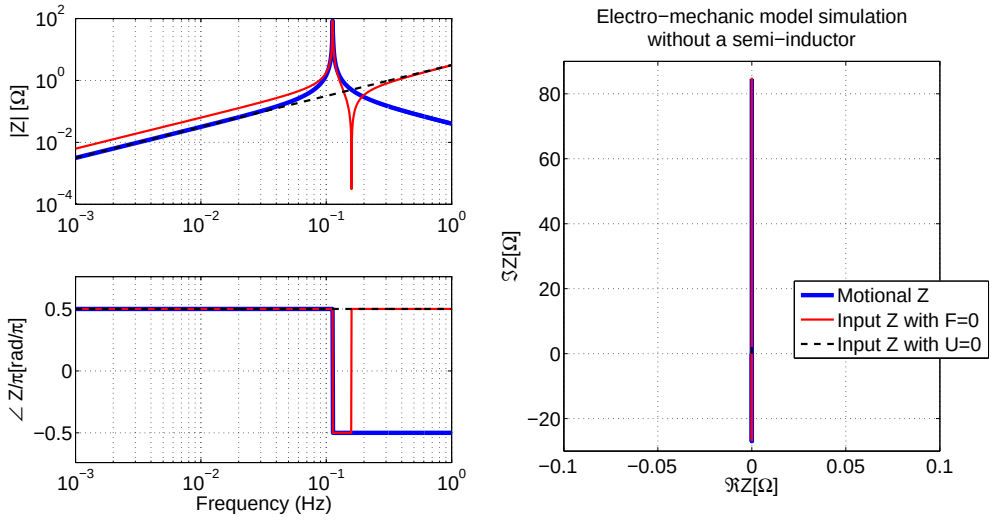

Figure B.3: Computed motional impedance (Eq. B.18), input impedances with both open(Eq. B.13) and short circuit conditions (Eq. B.18 and Eq. B.13) based on a simple electromechanic network shown in Fig. B.1.

APPENDIX C

SENSITIVITY ANALYSIS OF BAR'S SPICE MODEL

Figure C.1 shows the Knowles Electronics commercial SPICE circuit model (Killion, 1992). This SPICE model contains a gyrator and is meant to be equivalent to the physical system, but does not accordingly represent the system in a one-to-one physical manner.

In order to fully understand each component, we implemented the Knowles PSpice model in Matlab using transmission matrices. Unlike PSpice, Matlab provides a more flexible platform for a matrix model manipulation. Matlab does not critically depend on the user's operating system (Knowles' PSpice model is inflexibly tied to both the Cadence Orcad Schematics and Capture, and Windows XP). PSpice requires a DC path to ground from all nodes, thus R1, RK512, RK513, and RK514 components have been added for this purpose.

We then performed a *sensitivity analysis* on the Matlab model by changing each component value by $\pm 20\%$ to determine those components for which the output changed by less than -50 [dB], within the frequency range of 0.1 to 10 [kHz]. Once the small effect components were determined, we removed the components from the original PSpice design for a further Matlab analysis. To compare the difference between the original and the reduced components condition, we calculate each error computed across frequencies,

$$e(f) = \frac{|\text{Original} - \text{Small effect}|}{|\text{Original}|}, \tag{C.1}$$

where f is frequency. Our Matlab simulation result is shown in Fig. C.2(a) with the CMAG value defined in the PSpice circuit (in Fig. C.1, CMAG$= 0.92 \times 10^{-7}$). The Original simulation contains all circuit elements without any modification, whereas the Small effect simulation excludes the small effect components in Fig. C.1. The PSpice sensitivity analysis for the semi-capacitor is performed using Knowles PSpice library for the CMAG component[1] shown in Fig. C.2(b). The most important result of this sensitivity analysis was that the semi-capacitor in the PSpice model is one of these small effect components.

Using a series semi-capacitor on the right side of the gyrator is mathematically equivalent to using a shunt semi-inductor on the left side of the gyrator, because of mobility and

[1]This simulation result was provided by Knowles Electronics.

impedance analogies. However, ideally, circuit elements should be properly associated with their physical properties. It is important to take advantage of using a gyrator to describe the anti-reciprocity for a physically intuitive model of the system. The gyrator is the bridge between the electrical and mechanical systems. For this reason the coil of the receiver should be represented on the electrical side. This realization further motivated our objective to design a simplified and rigorous BAR model.

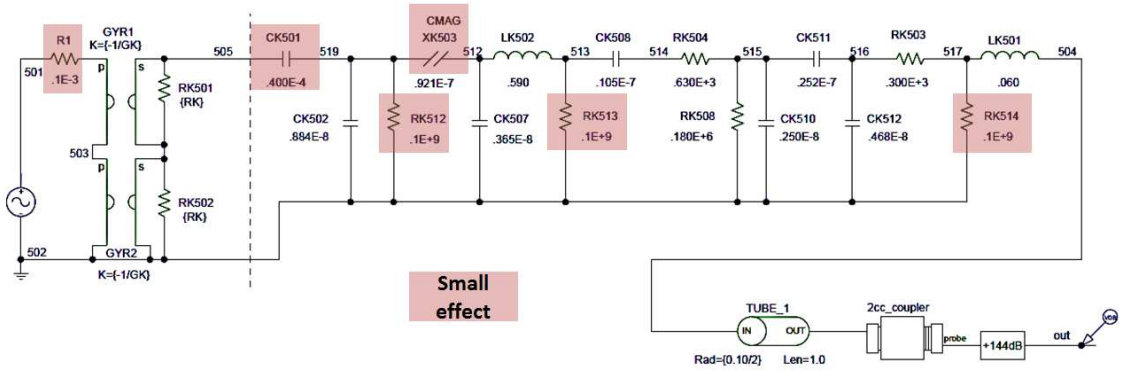

Figure C.1: Knowles PSpice model of the ED receiver: The refined PSice circuit model of ED receiver by reducing small effect components which are marked in red. R1, RK512, RK513, and RK514 resistors were added to maintain DC stability of PSpice. Note that the Spice model represents all ED series receivers, including ED7045, ED1744, ED1913, and etc., such that specific parameter value of components vary for each specific receiver.

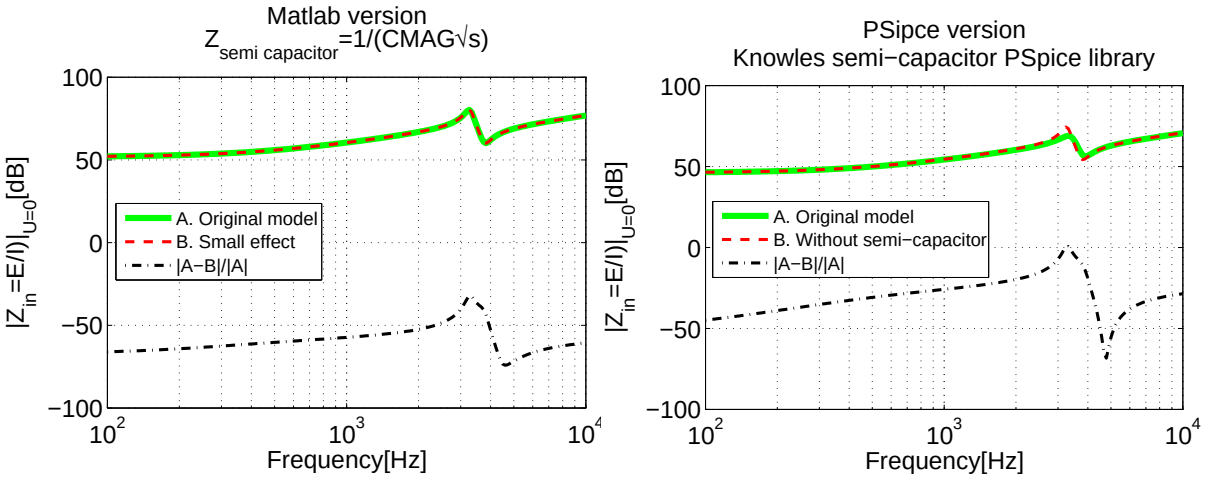

(a) Matlab simulation

(b) PSpice simulation

Figure C.2: The simulated electrical input impedance magnitude, $|Z_{in}|$, in dB scale. (a) shows the sensitivity analysis using Matlab based on Fig. C.1 where $s = j\omega$. The 'A. original model' and the 'B. Small effect' conditions are marked with a thick green line and a dashed red line, respectively. The 'B. Small effect' is the simulated result when all small effect components in Fig. C.1 are removed in the original PSpice circuit. It represents summed-up sensitivities of small effect components in Fig. C.1. (b) represents the sensitivity of the CMAG component only. This analysis is provided by Knowles Electronics using their PSpice library for the CMAG component. (This result is plotted in Matlab, but the data is acquired via PSpice simulation.) Similar to the (a), 'A. Original model' shows the PSpice simulation including all components in Fig. C.1, whereas 'B. Without semi-capacitor' simulates the original PSpice circuit only without the semi-capacitor. For both simulations (a) and (b), the difference between the original response and the reduced response is calculated based on Eq. C.1 shown as the black dashed line.

APPENDIX D

Z_{MOT}: SPATIAL RELATIONSHIPS BETWEEN Φ, I, B, F, AND I

In this section, we will research the fundamental spatial relationship of signals based on Maxwell's equation. There are four well-known Maxwell's equations both in integral and differential forms. Maxwell's equations can be reduced to two main equations, Faraday's law and Ampere's law. When Maxwell developed the electromagnetic relationship into mathematical equations, he ended up with 37 quaternion equations to describe all relationships in the electromagnetic world. Later on, Olive Heaviside reorganized Maxwell's quaternion equations into four reduced complex vector relationships using the $\bigtriangledown$ operator.

Therefore, it is a reasonable idea to revisit the electromechanic parameter's relationship in the spatial domain. In quaternion, three spatial rotation parameters (i, j, and k) are defined, which have the following properties

$$i^2 = j^2 = k^2 = ijk = (k)k = -1. \tag{D.1}$$

Note Eq. D.1 is noncommutative, also i or j are different from the imaginary parameter of the Laplace complex time-frequency domain.

Faraday-lenz's law explains the generator (a relationship between Φ and U through B)

$$\Phi = l(U \times B), \tag{D.2}$$

while Ampere's law is applied for explaining motor action (a relationship between F and I through B),

$$F = l(I \times B). \tag{D.3}$$

Let us consider Fig. D.2 picturing variables in the 3D spatial domain. Considering the spatial relationship of each variable shown in Fig. D.2, Eq. 2.1 is rewritten as

$$\begin{bmatrix} \Phi_x\hat{i} + \Phi_y\hat{j} + \Phi_z\hat{k} \\ F_x\hat{i} + F_y\hat{j} + F_z\hat{k} \end{bmatrix} = \begin{bmatrix} Z_e & T_{em} \\ T_{me} & Z_m \end{bmatrix} \begin{bmatrix} I_x\hat{i} + I_y\hat{j} + I_z\hat{k} \\ U_x\hat{i} + U_y\hat{j} + U_z\hat{k} \end{bmatrix}. \tag{D.4}$$

We can rewrite Eq. D.4 to consider the spatial relationship of each parameter depicted in

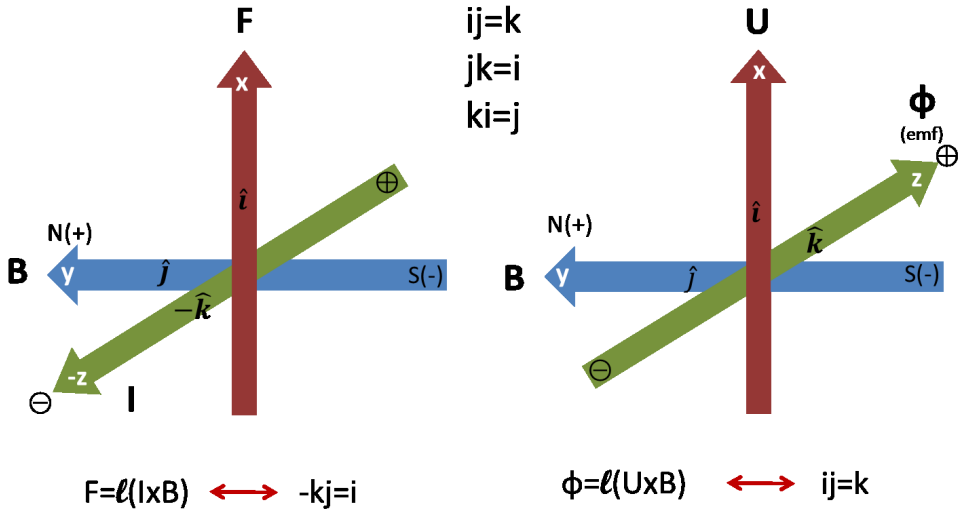

Figure D.1: Electromechanic system's variables in spatial domain by Beranek (1954).

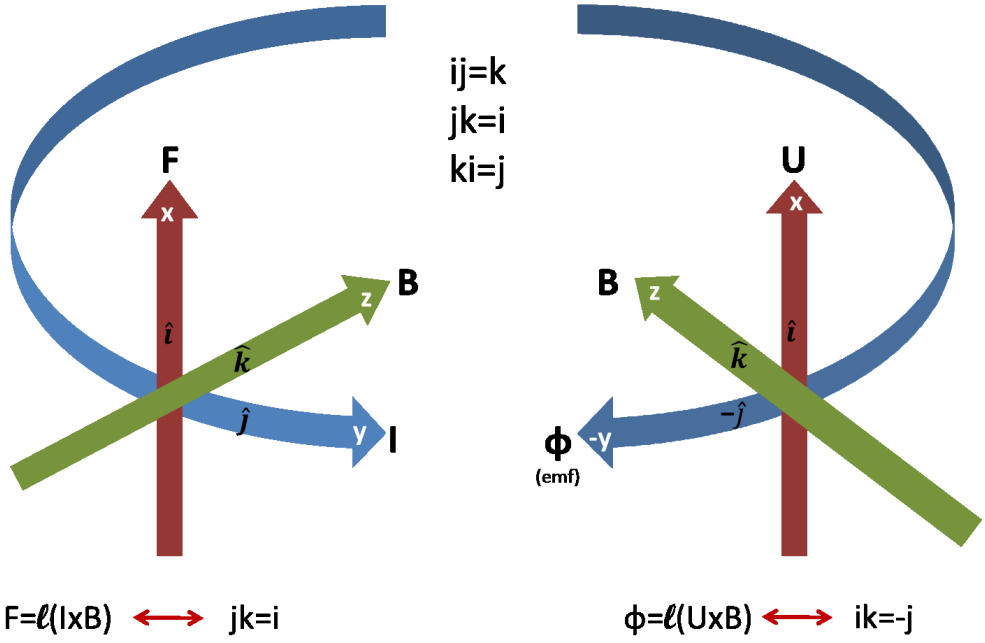

Figure D.2: Equivalent with Fig. D.1. The choice of each geometry is adapted from Hunt (1954).

Fig. D.2,

$$\begin{bmatrix} 0\hat{i} + \Phi_y\hat{j} + 0\hat{k} \\ F_x\hat{i} + 0\hat{j} + 0\hat{k} \end{bmatrix} = \begin{bmatrix} Z_e & T_{em} \\ T_{me} & Z_m \end{bmatrix} \begin{bmatrix} 0\hat{i} + I_y\hat{j} + 0\hat{k} \\ U_x\hat{i} + 0\hat{j} + 0\hat{k} \end{bmatrix}. \tag{D.5}$$

To finalize each relationship in Eq. D.5 we have,

$$\begin{bmatrix} \Phi_y\hat{j} \\ F_x\hat{i} \end{bmatrix} = \begin{bmatrix} Z_e & T_{em}\hat{k} \\ T_{me}(\hat{-k}) & Z_m \end{bmatrix} \begin{bmatrix} I_y\hat{j} \\ U_x\hat{i} \end{bmatrix}. \tag{D.6}$$

Considering spatial rotations in each parameter in Eq. D.6, we can repeat the Z_{mot} derivation shown in Eq. 2.40 and Eq. 2.41.

$$\Phi_y\hat{j} = Z_e I_y\hat{j} + T_{em}\hat{k}U_x\hat{i} = Z_e I_y\hat{j} + T_{em}U_x\hat{j} \tag{D.7a}$$

$$F_x\hat{i} = T_{me}(\hat{-k})I_y\hat{j} + Z_m U_x\hat{i} = -T_{me}I_y\hat{i} + Z_m U_x\hat{i} \tag{D.7b}$$

Setting $F_x\hat{i}$ to be zero, we have

$$\frac{\Phi_y}{I_y} = Z_e + T_{em}\frac{U_x}{I_y} \tag{D.8a}$$

$$\frac{U_x}{I_y} = -\frac{T_{me}}{Z_m} \tag{D.8b}$$

Plugging Eq. D.8b into Eq. D.8a, finally we have the same Eq. 2.42

$$Z_{in}|_{F_x=0} = \frac{\Phi_y}{I_y} = Z_e - \frac{T_{em}T_{me}}{Z_m}. \tag{D.9}$$

The result shown in Eq. D.9 is the same as Eq. 2.42; no spatial dependency is observed. Therefore the spatial relation is already considered in the motional impedance formula shown in Eq. 2.46 introduced in Chapter 2.

APPENDIX E

CALCULATION OF HUNT PARAMETERS

Equation 2.12 includes three unknown Hunt parameters (Z_e, Z_a and T_a) that we wish to find. In order to solve for three unknown parameters, three different electrical input impedances ($Z_{in|A}$,$Z_{in|B}$, and $Z_{in|C}$) are measured corresponding to three known acoustic loads, A, B, and C. The load conditions differ in length of the tubing, attached to the receiver's port. Each tube has the different impedance denoted as $Z_{L|A}$, $Z_{L|B}$, and $Z_{L|C}$, where $Z_{L|A}$=$Z_0 coth(a \cdot tube\_length)$ (for the blocked-end tube, $V = 0$), Z_0 is the characteristic impedance of a tube, and a is the complex propagation function. Parameters a and Z_0 assume viscous and thermal loss (Keefe, 1984). In 20 [^{o}C] room temperature, $c = 334.8$ [m/s]. Define diameter of $Z_L|_{A,B,C} \approx 1.4$ [mm]

Substituting these for Z_L in Eq. 2.12:

$$Z_{in|A} = \frac{\Phi}{I} = Z_e + \frac{T_a^2}{Z_{L|A} + Z_a} \tag{E.1}$$

$$Z_{in|B} = \frac{\Phi}{I} = Z_e + \frac{T_a^2}{Z_{L|B} + Z_a}$$

$$Z_{in|C} = \frac{\Phi}{I} = Z_e + \frac{T_a^2}{Z_{L|C} + Z_a}.$$

Given these three measured impedances, we can solve for Z_a, T_a, and Z_e via the following procedure:

1) Subtract two electrical impedance measurements to eliminate Z_e, such as

$$Z_{in|C} - Z_{in|A} = \frac{T_a^2}{Z_a + Z_{L|C}} - \frac{T_a^2}{Z_a + Z_{L|A}}. \tag{E.2}$$

2) Take the ratio of various terms as defined by Eq. E.2,

$$\left(\frac{Z_a - Z_{L|B}}{Z_{in|C} - Z_{in|A}}\right) = \left(\frac{Z_{in|A} - Z_{in|C}}{Z_{in|B} - Z_{in|C}}\right)\left(\frac{Z_{L|C} - Z_{L|B}}{Z_{L|C} - Z_{L|A}}\right).$$

From this we may solve for the first unknown Z_a,

$$Z_a = \frac{\left(Z_{in|A} - Z_{in|C}\right)\left(Z_{L|C} - Z_{L|B}\right)\left(Z_{in|C} - Z_{in|A}\right)}{\left(Z_{in|B} - Z_{in|C}\right)\left(Z_{L|C} - Z_{L|A}\right)} + Z_{L|B}. \tag{E.3}$$

3) Next we find T_a by substituting Z_a into Eq. E.2,

$$T_a = \sqrt{\frac{\left(Z_{in|C} - Z_{in|A}\right)\left(Z_a + Z_{L|C}\right)\left(Z_a + Z_{L|A}\right)}{Z_{L|A} - Z_{L|C}}}. \tag{E.4}$$

4) Finally, Z_e is given by Eq. E.1:

$$Z_e = \left(\frac{T_a^2}{Z_{L|A} + Z_a}\right) - Z_{in|A}. \tag{E.5}$$

APPENDIX F

HYSTERESIS LOOP FOR A FERROMAGNETIC MATERIAL: **B** VS. **H**

The word *Hysteresis* originates from the Greek, *hystérēsis*, (meaning a state of lagging behind or late); that is, the outcome depends on the history of past inputs, as well as current inputs. In the field of magnetism, the **B** and **H** relationship in ferromagnetic materials shows this hysteresis characteristic; plotting this relationship, we call it Hysteresis loop. The key formula for studying this effect is well known as $\mathbf{B} = \mu\mathbf{H}$; however, the most important thing to discern is, "whose **B**, **H**, and μ?":

$$\underbrace{\mathbf{B}}_{\text{Material's}} = \overbrace{\mu}^{\text{Material's}} \underbrace{\mathbf{H}}_{\text{Applied}}, \tag{F.1}$$

where **B** [Wb/m^2] is the total magnetic density in (ferromagnetic) material, **H** [A/m] is the external applied magnetic field to the material, and μ [H/m] is the permeability (one of properties, showing how easily the material can be magnetized) of the material.

Figure F.1 visualizes the magnetization process in a ferromagnetic material in a greatly simplified way. Without applied **H**, the ferromagnetic material (i.e., iron, nickel, etc.) does not show any magnetic properties (left drawing in Fig. F.1) having net $\mathbf{B} = 0$. Once it is exposed to the external magnetic field **H**, this material exhibits characteristics as shown in the right drawing in Fig. F.1. Now the net $\mathbf{B} \neq 0$; it has the same magnetic direction with the applied magnetic field. This is the simplified description of the magnetization; details of this process need advanced knowledge of quantum mechanics which is not relevant in our study (Ulaby, 2007).

Based on the magnetization process, we can discuss magnetic hysteresis. Figrue F.2 depicts a typical hysteresis loop shown in ferromagnetic materials. In general (not in a ferromagnetic material), **H** and **B** hold the linear relationship, meaning that μ of the material is constant. However it is not true for the ferromagnetic materials, as we can see in Fig. F.2. The shape of the curve has a specific pattern, and each step of the curve needs to be explained. In Fig. F.2, the x-axis represents magnetic field **H** that is applied to the material, and the y-axis shows the magnetic intensity (**B**) of the material.

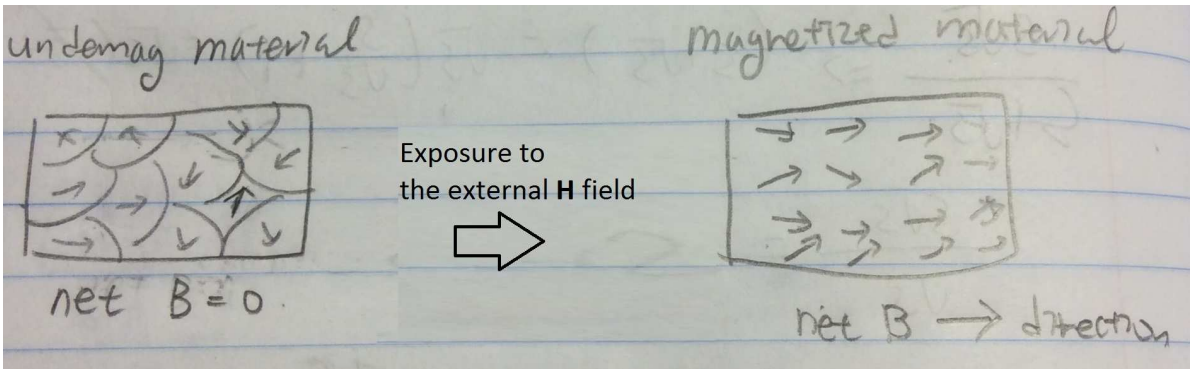

Figure F.1: Simplified magnetization process. Undemagnetized ferromagnetic material's net **B**=0. When ferromagnetic material is exposed to the magnetic field **H**, the net magnetic intensity (**B**) of the material is no longer 0. It becomes magnetized with the same direction of the applied **H**.

1) $(O \rightarrow A)$: The material's initial position starts from O. As strength of the **H** is increased to its positive maximum saturation point (1), the material's **B** also increases to reach the point A

2) $(A \rightarrow B_r)$: Then the **H** starts to decrease to zero, but the material's magnetic property still remains at B_r. This point is named the residual magnetic point. At this point, the ferromagnetic material has the magnetic characteristic without the applied magnetic field; therefore, it behaves like a permanent magnet.

3) $(B_r \rightarrow C)$: As the amplitude of the **H** is increased in the opposite direction (the direction of **H** is still backward), **B** becomes zero at C. The descenting from B_r to C is called demagnetization; that is, the permanent magnet loses its magnetic characteristic within this process.

4) $(C \rightarrow D)$: The line goes down to D, when the **H** reaches its (negative) maximum saturation limits at 2 (red).

5) $(D \rightarrow A)$: Finally, **H** is reversing its direction (i.e., current with sine wave, passing through $f = \pi/2$) and goes through the portion of the hysteresis loop from D to A.

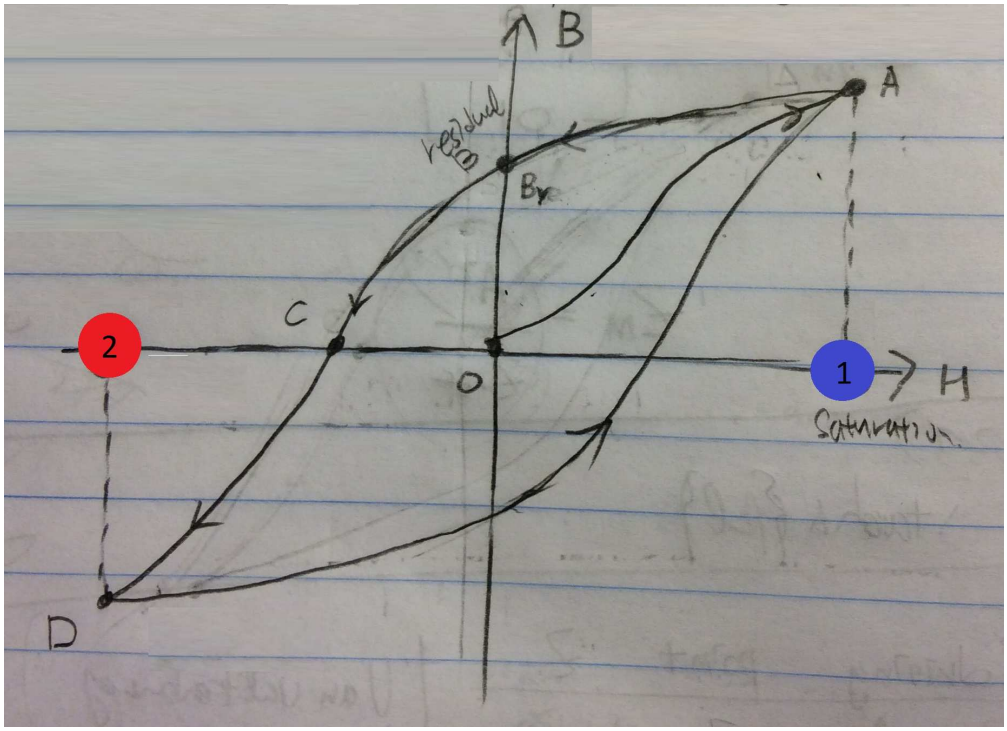

Figure F.2: A typical hysteresis curve in ferromagnetic materials. The x-axis represents magnetic field **H** that is applied to the material, and the y-axis shows the magnetic intensity (**B**) of the material. On the loop, there are five marked points, O, A, B_r, C, D, and two colored points on the x-axis blue (1) and red (2). The blue and red points are two saturation limits of **H** in each direction ($\pm$). The material's initial position starts from O. AS strength of the **H** is increased to its positive maximum saturation point (1), the material's **B** is also increased to reach the point A. Then the **H** starts to decrease to zero, but the material's magnetic property still remains at B_r. This point is called the residual magnetic point. At this point, the ferromagnetic material has magnetic characteristic without applied magnetic field; therefore it becomes a permanent magnet. As **H** increases its amplitude in the opposite direction (the direction of **H** is still backward), **B** becomes zero at C. The descenting from B_r to C is called demagnetization; that is, permanent magnet loses its magnetic characteristic in this process. The line goes down to D, when the **H** reaches its (negative) maximum saturation limits at 2 (red). Finally, **H** is reversing its direction (i.e., current with sine wave, passing through $f = \pi/2$) and goes through the portion of the hysteresis loop from D to A and repeating $A \rightarrow B_r \rightarrow C \rightarrow D...$ until **H** becomes zero.

REFERENCES

J. B. Allen. In J. B. Allen, J. L. Hall, A. E. Hubbard, S. T. Neely, and A. Tubis, editors, *Peripheral Auditory Mechanisms*, volume 64 of *Lecture Notes in Biomathematics*, pages 44–51, Berlin Heidelberg, 1986. Springer.

B. B. Bauer. A miniature microphone for transistor amplifiers. *Journal of the Acoustical Society of America*, 25(5):867–869, 1953.

L. L. Beranek. *Acoustics*. McGraw-Hill, New york, NY, 1954.

L. L. Beranek and T. J. Mellow. *Acoustics Sound Fields and Transducers*. Academic Press - Elsevier Inc., Waltham, MA, 2014.

R. P. Boas. *Invitation to complex analysis*. Random House, New York, NY, 1987.

O. Brune. *Synthesis of a finite two-terminal network whose driving-point impedance is a prescribed function of frequencyg*. PhD thesis, Massachusetts Institute of Technology, Massachusetts, May 1931.

H. J. Carlin and A. B. Giordano. *Network Theory, An Introduction to Reciprocal and Non-reciprocal Circuits*. Prentice-Hall, Englewood Cliffs NJ, 1964.

S. Cheng and D. P. Arnold. Defining the coupling coefficient for electrodynamic transducers. *Journal of the Acoustical Society of America*, 134(5):3561–3672, 2013.

R. D. Fay and W. M. Hall. The determination of the acoustical output of a thelephone receiver from input measurements. *Journal of the Acoustical Society of America*, 5:46–56, 1933.

F. A. Firestone. The mobility method of computing the vibration of linear mechanical and acoustical systems. *Journal of the Acoustical Society of America*, 10(1):83–83, 1938.

C. R. Hanna. Design of telephone receivers for loud speaking purposes. *Proceedings of the Institute of Radio Engineers*, 13(4):437–460, 1925.

F. V. Hunt. *Electroacoustics: The Analysis of Transduction and Its Historical Background*. Harvard University, Massachusetts, 1954.

J. Jensen, F. T. Agerkvist, and J. M. Harte. Nonlinear time-domain modeling of balanced-armature receivers. *Journal of the Audio Engineering Societ*, 59(3):91–101, 2011.

D. H. Keefe. Acoustical wave propagation in cylindrical ducts: Transmission line parameter approximations for isothermal and nonisothermal boundary conditions. *Journal of the Acoustical Society of America*, 75(1):58–62, 1984.

A. E. Kennelly. Impedance. *Transactions of the American Institute of Electrical Engineers*, pages 175–216, 1893.

A. E. Kennelly. The measurement of acoustic impedance with the aid of the telephone receiver. *Journal of the Franklin Institute*, 200:467–487, 1925.

A. E. Kennelly and H. A. Affel. The mechanics of telephone-receiver diaphragms, as derived from their motional impedance circles. *Proceedings of the American Academy of Arts and Science*, 51(8):421–482, 1915.

A. E. Kennelly and K. Kurokawa. Acoustic impedance and its measurement. *Proceedings of the American Academy of Arts and Science*, 56(1):3–42, 1921.

A. E. Kennelly and H. Nukiyama. Electromagnetic theory of the telephone receiver with special reference to motional impeance. *The 348th Meeting of the American Institute of Electrical Engineers*, 1919.

A. E. Kennelly and G. W. Pierce. The impedance of telephone receivers as affected by the motion of their diaphragms. *Proceedings of the American Academy of Arts and Science*, 48:113–151, 1912.

M. C. Killion. Elmer Victor Carson: A lifetime of achievement. *Bulletin of the American Auditory Society*, 17(1):10–21, 1992.

N. Kim and J. B. Allen. Two-port network analysis and modeling of a balanced armature receiver. *Hearing Research*, 301:156–167, 2013.

W. Lewin. Lecture 16: Non-conservative fields - do not trust your intuition. University Lecture, Electricity and Magnetism (Physics 8.02), 2002a.

W. Lewin. Lecture 20: Faraday's law - most physics college books have it wrong! University Lecture, Electricity and Magnetism (Physics 8.02), 2002b.

F. R. Lin, J. K. Niparko, and L. Ferrucci. Hearing loss prevalence in the United States. *Archives of Internal Medicine*, 171(20):1851–1853, 2011.

T. S. Littler. Motional impedance diagram. *Journal of the Acoustical Society of America*, V:235–241, 1934.

T. J. Lynch, V. Nedzelnitsky, and W. T. Peake. Input impedance of the cochlea in cat. *Journal of the Acoustical Society of America*, 72(1):108–130, 1982.

E. M. McMillan. Violation of the reciprocity theorem in linear passive electromechanical system. *Journal of the Acoustical Society of America*, 18:344–347, 1946.

E. E. Mott and R. C. Miner. The ring armature telephone receiver. *The Bell System Technical Journal*, pages 110–140, 1951.

P. Parent and J. B. Allen. Wave model of the human tympanic membrane. *Hearing Research*, 263:152–167, 2010.

S. Puria and J. B. Allen. Measurements and model of the cat middle ear: evidence of tympanic membrane acoustic delay. *Journal of the Acoustical Society of America*, 104(6): 3463–81, 1998.

S. Ramo, J. R. Whinnery, and T. Van Duzer. *Fields and Waves in Communication Electronics*. Wiley, New York, NY, 1965.

S. R. Robinson and J. B. Allen. Characterizing the ear canal acoustic impednace and reflectance by pole-zero fitting. *Hearing Research*, 301:168–182, 2013.

R. Serwy. The limits of brunes impedance. Master's thesis, University of Illinois at Urbana-Champaign, Illinois, May 2012.

A. Sommerfeld. *Electrodynamics*. Academic Press, New york, NY, 1964.

B. D. H. Tellegen. The gyrator, a new electric network element. *Philips research reports*, 3: 81–101, 1948.

K. Thorborg, A. D. Unruh, and C. J. Struck. A model of loudspeaker driver impedance incorporating eddy currents in the pole structure. *Journal of the Audio Engineering Societ*, 2007.

F. T. Ulaby. *Fundamentals of Applied Electromagnetics*. Prentice-Hall, Upper Saddle River, NJ, 2007.

M. E. Van Valkenburg. *Introduction to Modern Network Synthesis*. Wiley, New York, NY, 1960.

M. E. Van Valkenburg. *Network Analysis*. Prentice-Hall, Englewood Cliffs, NJ, 1964.

J. Vanderkooy. A model of loudspeaker driver impedance incorporating eddy currents in the pole structure. *Journal of the Audio Engineering Societ*, 37(3):119–128, 1989.

D. M. Warren and J. L. LoPresti. A ladder network impedance model for lossy wave phenomena. *Journal of the Acoustical Society of America*, 119(5):3377, 2006.

R. E. Weece and J. B. Allen. A clinical method for calibration of bone conduction transducers to measure the mastoid impedance. *Hearing Research*, 263:216–223, 2010.

R. L. Wegel. Theory of magneto-mechanical systems as applied to telephone receivers and similar structures. *Journal of the American Institute of Electrical Engineers*, 40:791–802, 1921.

H. H. Woodson and J. R. Melcher. *Electromechanical Dynamics*. Wiley, New york, NY, 1968.